

RCA REVIEW

BOARD OF EDITORS

Chairman

R. S. HOLMES
RCA Laboratories

E. I. ANDERSON
Home Instruments Division

A. A. BARCO
RCA Laboratories

G. L. BEERS
Radio Corporation of America

G. H. BROWN
Radio Corporation of America

A. L. CONRAD
RCA Service Company

E. W. ENGSTROM
Radio Corporation of America

D. H. EWING
Radio Corporation of America

A. N. GOLDSMITH
Honorary Vice President, RCA

J. HILLIER
RCA Laboratories

E. C. HUGHES
Electron Tube Division

E. A. LAPORT
Radio Corporation of America

H. W. LEVERENZ
RCA Laboratories

G. F. MAEDEL
RCA Institutes, Inc.

W. C. MORRISON
Defense Electronic Products

L. S. NERGAARD
RCA Laboratories

H. F. OLSON
RCA Laboratories

J. A. RAJCHMAN
RCA Laboratories

D. S. RAU
RCA Communications, Inc

D. F. SCHMIT
Radio Corporation of America

L. A. SHOTLIFF
RCA International Division

S. STERNBERG
Astro-Electronics Division

W. M. WEBSTER
RCA Laboratories

Secretary

C. C. FOSTER
RCA Laboratories

REPUBLICATION AND TRANSLATION

Original papers published herein may be referenced or abstracted without further authorization provided proper notation concerning authors and source is included. All rights of republication, including translation into foreign languages, are reserved by RCA Review. Requests for republication and translation privileges should be addressed to *The Manager*.

IN MEMORIAM

GEORGE M. NIXON

On February 10, 1963, George M. Nixon, a member of the *RCA Review* Board of Editors, died of a heart ailment. Mr. Nixon was the Manager, Equipment Development and Standards, of the National Broadcasting Company. He attended Pratt Institute in Brooklyn, New York, from which



he received the EE degree in 1927. After a year with the Electric Storage Battery Company, he joined the National Broadcasting Company in 1928 as a student engineer. Later, as a member of the Development Group concerned with the design and testing of loudspeakers and microphones, he was instrumental in the development of NBC's portable parabolic reflector microphone. In 1929 he was

made responsible for all acoustical work including studio design. He was a member of the industry group that developed what is now known as the Standard Volume Indicator. He was involved in early experiments on broadcasting of frequency-modulated signals and also participated in the experiments with "offset carrier" operation of cochannel television broadcast stations.

Mr. Nixon was a member of the Society of Motion Picture and Television Engineers and the American Institute of Electrical Engineers, a Senior Member of the Institute of Radio Engineers, and a Fellow of the Acoustical Society of America.

Mr. Nixon had been a member of the Board of Editors of *RCA Review* since 1960 and was also a contributor to the *Review*, his first paper having appeared in 1936. His loss will be felt keenly by all who knew him.



AN ELECTRON-BEAM MACHINE

By

A. B. EL-KAREH

RCA Laboratories
Princeton, N. J.

Summary—The theoretical and experimental design of an electron-beam machine is discussed in detail. An analysis is given of all the limitations inherent in an electron optical system of an electron-beam machine, and it is shown that the spot size is largely limited by the spherical aberration of the last focusing lens and by the thermal limitation long before space charge plays any important role. It is shown theoretically that at 100 kv, a probe current of 5 milliamperes can be focused to a .001 inch spot size. After reviewing all possible cathode and gun structures, a thermionic tungsten hairpin-filament emitter and a standard electron gun using a Wehnelt cylinder were chosen. An RCA EMU-3A electron microscope was converted according to the design specifications and a beam of 1 milliamperes was focused to .001 inch diameter. A multivibrator circuit was used to pulse the beam from a few microseconds to several milliseconds.

INTRODUCTION

HIGH-DENSITY ELECTRON BEAMS have been used for drilling, welding and milling various materials. The advantages of the electron-beam machine as compared to other heat sources are clearly shown in Table I.

The factors that determine the design of an electron-beam machine obviously depend to a large degree upon the nature of the job to be done. Among the factors to be considered are the ultimate spot size, the size of the workpiece, the volume of the vacuum chamber, the gas evolution expected, the level of energy concentration required, and the distance from the gun to the workpiece. After all these factors have been established, it is possible to select a suitable electron optical system, cathode, gun assembly, accelerating voltage and other elements and parameters.

Table I

Heat Source	Min. Area (cm ²)	Max. Power Density Watts/cm ²
Oxyacetylene Flame	10 ⁻²	10 ⁴
Electric Arc	10 ⁻³	10 ⁵
Electron Beam	10 ⁻⁷	10 ⁹

GENERAL CONSIDERATIONS

It was decided to design a machine with a high power concentration. The quality and versatility of a machine are appreciably improved as the spot size is decreased and the power concentration increased. For the applications we had in mind, a spot size of 0.001 inch (25 microns) and a power concentration of 100 megawatts/cm² was desirable. For a 100-kv accelerating voltage, this represents a current of 5 milliamperes at the probe.

This objective presented a formidable task. As a first guess it might seem desirable to increase the energy by increasing the accelerating voltage; however, there is a practical limit to the voltage which may be used. Besides the increase in cost and the necessity of x-ray shielding, insulation of the intricate parts becomes very complicated as the voltage is raised beyond a certain point. The task was therefore to design an electron optical assembly which could realize the indicated objective at a prescribed accelerating voltage.

It was necessary to investigate the limitations inherent to the electron optical system before a detailed theoretical and experimental study of the design and performance of the electron machine could be undertaken.

In general, there are four limitations that must be considered in this case. In the first place, there is no such thing as a perfect lens, i.e., a lens which will focus the electrons emitted from a point source into a point image. Second, the electrons forming the beam tend to repel one another, a phenomenon generally known as space-charge repulsion. Third, the electrons emerging from the emitter have a Maxwellian velocity distribution. Finally, diffraction effects will tend to set a lower limit to the beam diameter. An analysis is given here to show which of the above are instrumental in setting an upper limit to the current density and lower limit to the spot size for a given electron optical system, beyond the values that have already been selected.

DIFFRACTION LIMITATION

Let us consider a system where r_a is the focused spot radius and θ the half-angle of convergence of the beam. The radius of the first minimum of the diffraction image is given by

$$r_a \cong \frac{0.6\lambda}{\theta}; \quad (1)$$

λ is the electron wavelength

$$\lambda \cong \frac{12.3}{\sqrt{V}}, \quad (2)$$

where λ is in angstrom units and V in volts. From Equations (1) and (2),

$$r_a \cong \frac{7.4}{\theta\sqrt{V}} \text{ angstroms.} \quad (3)$$

For $V = 10^5$ volts, $\theta = 5 \times 10^{-3}$, $r_a = 4.75 \times 10^{-7}$ mm. It is obvious that in the system we have in mind the diffraction limitation is of no concern.

SPACE-CHARGE LIMITATION

The question of space-charge and thermal limitations has been investigated by many workers. However, each limitation has been investigated separately, and the physical assumptions on which they are separately based are very different. Attempts have been made by Cutler and Hines¹ and Danielson et al.² to analyze exactly the situation when both space-charge and thermal limitations are taken into account simultaneously. Their results are very intricate, being arrived at after a series of complex derivations. Fortunately, it is not imperative to study both limitations at the same time, because the transition region between the dominance of either effect is quite abrupt. Electron beams, over a rather wide range, are either almost totally space-charge limited or thermally limited. There is, indeed, a narrow region where both limitations are present, but this need not be taken into account in this analysis.

Schwartz³ arrived at one of the most elegant solutions to the space-charge problem. By means of an ingenious normalization procedure he plotted a universal curve which can be used to obtain the space-charge-limited spot size quite readily as a function of other beam parameters and for a wide range of operating conditions. Following the excellent work of Thompson and Headrick,⁴ Schwartz started out by considering the charge per unit length of the beam, which is given by

¹ C. C. Cutler and M. E. Hines, "Thermal Velocity Effects in Electron Guns," *Proc. I.R.E.*, Vol. 43, p. 307, 1955.

² W. E. Danielson, J. L. Rosenfeld, and J. A. Saloom, "A Detailed Analysis of Beam Formation with Electron Guns of the Pierce Type," *Bell Syst. Tech. Jour.*, Vol. 35, No. 2, p. 375, March 1956.

³ J. W. Schwartz, "Space-Charge Limitation on the Focus of Electron Beams," *RCA Review*, Vol. 18, No. 1, p. 3, March 1957.

⁴ B. J. Thompson and L. B. Headrick, "Space-Charge Limitations on the Focus of Electron Beams," *Proc. I.R.E.*, Vol. 28, No. 7, p. 318, July 1940.

$$\frac{I}{V_z}, \quad (4)$$

where I is the beam current and V_z the axial velocity. He used Gauss' law to express the electric field just outside a long cylinder of charge as

$$F = \frac{I}{\pi \epsilon d \sqrt{2\eta V_0}}, \quad (5)$$

where V_0 is the accelerating potential,

η is the electronic charge to mass ratio: $e/m = 1.76 \times 10^{11}$ coulomb/kg,

ϵ is the permittivity of vacuum: 8.85×10^{-12} farad/meter,

d is the beam diameter.

After some manipulations Schwartz obtained

$$\sqrt{\frac{\eta I}{\pi \epsilon \sqrt{2\eta V}} \frac{Z}{\sqrt{2\eta V}} \frac{2}{D_i}} = \frac{f(\beta)}{\beta}, \quad (6)$$

where Z is the gun-to-screen axial distance and D_i is the initial beam diameter. $f(\beta)$ and β are defined by the transcendental equation

$$\begin{aligned} f(\beta) &= 2\beta e^{-\beta^2} \left\{ U(\beta) + U \left(\sqrt{\beta^2 - \ln \frac{D_i}{d}} \right) \right\} \\ &= 1 + \frac{d\beta}{D_i} \left\{ \sqrt{\beta^2 - \ln \frac{D_i}{d}} \right\}^{-1}, \end{aligned} \quad (7)$$

where r is the instantaneous radius of an electron on the edge of the beam at its narrowest constriction, and β is so chosen as to make Equation (7) valid, and

$$U(x) = \int_0^x e^{t^2} dt. \quad (8)$$

Equation (6) simplifies to

$$I = 8.24 \times 10^{-6} \left(\frac{D_i}{Z} \right)^2 \left(\frac{f(\beta)}{\beta} \right)^2 V^{3/2}. \quad (9)$$

Schwartz made the same assumptions as Thompson and Headrick, namely,

- (1) the electron current density in the aperture is uniform,
- (2) all the electrons have the same axial velocity,
- (3) the radial velocity of the electrons, directed inwards, is proportional to their distance from the axis,
- (4) the electrons move in a region which is field-free except for the field caused by the charge density of the beam.

It is clear that the above assumptions do not always hold in every electron optical system, but the errors involved are not serious in our system.

Now let

$$\beta = \sqrt{\ln \frac{D_i}{d} + \delta^2}. \quad (10)$$

Substituting this into Equation (7),

$$2\beta e^{-\beta^2} U(\beta) + 2\beta e^{-\beta^2} U(\delta) = 1 + \frac{d\beta}{D_i \delta}, \quad (11)$$

$$U(\beta) = \int_0^1 e^{x^2} dx + \int_1^\beta e^{x^2} dx \quad (12)$$

$$\begin{aligned} U(\beta) = & 1 + \frac{1}{3} + \frac{1}{5.2!} + \cdots + \frac{1}{2} \left(\frac{e^{\beta^2}}{\beta} - e \right) + \frac{1}{4} \left(\frac{e^{\beta^2}}{\beta^3} - e \right) \\ & + \frac{3}{4} \left(\frac{e^{\beta^2}}{\beta^5} - e \right) + \frac{15}{8} \left(\frac{e^{\beta^2}}{\beta^7} - e \right) + \frac{105}{8} \int_1^\beta \frac{e^{x^2}}{x^8} dx. \end{aligned} \quad (13)$$

This is found by repeated integration by parts. If we consider D_i/d as very large, $\delta = \{\beta^2 - \ln D_i/d\}^{1/2}$ is small and β is large. The value of the first series is 1.463, which is small compared to the second part of the expression, as β is large. The residual integral in the second expression decreases with continued integration by parts, but begins to increase again when $\beta^2 \approx n + 1/2$. Thus, the error is least if the series is broken off near this point. For very large β , it is advisable to break off the series slightly sooner to make the neglected series

$$- e \left(\frac{1}{2} + \dots + \frac{2n-1}{2n} \right)$$

small. Thus we obtain the semiconvergent expression

$$U(\beta) = \frac{1}{2} \frac{e^{\beta^2}}{\beta} \left(1 + \frac{1}{2\beta^2} + \frac{3}{4\beta^4} + \frac{15}{8\beta^6} + \dots \right). \quad (14)$$

Therefore, Equation (11) can be written

$$\begin{aligned} & \frac{1}{2\beta^2} + \frac{3}{(2\beta^2)^2} + \dots + \frac{2\beta}{e^{\beta^2}} (\delta) \left(1 + \frac{\delta^2}{3.1!} + \dots \right) \\ &= \frac{d}{\delta D_i} \left(\ln \frac{D_i}{d} + \delta^2 \right)^{\frac{1}{2}}, \end{aligned} \quad (15)$$

or

$$\begin{aligned} & \frac{1}{2 \ln \frac{D_i}{d}} \left\{ 1 - \frac{\delta^2}{\ln \frac{D_i}{d}} \dots \right\} + \frac{3}{4 \left(\ln \frac{D_i}{d} \right)^2} \left\{ 1 - \frac{2\delta^2}{\ln \frac{D_i}{d}} \dots \right\} + \dots \\ &+ \frac{\frac{2d}{D_i} \sqrt{\ln \frac{D_i}{d}}}{1 + \delta^2 + \frac{\delta^4}{2!}} \left\{ \delta + \frac{\delta^3}{3.1!} + \dots \right\} \\ &= \frac{d}{\delta D_i} \sqrt{\ln \frac{D_i}{d}} \left(1 + \frac{1}{2} \frac{\delta^2}{\ln \frac{D_i}{d}} - \frac{1}{8} \frac{\delta^4}{\left(\ln \frac{D_i}{d} \right)^2} + \dots \right) \end{aligned} \quad (16)$$

We multiply throughout by δ and solve for δ ,

$$\begin{aligned} \delta \left\{ \frac{1}{2 \ln \frac{D_i}{d}} + \frac{3}{\left(2 \ln \frac{D_i}{d} \right)^2} + \dots + \frac{2d}{D_i} \sqrt{\ln \frac{D_i}{d}} \delta - \frac{\delta^2}{2 \left(\ln \frac{D_i}{d} \right)^2} \right. \\ \left. - \frac{3}{2} \frac{\delta^2}{\left(\ln \frac{D_i}{d} \right)^3} + \dots \right\} \end{aligned}$$

$$= \frac{d}{D_i} \sqrt{\ln \frac{D_i}{d}} \left(1 + \frac{1}{2} \frac{\delta^2}{\ln \frac{D_i}{d}} + \dots \right) \quad (17)$$

$$\delta \approx \frac{\frac{d}{D_i} \sqrt{\ln \frac{D_i}{d}}}{\frac{1}{2 \ln \frac{D_i}{d}} + \frac{3}{\left(2 \ln \frac{D_i}{d}\right)^2} + \dots} \quad (18)$$

with a relative error of the order

$$\delta^2 \approx 4 \left(\frac{d}{D_i} \right)^2 \left(\ln \frac{D_i}{d} \right)^3.$$

Therefore

$$\begin{aligned} \frac{f(\beta)}{\beta} &= \frac{1}{\beta} + \frac{d}{D_i \delta} = \frac{1}{\sqrt{\ln \frac{D_i}{d}}} \left(1 - \frac{\delta^2}{2 \ln \frac{D_i}{d}} \dots + \frac{1}{2 \ln \frac{D_i}{d}} \right. \\ &\quad \left. + \frac{3}{\left(2 \ln \frac{D_i}{d}\right)^2} + \dots \right) \\ &= \frac{1}{\sqrt{\ln \frac{D_i}{d}}} \left(1 + \frac{1}{2 \ln \frac{D_i}{d}} + \frac{3}{\left(2 \ln \frac{D_i}{d}\right)^2} + \dots \right). \quad (19) \end{aligned}$$

We thus obtain, for $V = 10^5$ volts,

$$\begin{aligned} I &= \frac{260}{\ln \frac{D_i}{d}} \left(\frac{D_i}{Z} \right)^2 \left\{ 1 + \frac{1}{2 \ln \frac{D_i}{d}} + \frac{3}{\left(2 \ln \frac{D_i}{d}\right)^2} \right. \\ &\quad \left. + \frac{15}{\left(2 \ln \frac{D_i}{d}\right)^3} + \frac{105}{\left(2 \ln \frac{D_i}{d}\right)^4} + \dots \right\}^2, \quad (20) \end{aligned}$$

where I is in amperes. The upper value of the space-charge-limited probe current has been computed with the use of this expression for $d = 0.001$ inch for two different working distances Z (1 inch and 4 inches) as a function of the initial beam diameter D_i . These values of Z correspond to the desirable working distances in the machine. The results are plotted in Figure 1.

Similar curves can be obtained for the gun we have chosen by reading directly from Schwartz's curve, reproduced and enlarged in Figure 2. It can be seen that for values of $d/D_i > 0.04$ the curve is double valued. Here the space-charge effects are appreciable, and a plane of minimum sectional area exists between the screen and the lens where the minimum-focused-spot condition is achieved. However, our values fall well below 0.04.

Hollway⁵ gives a somewhat equivalent treatment, and has since⁶ published a design chart for calculating electron-beam parameters. Using the chart, it is possible to determine not only the space-charge-limited spot size for given gun data, but also thermal velocity spreading limitations. Reference to Hollway's charts will show that his results correspond very closely to those derived by Schwartz.⁷ The chart shows that for the system being designed, there is no space-charge limitation.

The whole derivation was made on the assumption that the beam travels in absolute vacuum. It has been shown⁷ that under certain conditions, ions formed from the residual gas may be trapped in the beam, thus neutralizing some of the space-charge forces.

THERMAL LIMITATIONS

We use the well-known formula derived by Langmuir for the maximum current density achievable in an electron spot as limited by the thermal velocity distribution of the emitted electrons:

$$j_0 = j_c \left\{ \frac{eV}{kT} + 1 \right\} \sin^2 a. \quad (21)$$

⁵ D. L. Hollway, "The Optimum Space-Charge Controlled Focus of an Electron Beam," *Australian Jour. Sci. Research*, Vol. 5, Series A, p. 430, 1952.

⁶ D. L. Hollway, "Design Chart for Calculating Electron-Beam Parameters," *Electronics*, Vol. 35, No. 7, p. 50, Feb. 16, 1962.

⁷ K. G. Hernqvist and E. G. Linder, "Space-Charge Effects in Electron Beams and Their Reduction by Positive Ion Trapping," *Jour. Appl. Phys.*, Vol. 21, No. 11, p. 1088, Nov. 1950.

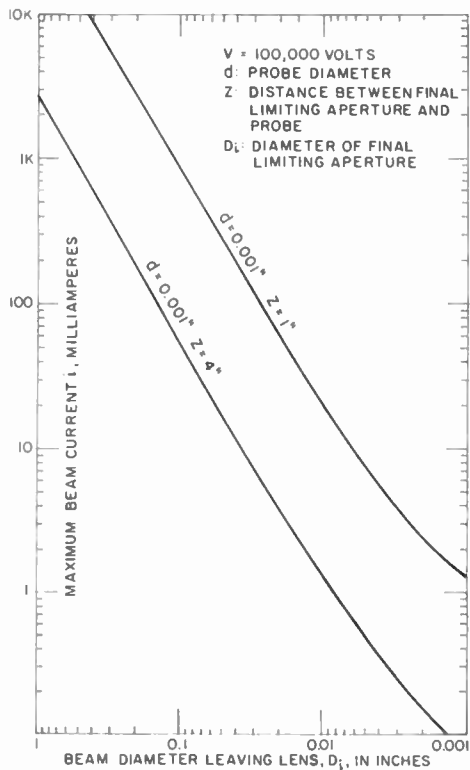


Fig. 1 Upper limit to probe current established by space charge.

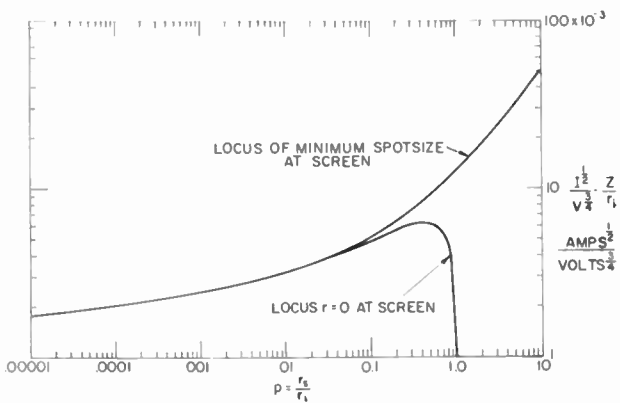


Fig. 2—Space-charge limitations as derived by Schwartz.⁵

Here the assumption is made that the electrons originate from a unipotential cathode having a Maxwellian velocity distribution corresponding to a uniform absolute temperature T . j_c is the emission density, which is considered to be uniform. The converged electrons are in a field-free region and of uniform velocity V . a is the half angle of arrival at the plane where j_0 is being defined. For small values of a , Equation (21) can be written

$$I = \frac{\pi d_0^2}{4} a^2 \frac{11600 V}{T} j_c \text{ amperes.} \quad (22)$$

T is the temperature of the cathode in $^{\circ}\text{K}$ and j_c the emission per unit area (amperes/cm²). Since the system is demountable and the filament or cathode can be replaced, we may assume for a tungsten cathode, $T = 3000^{\circ}\text{K}$. With $V = 10^5$ volts we then have

$$I = 3.00 a^2 d_0^2 10^5 j_c \text{ amperes.} \quad (23)$$

The permissible angle, a , is limited by the spherical aberration of the last lens. There is no point in computing Equation (23) for values of a for which the spherical aberration is already the limiting factor. It is therefore appropriate to consider together the limitations imposed by the temperature spread of the initial velocities and by spherical aberration.

The value of a is determined by

$$d = d_0 + \frac{Cfa^3}{2}, \quad (24)$$

where d_0 is the beam diameter in the absence of spherical aberration, C is the spherical aberration constant and f is the focal length. This gives the beam diameter of a pencil with aperture angle a in the plane of narrowest constriction.

Combining Equation (24) with (23),

$$I = 3 \times 10^5 a^2 \left(d - \frac{Cfa^3}{2} \right)^2 j_c \text{ amperes.} \quad (25)$$

We shall now choose a to maximize I ; by setting $dI/da = 0$, we get

$$2a \left(d - \frac{Cfa^3}{2} \right) - 3a^4 Cf \left(d - \frac{Cfa^3}{2} \right) = 0, \quad (26)$$

or

$$a^3 = \frac{d}{2Cf}. \quad (27)$$

We then have

$$\frac{I}{j_c} = 3 \times 10^5 \left(\frac{d}{2Cf} \right)^{2/3} \left(\frac{3d}{4} \right)^2 = 1.06 \times 10^5 \frac{d^{8/3}}{Cf^{2/3}}. \quad (28)$$

The smallest value of Cf which has been obtained for any symmetric electron lens is of the order of 0.1 cm. Therefore, for a beam diameter of 25μ , this represents a current I in ma, with j_c assumed to be 5 amps/cm²

$$I = 5 \times 1.06 \times 10^5 \times 10^{-8} \times 11.85 \times 10^{2/3} = 0.291 \text{ ampere}. \quad (29)$$

This enormous current, attractive as it may seem, is of purely academic interest, since the value of Cf used represents a lens of almost no working distance.

In computing the Cf of a lens, it is necessary to know the lens configuration and the working distance. Some approximate values are selected initially for the purpose of the analysis; exact values are computed later, after the geometry of the system has been outlined.

Using the curves of Liebmann and Grad⁸ and those given by Zworykin et al.,⁹ it is possible to derive the value of Cf for various lens configurations. Figure 3 shows the assumed lens cross section. Using the same notation as that of Liebmann and Grad, we have set the pole piece separation, a_p , equal to the bore diameter, D . For the range of working distances and lens diameters to be considered, the principal planes of this lens can be regarded as coinciding with its geometrical plane of symmetry, and thus the working distance is

$$Z = f - D. \quad (30)$$

Table II gives the results obtained with the chosen lens for various values of D and Z .

In making a comparison between the space-charge and thermal limitations, it should be noted that the beam does not fill the whole

⁸ G. Liebmann and E. M. Grad. "Imaging Properties of a Series of Magnetic Electron Lenses," *Proc. Phys. Soc. (London)*, Vol. 64, Sec. B, Part 11, p. 956, Nov. 1951.

⁹ V. K. Zworykin, G. A. Morton, E. G. Ramberg, J. Hillier, and A. W. Vance, *Electron Optics and the Electron Microscope*, p. 614, John Wiley and Sons, Inc., New York, N. Y. 1945.

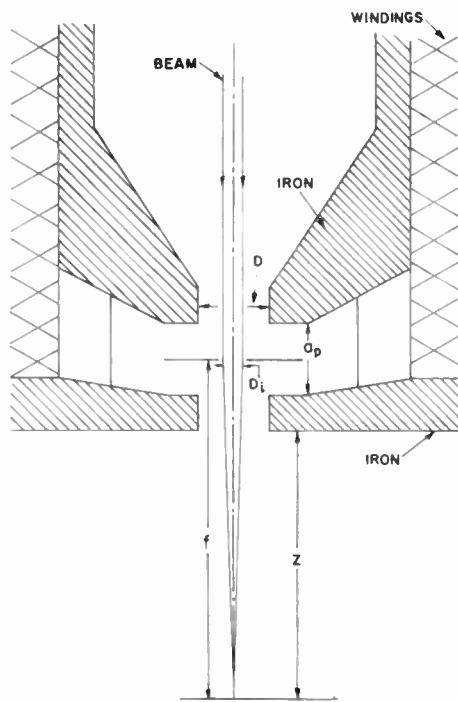


Fig. 3—Assumed magnetic-lens configuration.

diameter of the lens. The diameter of the beam, D_i , and the lens diameter, D , are related by the following equation:

$$D_i = 2(Z + D)a = 2(Z + D) \left(\frac{d}{2Cf} \right)^{1/3}. \quad (31)$$

Table II
(For $d = 0.001$ inch)

Z (inches)	D (inches)	Cf (centimeters)	$\frac{I}{j_0} \times 10^3$
1	1.6	27.00	1.39
1	0.4	62.50	0.794
1	0.1	490.00	0.203
4	1.6	250.00	0.323
4	0.4	1960.00	0.083
4	0.1	26000.00	0.014

Table III gives a comparison for the values obtained with the two limitations taken one at a time. As stated previously, the spherical aberration of the focusing lens is already implied in the thermal limitation. It seems obvious that the minimum spot size will be limited by the spherical aberration of the last lens and the thermal limitation of the system long before space charge plays any important role.

Table III

Lens Bore Diameter, D (inches)	Beam Diameter at the Lens, D_i (inches)	Working Distance Z (inches)	$\frac{I}{j_0} \times 10^3$	Space-Charge Limited Current (ma)
1.6	0.19	1	1.39	2500
1.6	0.19	4	0.323	160
0.4	0.076	1	0.794	500
0.4	0.076	4	0.083	30
0.1	0.030	1	0.203	115
0.1	0.030	4	0.014	7

CHOICE OF CATHODE

An ideal cathode is one which will require a minimum of attention for the maximum length of time. A cathode must be more or less self-supporting, it must not be poisoned by the gases released from the metal or by the metal vapor itself and, above all, it must have enough electron emission to satisfy the electron optical requirement of the system. Generally, highest electron emissions are the most desirable.

If the criterion in the choice of a cathode for an electron beam machine is the emission of the largest possible number of electrons, a field emitter should theoretically surpass all other cathodes because of the almost inexhaustible reservoir of electrons inside a metal; current densities of millions of amperes per cm^2 should be obtainable. It is therefore worthwhile to investigate this emitter to see whether it could be applied for our purpose.

Dolan and Dyke¹⁰ recognize three kinds of field emission: (1) temperature emission at high temperatures and low fields, as described

¹⁰ W. W. Dolan and W. P. Dyke, "Temperature-and-Field Emission of Electrons from Metals," *Phys. Rev.*, Vol. 95, No. 2, p. 327, July 15, 1954.

by Richardson and Schottky; (2) the field emission at low temperatures and high fields investigated by Nordheim; and (3) the temperature-field or T - F emission at temperatures and fields intermediate between the two extremes, studied by Dolan and Dyke.

Schottky's¹¹ equation in its simple form is as follows:

$$j = j_0 \exp \left\{ \frac{e}{k} \left[\frac{e}{4\pi\epsilon_0} \right]^{\frac{1}{2}} \frac{F^{\frac{1}{2}}}{T} \right\} \quad (32)$$

where j_0 is the thermionic emission at zero field, e is the electron charge, k is Boltzmann's constant, ϵ_0 is the permittivity of free space, and T

Table IV—Free-field emission of tungsten as a function of temperature.

j_0 amps/cm ²	T in °K
0.12	2400
0.30	2500
0.70	2600
1.6	2700
3.5	2800
7.3	2900
14.0	3000

is the temperature in °K. This can be written in its logarithmic form as

$$\log_{10} \left(\frac{j}{j_0} \right) = 0.1912 \frac{F^{\frac{1}{2}}}{T}. \quad (33)$$

Taking tungsten as an example, the work function $\phi = 4.5$ ev, Table IV, gives values of j_0 for various temperatures. Thus, at 2600°K and a field of say 10^6 volts per cm, we have

$$\log_{10} \left(\frac{j}{0.70} \right) = 0.1912 \times \frac{10^3}{2600}; \quad (34)$$

¹¹ W. B. Nottingham, "Thermionic Emission," *Handbuch der Physik*, Vol. 21, p. 1, Springer-Verlag, Berlin, 1956.

the emission is increased by a factor of less than 1.2. Schottky's relation holds as long as the field $F > 8.83 \times 10^3 \phi^{1/2} T$, where ϕ is the work function of the material. For tungsten, $F > 1.87 \times 10^4 T$. At higher fields the expression for the emission can be written¹²

$$\frac{j}{j_0} \approx 1 + \frac{\left\{ 2.8 \times 10^4 \frac{\phi^{1/2} T}{F} \right\}^2}{6}. \quad (35)$$

Table V

j_0 amps/cm ²	$F \times 10^7$ volts/cm
0.00047	2
37	3
1.1×10^4	4
3.9×10^5	5
4.2×10^6	6
2.3×10^7	7
8.7×10^7	8

Here j_0 is the field emission current at low temperatures. This should be sufficiently accurate because low temperatures are considered. Again, if tungsten is considered, we have

$$\frac{j}{j_0} = 1 + 6 \times 10^8 \frac{T^2}{F^2}. \quad (36)$$

Table V gives the values of j_0 as a function of F which are applicable in this relation.

When both the temperature and the field are high, the emission process is strongly dependent on both variables, and Dolan and Dyke¹⁰ have shown that the enhancement of electron emission due to added thermal energy is much larger at low fields than at high fields, which is to be expected. An increase of current density by a factor of 5 over

¹²R. H. Good and E. W. Müller, "Field Emission," *Handbuch der Physik*, Vol. 21, p. 190, Springer-Verlag, Berlin, 1956.

the value expected for the low-temperature emitter could be obtained. From the above analysis and examples, it can easily be seen that for large current densities, Schottky effect is not the answer. One has to depend on either true field emission or the T - F emission.

If we consider a pointed cathode of hyperbolic shape and of radius of curvature r_0 , and an anode separated from it by a distance R , the field can be expressed¹³

$$F = \frac{2V}{r_0 \ln \frac{4R}{r_0}} \quad (37)$$

where V is in volts. Thus, if $R = 1$ cm and $r_0 = 4$ microns, a field of about 5×10^7 volts per cm is obtained for $V = 100$ kv. The electrons are accelerated normally to the surface. Since, in order not to exceed the limit imposed by the spherical aberration of the focusing lens, the beam has to be restricted to 0.1 radian, the effective emission area is 1 micron. Strictly speaking, there is some convergence of the particles, but this is minor and will be neglected in this analysis. If now we wish a 5-ma total current, the emission density must be of the order of 5×10^5 amperes/cm². Reference to Table IV will show that it is possible to obtain such a condition. Slightly better results can be obtained with a T - F emitter. It seems therefore as though field emitters would be very suitable for electron-beam machines. However, one major difficulty is lifetime. Experience with field emitters reveals erratic and unstable performance even in a clean and dust free tube, mainly due to cathode sputtering. Muller¹⁴ measured the sputtering rate and found it to be approximately

$$t = \frac{10^{-8}}{ip}, \quad (38)$$

where t is the time, in seconds, required to remove one layer; i is the emission current in amperes; and p the gas pressure in mm of Hg. On the assumption that the life of an emitter extends to the point where 100 monolayers have been removed, the life can then be $10^{-6}/ip$. Thus, in a vacuum of about 10^{-5} mm Hg and with a current of 1 ma, the

¹³ C. F. Eyring, S. S. Mackeown, and R. A. Millikan, "Field Currents from Points," *Phys. Rev.*, Vol. 31, No. 5, p. 900, May 1928.

¹⁴ E. W. Müller, "Field Emission and Cathodic Dispersion of Thoriated Tungsten," *Z. Physik*, Vol. 106, p. 132, 1937.

emitter life will be less than two minutes. Dolan and Dyke¹⁵ have shown how favorable results could be obtained from a T - F field emitter under pulsed conditions. Here the buildup is limited during the time the field is on, and while the field is off, it permits surface forces to restore the original smooth, clean cathode surface. A tungsten cathode in the temperature range of 1700-2200° K was used and fields up to 7×10^7 volts per cm were applied in pulses as long as 0.01 second and duty cycles up to about 0.25. Stable current-voltage relationship was obtained even in vacuum as low as 10^{-4} mm Hg.

Even if the cathode life problem is solved, there seems to be very little advantage in cold-cathode field emission for spot radii of more than 1μ . The optimum magnification for imaging such small sources as are available with field emitters is close to unity. Also, there are unavoidable aberrations in the imaging lenses. From these facts, Cosslett and Haine¹⁶ deduced that the current at the probe is limited, and is much less than might be expected from the high brightness of the emitter.

One can therefore conclude that for our present application field emitters are not as attractive as hot cathode tungsten emitters. However, it seems quite likely that for small spot sizes, that is, of the order of less than 1μ , field emission might very well be the best choice.

Due to adverse conditions under which the cathodes would be called to operate, it is obvious that oxide cathodes, despite their many advantages, are totally unsuitable for our purpose.

Lanthanum hexaboride (LaB_6) cathodes and uranium and zirconium carbide cathodes have been considered, but since insufficient data is available about them, they were discarded for the present.

The possibility of heating a refractory metal by electron bombardment using the scheme shown in Figure 4 was not very attractive because this is a somewhat complicated structure which requires an additional bombarding power supply floating at the cathode potential, in our case 100 kv.

It was therefore concluded that for our immediate application, the cathode that best satisfies the requirements is the pure hairpin tungsten filament. The emission is 5 amperes/cm² at a temperature of 2850 °K. The life under those conditions is about 10 hours for a 4-mil-diameter filament and 100 hours for a 40-mil filament. It is usually accepted

¹⁵ W. P. Dyke and W. W. Dolan, "Field Emission," *Advances in Electronics and Electron Physics*, Vol. 8, p. 167, Academic Press, Inc., New York, N. Y., 1956.

¹⁶ V. E. Cosslett and M. E. Haine, *Proc. International Conf. on Electron Microscopy*, London, p. 639, 1954.

that the useful life of a filament is determined by the time taken for its diameter to be reduced by approximately 12 per cent. The life figures are given for good vacuum; obviously the life will be considerably reduced if water vapor is liberated in the column. At poor vacuum levels, oxidation is a dominant factor in determining the life of the tungsten cathode.

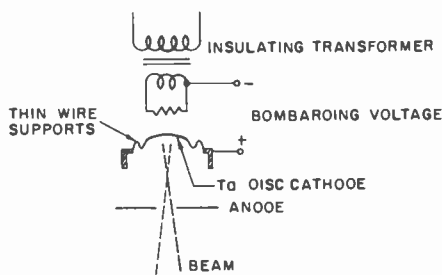


Fig. 4—Bombarded cathode in the shape of a disc.

CHOICE OF GUN

The electron gun is basically a triode. Sometimes the workpiece itself serves as the positive electrode and the system is then referred to as "work accelerated." Usually, as in our case, the accelerating anode is a separate electrode with a hole in the center to permit the passage of the electrons. Such an arrangement is called "self-accelerated."

There are three kinds of guns which seem of interest and which use the hairpin tungsten emitter as a cathode.

- (1) The classical gun which is normally used in the electron microscope.
- (2) The Steigerwald gun.
- (3) The Bricka and Bruck gun.

These three guns are shown in Figure 5. The Steigerwald gun¹⁷ has been studied in detail by Braucks.¹⁸ It is sometimes referred to as the distant focus or telefocus gun. The fundamental reason for the long focus effect is that the equipotential lines are concave towards the

¹⁷ K. H. Steigerwald, "Ein Neuartiges Strahlerzeugungs-System für Elektronenmikroskope," *Optik*, Vol. 5, p. 469, Nov.-Dec. 1949.

¹⁸ F. W. Braucks, "Untersuchungen an der Fernfokuskathode Nach Steigerwald," *Optik*, Vol. 15, p. 242, April 1958.

cathode due to the hollow shape and negative bias of the surrounding cup. Thus, electrons starting from the cathode are given radial outward velocity and the beam begins to diverge. Between the control electrode and the anode the equipotentials first become flat and then convex towards the cathode. The beam therefore is given radial inward acceleration but this only gradually overcomes the initial outward velocity. Consequently, the beam converges quite slowly and the beam forming field has a large focal length. The focal length can obviously be controlled by the bias voltage. A first look at the Steigerwald gun

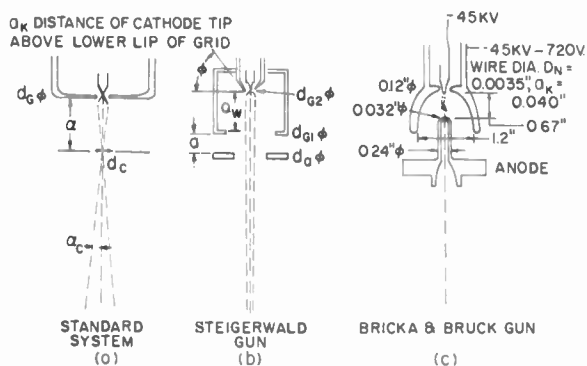


Fig. 5—Beam-forming systems with thermionic cathodes.

might indicate that a great advantage is to be gained by the elimination of the crossover and a consequent reduction of the aberrations. However, the sharply shaped grid field may be expected to be very sensitive to filament displacements, so that the image will be affected appreciably by any misalignment and improper placement of the filament.

In the Bricka and Bruck gun¹⁹ a crossover is formed just beyond the cathode and this is reimaged at a considerable distance from the gun. It is said to be particularly satisfactory as far as alignment is concerned since the current drawn through the anode aperture is not affected by small filament displacements.

The classical gun was investigated by Borries²⁰ and by Dosse.²¹

¹⁹ M. Bricka and H. Bruck, "Sur Un Nouveau Canon Electronique Pour Tubes A Haute Tension," *Annales Radioelectricité*, Vol. 3, p. 339, Oct. 1948.

²⁰ B. v. Borries, "Die Energetischen Daten Und Grenzen Der Übermikroskopie," *Optik*, Vol. 3, p. 389, July-Aug. 1948.

²¹ J. Dosse, "Theoretical and Experimental Investigations of Electron Emitters," *Z. Physik*, Vol. 115, p. 530, 1940.

Further details are given by Haine and Einstein.²² The crossover lies between the anode and the cathode, nearer to the cathode. Despite the possible advantages presented by the other two types of guns, it was decided to use the standard gun since this presented the least modification in the equipment available for experimental verification.

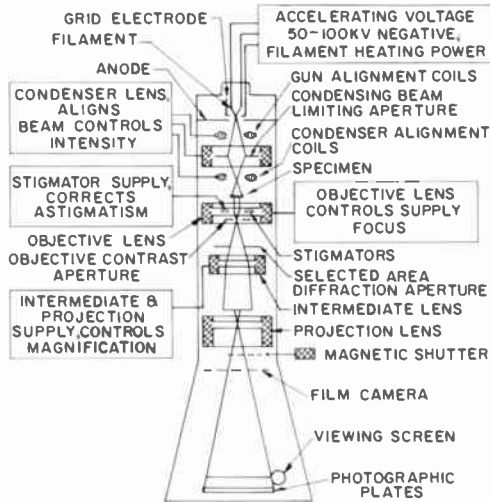


Fig. 6—Functional diagram of microscope column.

DESIGN OF THE MACHINE

In order to speed up the construction of the electron beam machine, it was decided to convert an existing electron microscope—the RCA EMU-3A. Figure 6 shows a functional diagram of the microscope column. The objective and the intermediate lens were removed. The projector lens was reversed. Figure 7 shows the simplified version of the column when adapted as an electron beam machine.

The accelerating voltage is 100 kv. The probe diameter of 0.001 inch is to be focused 2 inches below the lens center of the projector, leaving approximately 1 inch working distance for accommodating the deflection system and allowing vertical movement of the work. The standard electron gun is used. The data given by Borries on that gun

²² M. E. Haine and P. A. Einstein, "Characteristics of the Hot Cathode Electron Microscope Gun," *Brit Jour. Appl. Phys.*, Vol. 3, p. 40, Feb. 1952.

refer to smaller currents than those required in our present system. However, since we are heating the filament to a temperature where space-charge limitation occurs, it is possible to scale voltages, distances and currents according to the rule

$$\begin{aligned} V' &= AV \\ d' &= A^{3/4}d \\ I' &= A^{3/2}I \end{aligned} \quad (39)$$

where A is a scaling factor. These are the well-known relations that

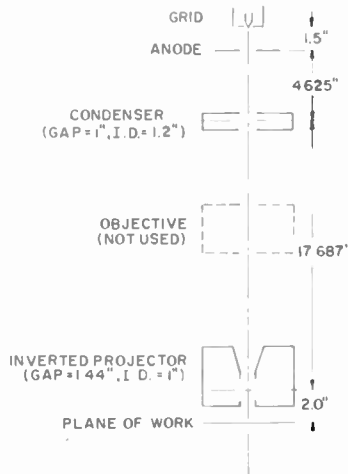


Fig. 7—Electron optics of EMU-3A adapted for beam-drilling.

prevail under space-charge-limited conditions. The crossover diameter, d_c , determined by the product of the time of flight d'/V' and the fixed initial lateral velocity component, transforms according to the relation $d_c' = A^{1/4}d_c$.

The dimensions given by Borries, which lead to very nearly optimal performance, and those obtained by scaling are shown in Table VI. The position of the crossover is not specified. The crossover lies near the cathode close to cutoff and moves forward towards the anode as the beam current is increased by reduction of the bias voltage. However, to a sufficiently close approximation, the crossover will be assumed to lie in the plane of the anode aperture.

These optimum dimensions, based on the results obtained by Borries, do not agree with those of Haine and Einstein.²² According

to the latter, the efficiency, defined as the ratio of probe current to total emission current, increases as the diameter of the hole in the Wehnelt cup and the distance from that hole to the tip of the filament is decreased. It is possible that as the filament is recessed further from the Wehnelt control cup, the field that penetrates imparts a radial velocity to the electrons and therefore decreases the over-all efficiency.

Table VI

	(Borries)	(Scaled)
V	20 kv	100 kv
T	2650° K	2650° K
d_p	0.060 inch	0.200 inch
a_k	0.040 inch	0.133 inch
a	0.400 inch	1.333 inches
D_w	0.005 inch	0.017 inch
I_b	0.200 ma	2.220 ma
d_c	0.0031 inch	0.0046 inch

d_p is the aperture diameter of the Wehnelt cylinder,
 a_k is the distance of filament point above grid aperture,
 a is the distance between grid and anode,
 D_w is the diameter of the filament wire,
 I_b is the beam current,
 d_c is the crossover diameter.

If we let u_1 and v_1 be the object and image distances of the condenser lens, and u_2 and v_2 those of the projector lens, reference to Figure 7 will give

$$\begin{aligned}
 u_1 &= 4.625 \text{ inches,} \\
 v_1 + u_2 &= 17.687 \text{ inches,} \\
 v_2 &= 2 \text{ inches.}
 \end{aligned}$$

Therefore,

$$\frac{2}{u_2} \times \frac{17.687 - u_2}{4.625} = \frac{0.001}{0.0046} \quad (40)$$

Hence, $u_2 = 11.75$ inches and $v_1 = 5.94$ inches. The magnification and the focal lengths of the two lenses become

$$M_1 = 1.28,$$

$$\frac{1}{M_2} = 5.88,$$

$$f_1 = \frac{v_1}{M_1 + 1} = 2.60 \text{ inches},$$

$$f_2 = \frac{u_2}{\frac{1}{M_2} + 1} = 1.71 \text{ inches},$$

and the over-all magnification is $M = 4.6$. The spherical aberration of the condenser lens is negligible because of the small aperture angle of the beam. The spherical aberration of the projector lens is significant since, as we have seen previously, it might very well set a limit to the spot size. If we use the notations of Liebmann and Grad, as was done in the section dealing with limitations, the final lens in the present scheme has a ratio a_p/D (pole-piece separation to the internal pole-piece diameter) equal to 1.44. Interpolation of the results given by Liebmann and Grad gives $Cf = 5$ inches. This coefficient is computed for infinite magnification. It is therefore necessary to compute it for the actual magnification of the system.

Considering the lens as a thin lens, this can be done as follows. The usual lens equation is

$$\frac{1}{u} + \frac{1}{v} = \frac{1}{f}, \quad (41)$$

where u and v are the object and image distances, respectively.

$$\frac{1}{u} + \frac{1}{Mu} = \frac{1}{f}, \quad (42)$$

or

$$u = \frac{M + 1}{M} f. \quad (43)$$

If r_u is the height of incidence on the lens,

$$r_a = \frac{M+1}{M} fa. \quad (44)$$

Now for a thin lens* we can write

$$\Delta r = Mu Kr_a^3. \quad (45)$$

K is independent of object position, hence the angular displacement due to spherical aberration,

$$\Delta\delta = \frac{\Delta r}{Mu} = Kr_a^3, \quad (46)$$

depends only on the height of incidence, r_a . For the object near the focal point,

$$\frac{\Delta r_\infty}{Mf} = \frac{MC_\infty r_a^3}{Mf^4} = Kr_a^3, \quad (47)$$

leads to

$$K = \frac{C_\infty}{f^4}. \quad (48)$$

Hence

$$\Delta r = v\Delta\delta = Mu K_x r_a^3, \quad (49)$$

or

$$\Delta r = (M+1)fK_x \left(\frac{M+1}{M}\right)^3 f^3 a^3, \quad (50)$$

$$\Delta r = C \left(\frac{M+1}{M^3}\right)^4 a^3 = MC_x \left(\frac{M+1}{M}\right)^4 a^2. \quad (51)$$

Now

$$\Delta r = C_s Ma^3. \quad (52)$$

We then have

$$C_s = \left(\frac{M+1}{M}\right)^4 C_\infty = 9.4 \text{ inches}. \quad (53)$$

To compute the convergence of the beam at the crossover we shall use the Langmuir relation given in Equation (22).

* See e.g. Eq. 17.4 of reference (9).

$$I = c \frac{\pi d_0^2}{4} a^2 \frac{V}{V_T} j_c. \quad (54)$$

$V_T = kT/e = 0.25$ volt which corresponds to the operating temperature of the filament. V is the beam voltage, d_0 is the spot diameter, and j_c is the emission density at the cathode. The factor c would be unity if the current density at the spot were constant up to the edge and zero beyond, and if the same condition applied for the distribution of current in angle, i.e., constant current per unit solid angle up to the convergence angle a , and zero beyond.

In actual practice this is not the case. If the gun is not operated at a very low bias and low filament temperature, the intensity distribution across the crossover can be assumed to be Gaussian. If now we define the edge of the spot at crossover as the point where the current density has dropped by the factor $1/e$, and if we assume that the emission also falls off in Gaussian fashion by the factor $1/e$ at the point corresponding to the limiting convergence angle a , the value of c is about $1/3$.

Strictly speaking, the angular distribution of current density across the beam is of Gaussian nature only at low beam currents. As the beam current is increased by decreasing the bias, the beam becomes "hollow." This was reported by some authors and shown by Haine and Einstein.²² Borries assumed that the crossover diameter is that which encloses 93 per cent of the beam, based on a visual measurement. Borries crossover diameter must therefore be divided by

$$\sqrt{\frac{\ln 0.07}{\frac{1}{e}}} = \sqrt{-\ln 0.07} = 1.63. \quad (55)$$

This was done in the tabulation of the results derived from the data of Borries. We therefore have at the crossover,

$$a_c = \frac{1}{d_0} \sqrt{\frac{4}{\pi c} \frac{V_T}{V} \frac{I_b}{j_c}}. \quad (56)$$

For $V = 10^5$ volts, $c = 1/3$ and $V_T = 0.25$ volt, this gives

$$a_c = \frac{0.00121}{d_0} \sqrt{\frac{I_b}{j_c}}, \quad (57)$$

where I_b is in amperes, j_0 in amperes/cm², and d_0 in inches. We can now use the scaled values of Borries;

$$a_c = \frac{0.00121}{0.0046} \sqrt{\frac{2.22 \times 10^{-3}}{j_0}} \quad (58)$$

At $T = 2650^\circ\text{K}$, $j_0 = 1.41$ amperes/cm². We then have $a_c = 0.0116$ radian. Thus a_s at the spot will be

$$a_s = M a_c = 4.6 \times 0.0116 = 0.0533 \text{ radian.}$$

The minimum disc of confusion is then

$$\frac{1}{2} C_s a_s^3 = \frac{1}{2} (9.4) (0.0533)^3 = 0.000715 \text{ inch.} \quad (59)$$

This is less than 0.001 inch, so the dimensioning is adequate. The probe current is given as 2.2 ma. In order to increase the current to 5 ma, which was the initial objective, the filament temperature must be increased to approximately 2750°K. The spot size will not change under these conditions. The life of the filament as defined earlier should be of the order of 100 hours, assuming, of course, that the chamber is not opened too frequently. From the results obtained by Maloof,²³ it seems possible that filaments formed from single-crystal tungsten wires have longer lives. However, no experimental data are available to prove this point.

DESCRIPTION OF THE MACHINE

Figure 8 shows a schematic diagram of the electron-beam machine. The filament and control cylinder are at -100 kv with respect to ground. All of the remaining parts are at ground potential. The bias and pulses are fed between the cathode and Wehnelt control cylinder at 100 kv level.

It was desirable to convert the EMU-3A electron microscope to an electron beam machine with a minimum of modifications. The chamber was considerably enlarged to allow more working space. The new housing, shown in Figure 9, has a pyramidal shape and is made of aluminum. Several ports were installed for viewing, access to the housing, and for vacuum-tight electrical connections. Inside the housing a positioning table was incorporated to permit mechanical move-

²³ S. R. Maloof, "Growth of Tungsten Single Crystals by the Strain-Anneal Method Using Electron-Beam Heating," *Proc. 4th Symp. Electron Beam Technology*, Boston, p. 190, March 1962.

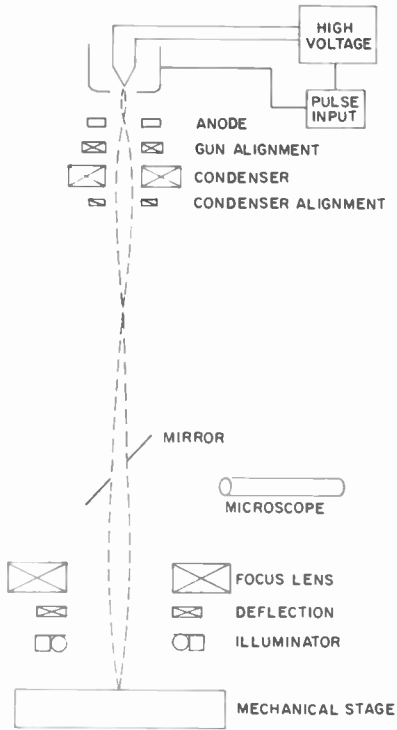


Fig. 8—Electron-beam machine.

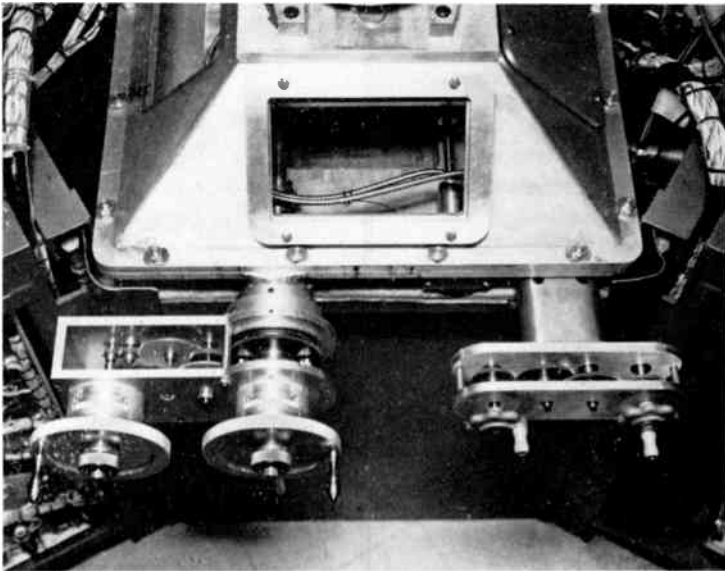


Fig. 9—Controls for mechanical table and aluminum housing frame.

ment of the workpiece. The table is designed to have X and Y motion in the horizontal plane as well as rotation and elevation control. The X and Y motion have to be very accurate, preferably within one thousandth of an inch. There was no need to require the same kind of accuracy in the rotation and elevation control.

The drives for the X and Y motion were compounded and made concentric with each other. In this way, only one vacuum seal to the housing is necessary. There are two additional seals in the concentric shafts. Figure 10 shows a schematic of the arrangement. A lead screw mated with a nut and supported on its ends, free to rotate, forms the basic design. When the nut is locked by means of a long tubular con-

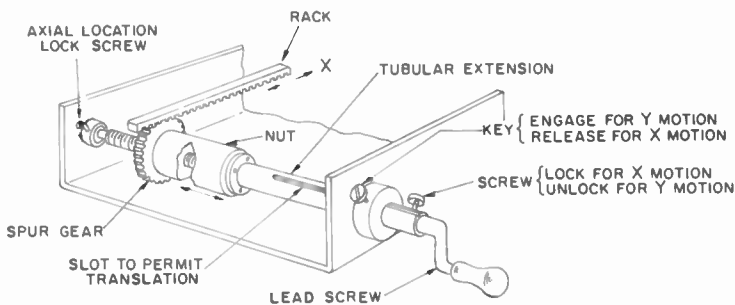


Fig. 10—Schematic of the mechanical table.

nection, a motion in the Y direction is obtained by rotating the appropriate wheel at the control. If the screw and nut are locked together, the rotation at the control results in an X directed motion. The controls for the elevation and rotation are connected through flexible shafts. The connection to the vacuum chamber is made through O-rings. Figure 11 shows the positioning table and Figure 9 shows the mechanical controls. Whenever a workpiece calls for precision in the rotation control, a special jig, electrically motorized, is placed on the mechanical table. The motors are kept dry in a vacuum desiccator. Since the vacuum level at which the machine normally operates is poor (about 10^{-4} mm Hg), the introduction of motors does not increase the pumping time. Another jig, designed to provide rotation along an axis perpendicular to that of the beam is also used when two tubular sections are to be welded together. Electrical motors with variable speeds provide the necessary rotation.

The mechanical table is electrically insulated from the housing. It is connected to ground through an ammeter. The probe current can

thus be measured continuously. For accurate measurement, the table is moved until the beam strikes a Faraday cage so as to avoid any error due to secondary emission. For rough indications, secondary emission is generally neglected. The voltage across a resistor in series with the probe meter is fed to an oscilloscope which shows the waveform of the pulses at the probe.

The opening of the column that was formerly used for the intermediate lens was enlarged to provide room for the installation of a

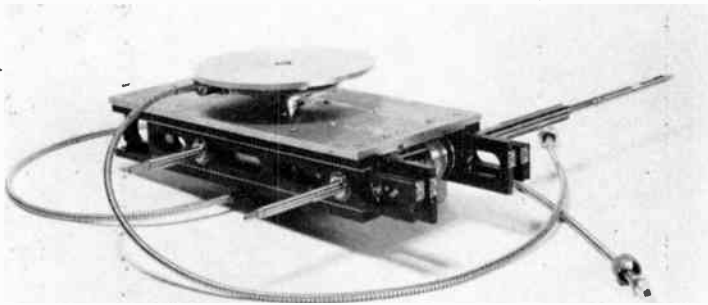


Fig. 11—Mechanical table.

viewing system. A reflected view is provided by a mirror inclined at 45° with respect to the beam axis. A hole is drilled in its center large enough to let the beam pass freely. Observation is made with a microscope mounted at right angles to the column axis and facing the mirror. The mirror is located in the geometrical and optical center of the column. In order to maintain the field of view of the spot, it is necessary to move either the microscope or the mirror. The microscope is large and heavy, hence, it was found simpler to move the mirror. The mirror is mounted on a rectangular frame in such a way that the mirror center and that of the housing are coincident. A vacuum-sealed lead glass window in the wall of the housing permits observation of the mirror and workpiece. Separate drives through the vacuum provide the control of the position of the mirror. It can be pivoted about the beam axis or about an axis perpendicular to that of the beam. Figure 12 shows the mirror housing. The microscope used for observation must have a focal length of nearly nine inches. Consequently, it measures 32 inches and weighs 35 pounds. It was therefore necessary to mount it on a boom pivoted from a right column so that it can be moved

aside to permit access to the work chamber. A manually operated slide is used for positioning the microscope.

POWER SUPPLY

Many of the power supplies require a high degree of stability of the operating voltages and currents. The high-voltage supply is generated by a resonating LC series network. An inductor and its stray capacitor are connected in series, and a-c voltage at resonant frequency

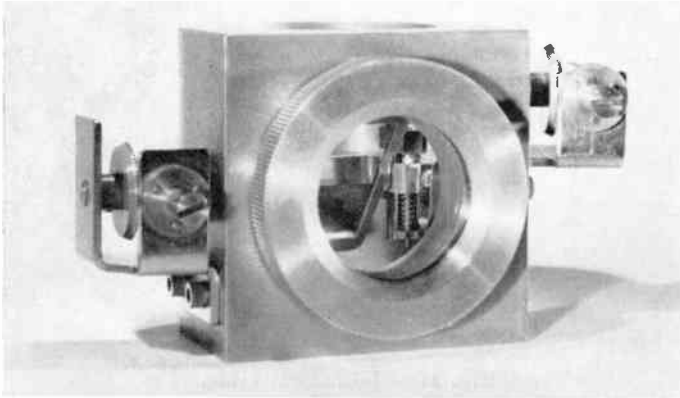


Fig. 12—Micropositioner for the viewing mirror.

is applied. By careful design, the electrical losses are minimized and a high voltage is obtained across the inductor. The peak r-f voltage developed across the coil can be either 25 or 50 kv depending upon the plate and screen voltages supplied to the oscillators. The high resonant voltage is rectified and doubled by conventional means.

Stabilization is achieved by a feedback network. The high-voltage output is stabilized by changing the screen voltage of the oscillator tubes whenever the high-voltage output begins to deviate from its normal value.

The heating current for the filament is delivered at high-voltage level by means of r-f induction. A conventional oscillator circuit provides a 100 kc resonant frequency. The output is inductively coupled to the gun-filament circuit.

VACUUM INSTALLATION

The vacuum installation consists of a mechanical pump and a diffu-

sion pump. An automatic system permits the admission of air to the column only after the diffusion pump has been sealed off. Thus, during loading, the fore pump is connected to the diffusion pump while the column is filled to atmospheric pressure. Before operation, the diffusion pump is sealed off at both ends. The fore pump is connected directly to the column. When the pressure reaches a sufficiently low value, the fore pump is connected to the diffusion pump which, in turn, is opened to the column. The complete vacuum valving is carried out automatically. Electric motors actuate the valves and correct sequencing is obtained by the action of limit switches and relays. The danger of accidentally letting air to a hot diffusion pump is thus minimized.

Two vacuum gauges are used—a thermocouple gauge and a cold discharge gauge. The thermocouple gauge indicates the pressure reached by the fore pump. The cold discharge or ionization gauge is used to indicate the pressure in the column when the diffusion pump is connected to the column. The electrical signal from the cold discharge vacuum gauge is amplified and used to change the system from rough pumping to final pumping at the correct column pressure. The same gauge is also utilized to control the automatic valving sequence and prevent application of high voltage until the required degree of vacuum is obtained. This prevents the operator from touching the electron gun while the high voltage is on.

To avoid the resistance to pumping offered by the column, a by-pass connection is made from the housing to the gun area.

ALIGNMENT

The tungsten filament is 8 to 10 mils in diameter. It is positioned and spot welded to the holder with the help of a jig shown in Figure 13. The filament holder is installed in the cone with the help of two screws. A second jig, shown in Figure 14, is used to provide the alignment of the filament with the Wehnelt cup. Should there still be any misalignment, there is enough play in the assembly to maneuver the filament holder until the correct position is found. The jig can then be removed and, with the help of a depth microscope, the distance from the tip of the filament to a fixed reference shoulder can be measured. By measuring the length of the Wehnelt cup, the correct spacing between the filament and cup can be determined. The gun can then be connected to the assembly.

The concentricity of the cathode and control electrode with the periphery of the column is effected with the help of a special jig. This screws to the cathode holder exactly as does the Wehnelt cup and is slightly smaller than the inside diameter of the column. With the help

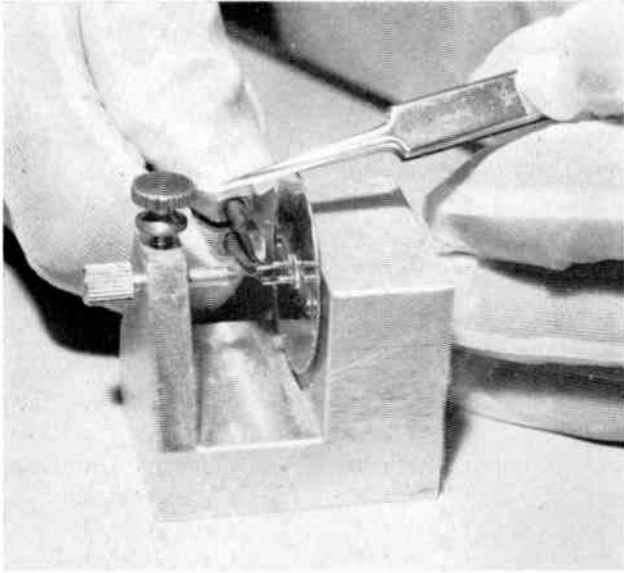


Fig. 13—Jig for spot-welding the filament.



Fig. 14—Jig for positioning filament in the gun assembly.

of feelers, concentricity is verified. The cone assembly can be shifted until alignment is obtained. The whole procedure has to be repeated only when the cone is removed for replacement or for trouble shooting.

The gun assembly can be mechanically displaced with respect to the condenser lens. This latter is fixed and its mechanical alignment with the rest of the column is obtained by carefully machined surfaces. Three screws spaced 120 degrees apart can be used to align the gun to the condenser.

The projector lens is held on the column by means of three screws. These allow the alignment of the lens with respect to the column and condenser. The mechanical alignment cannot be relied upon for perfect alignment due to the tolerances involved. Once the best mechanical alignment is obtained, final alignment is achieved with the help of electrical deflectors in the column.

There are two separate deflectors. One preceding the condenser lens which serves to align the gun assembly with the condenser, and another immediately after the condenser lens which serves to align the condenser with the projector. The deflectors are connected across a bridge circuit of resistors. If the bridge is in balance, there is no current flowing in either deflection coil. This is the neutral position. The knobs are then positioned in the center of the dial. Rotation of the knobs one way or another will allow current to flow in one direction or another with a corresponding deflection of the beam. The machine can be operated at either 50 or 100 kv depending on whether the input to the doubler is 25 or 50 kv. The field necessary to deflect the beam at 50 kv is less than that at 100 kv. A resistance is therefore introduced in series with the bridge circuit. This limits the current when operating at 50 kv but is disconnected by a relay when operation is at 100 kv. Smooth deflection control is obtained in this fashion. Alignment can be recognized by noting that a beam of electrons coincident with the axis of a magnetic electron lens does not shift as the strength of the lens is changed. If the beam is off the axis, it shifts as the strength of the lens is changed. The shift of an image point from a magnetic lens as the strength of the lens is changed becomes therefore a criterion for recognizing alignment. There can be a condition where the direction as well as the position are both off the axis in such a way as to obtain a stationary spot as the lens is energized. It is therefore necessary to reverse the magnetic field during the alignment procedure.

Sometimes, the aperture in the condenser lens becomes contaminated. By carefully defocusing the beam and increasing the emission, the aperture is heated and this generally eliminates the charging up.

ILLUMINATION

Correct observation of the workpiece during operation is very important for the successful operation of the machine. The illumination of the target presents some problems because of the close spacing between the final lens and the workpiece. The illumination was therefore provided by inserting six equidistant bulbs immediately above the working area. The bulbs have given some difficulties because of the insulated glass which charges up and distorts the beam and because of the loss of light when they get coated with the metal vapor after operation. The final solution was found by removing the glass and using bare filaments. By careful interlocking, the filaments are lit only when good vacuum is obtained. In order to be able to position the target properly, two bulbs are located at the extreme corners of the housing. These serve only during the time air is let inside the chamber and are not sufficient to illuminate the target during operation. The observation of the target while it is being bombarded by the beam is rather difficult due to the brightness of the spot. The microscope iris is used to cut down on the illumination, but this in turn results in loss of detail. Another method would be to use a television camera on the target; however, there are problems to be solved here too.

DEFLECTION

The deflection control is provided by means of four pole deflectors. The four coils are wound on a ferrite core and are arranged 90 degrees apart with their axis pointing inward at a common center. One method of deflection is achieved as follows: Two of the coils, 180 degrees apart, are connected in series and a sawtooth voltage is applied to these coils. The other two coils are also connected in series and a square wave is applied to them. Now the beam will travel back and forth and is deflected left and right across the straight line of the sawtooth wave. If the two waves are not synchronized, the spot will hit all points of the periphery of the rectangle bounded by both wave-form amplitudes. As an example, if the two wave forms are periodically interchanged, a cross will be formed. The use of more poles will increase the number of geometrical configurations that can be machined. The maximum deflection is of the order of 1/8 inch from the center point due to the limit imposed by astigmatism.²⁴

PULSE SYSTEM

As was indicated earlier, it is necessary to pulse the beam to reduce

²⁴ W. Glaser, *Grundlagen der Elektronenoptik*, Springer-Verlag, Wien, 1952. See Equation (143.6), page 485.

unwanted heating and melting at the target. The beam is biased off by applying a sufficiently negative voltage on the Wehnelt cylinder. If now a positive pulse is applied on the Wehnelt cylinder, the beam is automatically switched on for the length of time the pulse is applied. A first look at the problem might indicate that this is a simple matter, quite readily solvable. However, there are many difficulties involved which necessitate careful design of circuitry and insulation.

As indicated earlier, the anode and column are at ground potential, while the cathode and cup are at -100 kv with respect to the anode. Accordingly, the pulse has to be delivered at 100 kv level.

The requirement for the successful operation of the machine was

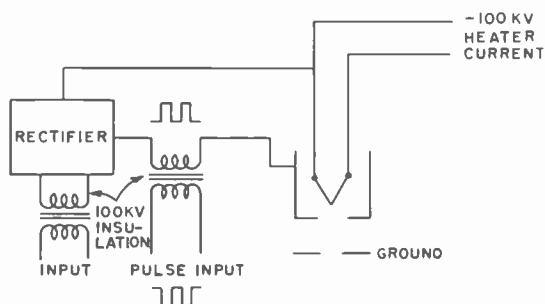


Fig. 15—Pulse control using insulated high-voltage pulse transformer.

to have a pulsing circuit that can deliver pulses from two to several hundred milliseconds in duration. For short pulses, the rise and decay time must be very short. This sets up an upper limit to the RC of the network. The capacitance is already present in the gun system and it is estimated as 50 picofarads. In addition there is the stray capacitance of the circuit.

For long pulses, relatively long rise and decay times can be tolerated. However, it is preferable not to have any exponential decay of the pulse. This in turn presents some difficulties due to the RC of the network. A compromise must therefore be sought.

One method of obtaining the pulses is to feed the pulses through a pulse transformer insulated for 100 kv. The pulses are supplied to the primary winding from a pulser at ground potential. The pulse transformer is a $1:1$ inverting transformer and can be designed to have a bandwidth which enables it to transmit rectangular pulses over a certain range. This scheme is shown in Figure 15. It has many advantages. However, it is well-known that a pulse transformer can only work over a narrow bandwidth. It is very difficult, if not impossible,

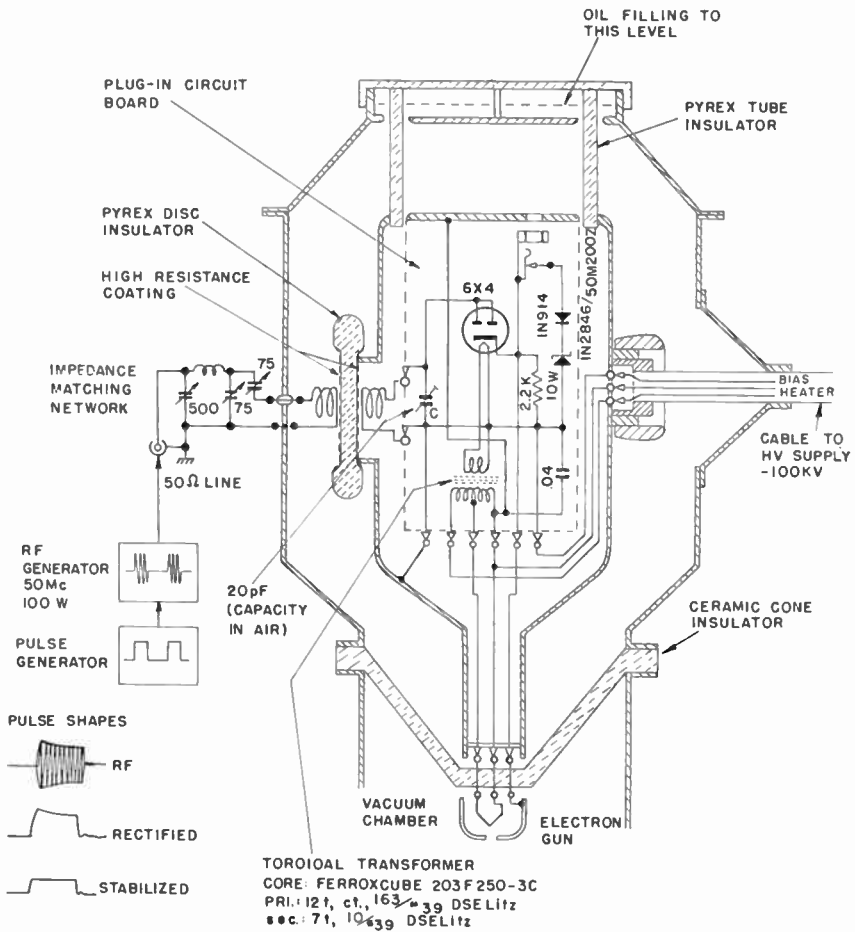


Fig. 16—Pulse-coupling lead using r-f scheme.

to design a pulse transformer that will transmit undistorted pulses up to several hundred milliseconds. This scheme was therefore not chosen.

Another method considered was the use of a pulsed r-f carrier system by which the pulses can be brought to 100-kv potential and there rectified and stabilized in amplitude.

Figure 16 shows details of such a scheme. A 1/2-inch thick Pyrex insulator is used between the primary and secondary of the r-f coupling transformer. The circuit at the 100-kv level is a parallel tuned circuit

with a half-wave series rectifier across it. The rectified pulses can be stabilized to the desired pulse amplitude by means of a Zener diode. In order to avoid the long tail at the trailing edge of the pulse due to the charge stored in the Zener diode, a rectifier diode was connected in series with the Zener diode. This scheme has many merits but at the same time presents many difficulties due to the critical tuning involved.

A variation of this scheme is to use the r-f to supply not only the pulses, but also the bias. Thus, by simple amplitude modulation the potential difference between the Wehnelt cup and filament can be varied at will, thereby eliminating the bias supply with its own 100-kv insulated transformer. However, a simple computation will show that such a scheme is not feasible. The load capacitance is of the order of 50 picofarads.

If we require a minimum pulse width to be of the order of two microseconds, the minimum permissible rise and decay time would be of the order of 0.4 microsecond. The load resistance would have a maximum value

$$R = \frac{\tau}{C} = \frac{0.4 \times 10^{-6}}{50 \times 10^{-12}} = 8 \times 10^3 \text{ ohms.} \quad (60)$$

For a bias of about 1500 volts, this would present a power dissipation of

$$P = \frac{(1500)^2}{8 \times 10^3} = 280 \text{ watts.} \quad (61)$$

It is clear that such a power dissipation at r-f frequency would not be very practical.

It was therefore decided to discard the r-f pulsing scheme. In view of the fact that the pulse circuit was to deliver pulses over a wide range, the best solution was found by using a bistable multivibrator. The power supply which provides the variable bias voltage circuit provides the d-c plate voltages to the multivibrator at the same time. Figure 17 shows the circuitry used in such a scheme.

All of the electric components at 100-kv level are mounted inside a highly polished shielding bottle which plugs into sockets in the bottom of a ceramic insulator core.

The high-voltage cable plugs into one side of the container or "bottle." A corona shield is provided around the cable to minimize the field strength. On the opposite side, a glass insulator with the differentiating transformer is mounted. The glass insulator is 1/2-inch

thick in the center and is thicker at the rim. It is coated with a high resistance "TIC" (transparent iridized coating) coating of the order of 10^4 ohms/cm in the depressions of both sides. These coatings serve as field equalizers for the high voltage. The coupling transformer is made of a ferrite core split in two and mounted face to face on each side of the glass insulation. This provides the high-voltage insulation as well as the leakage for the differentiation of the pulses. All outside corners of the shield are well rounded to eliminate any high field regions, thus eliminating the chance of breakdown.

Tube T_2 is normally conducting while tube T_3 is kept close to cutoff by means of resistor R_4 . A positive trigger pulse at the grid of tube T_1 turns this tube on and cuts off tube T_2 . As a consequence, tube T_3

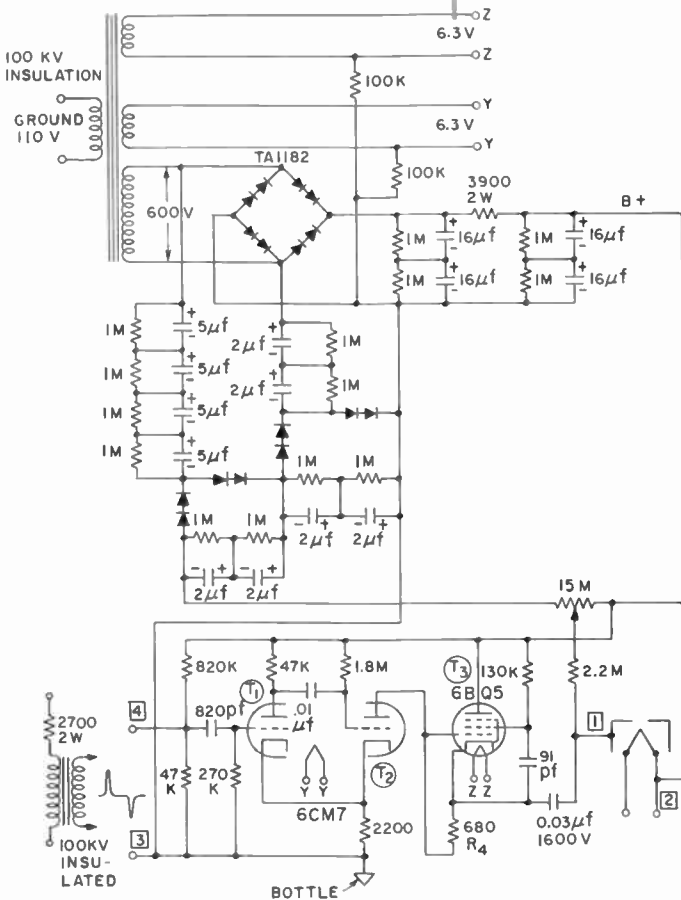


Fig. 17—Multivibrator pulsing and bias supply.



Fig. 18—Pulse circuit attached to transformer and ready to be inserted in the bottle and oil bath.

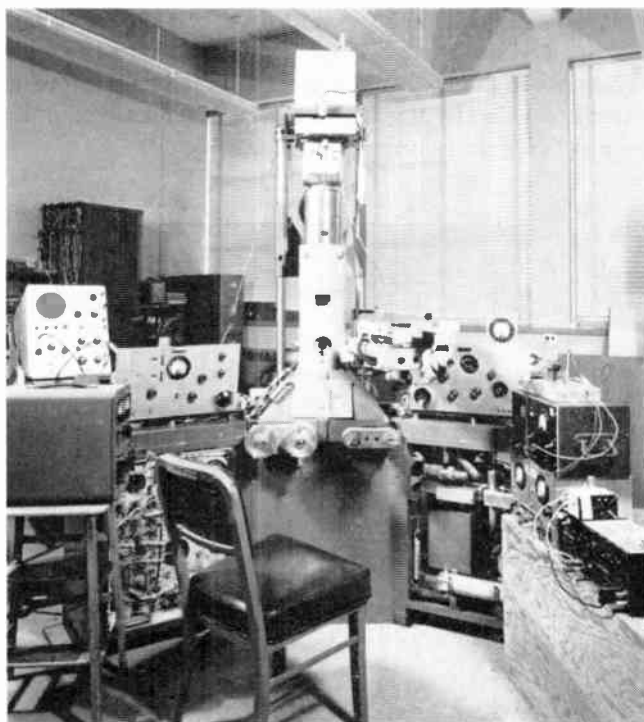


Fig. 19—Electron-beam machine.

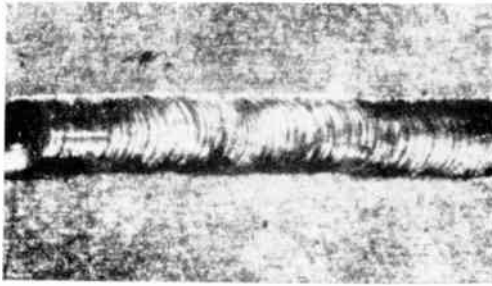


Fig. 20—A butt weld of two pieces of molybdenum 5/1000 inch thick.

loses its bias voltage and becomes fully conductive. The bias voltage between the cathode and the control grid drops accordingly. The negative trigger pulse resets the system to the original conditions.

The advantage of this system as against others is the fact that very wide bandwidths can be covered by the same setup. In the very short pulse-width range, a fast rise and decay time is essential, but the exponential decay of the pulse due to the charging and discharging of the inherent capacitance in the system is negligible. For large pulse widths, the rise and decay time is negligible, but here the maintenance of a relatively horizontal pulse is important. It is therefore necessary to design two separate circuits which can be interchanged quite readily to suit the pulsing requirement at the target.

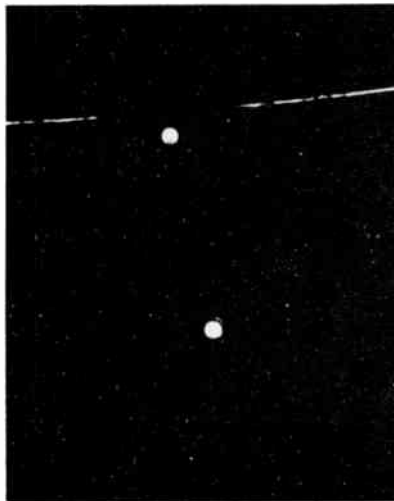


Fig. 21—2½-mil holes drilled in molybdenum 5 mils thick.

It was found advisable to set up the circuit in such a way as to maintain a fixed pulse amplitude. The level between the Wehnelt cylinder and cathode can be adjusted with the bias control. In this way only one 100-kv insulated control is necessary.

The "bottle" or shield is mounted inside a grounded container. The clearance between the two is maintained to a minimum of $1\frac{1}{4}$ inches throughout. Dow Corning silicone oil is used as an insulator. A viscosity of 1.0 centistoke at 25°C was chosen. The electric strength is 325 volts/mil.

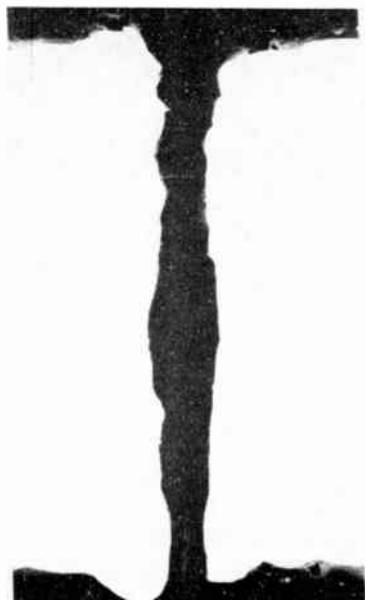


Fig. 22—Cross section of 1/4000 hole drilled in ferrite 10 mils thick.

The diodes used were good for 1000 volts peak inverse voltage and can carry from 300 to 400 ma d-c forward current depending on whether they are capacitively or inductively loaded. Figure 18 shows the circuit attached to the transformer and ready to be inserted in the bottle and oil. Figure 19 shows the complete electron-beam machine during operation.

While the objective of this paper is to describe the considerations which underlie the design of an electron-beam machine and its actual design, some examples of work performed with the completed machine are shown in Figures 20 to 23.

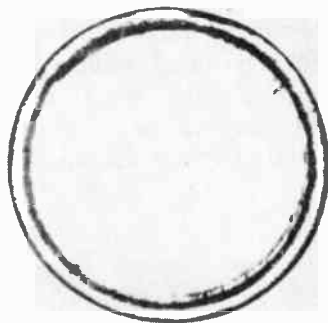


Fig. 23—Weld of two concentric nichrome tubes.

CONCLUSION

In conclusion, it has been shown that an electron-beam machine can be designed to obtain a high probe current of 5 milliamperes in a spot of .001 inch diameter. The spot can be deflected $\frac{1}{4}$ inch without appreciable distortion. The beam can be pulsed from a few microseconds to several milliseconds very satisfactorily, using a multivibrator circuit. A mechanical table to provide flexibility in positioning and displacing the object is incorporated in the electron-beam machine. The viewing mechanism consists of a long-focus microscope and a 45° mirror with a hole through which the beam passes freely.

ACKNOWLEDGMENTS

The work described in this report was performed under the leadership of H. B. Law. L. Davne was largely responsible for the mechanical design. The circuits in the pulse head were designed and improved by R. Lochinger and W. Moles. J. Reisner was consulted numerous times during experiments with the machine, and supplied the pole pieces for the final lens. A considerable part of the theoretical work was contributed by E. G. Ramberg. Finally, the author wants to thank L. S. Nergaard and F. Norman for suggesting the use of a multivibrator to pulse the beam.

HIGH-SPEED ARITHMETIC EMPLOYING TUNNEL DIODES*

BY

H. S. MILLER

RCA Laboratories
Princeton, N. J.

Summary—Straight-forward tunnel-diode circuitry was developed which sequentially propagates (and stores) both carries and borrows in parallel adders. Measured stage delays average 0.3 nanosecond (0.3×10^{-9} second); worst-case stage delay is 0.4 nanosecond. The power supply for the tunnel-diode circuitry comes from conventional transistor logic circuits. Transistorized amplifiers are used to increase the signal level of the tunnel-diode circuits to that required by other transistor logic circuits. Extrapolating from experimental results, the "wait" time for generation of a set of carries or borrows after both operands are present would be on the order of 80 nanoseconds for a 50-bit word length.

INTRODUCTION

THE PRINCIPAL LIMITATION on the speed of parallel arithmetic units is the time required to communicate information sequentially from its least-significant bit positions to its most-significant bit positions. Carries and borrows are examples of this type of information. Approaches taken in the past to shorten this communication time include: (a) techniques for partially or fully eliminating the need for this sequential communication by using redundant number systems, such as carry-save^{1,4} and extended-base⁵

* Manuscript received 23 January 1963.

¹ "On the Design of a Very High-Speed Computer," *Report No. 80, Digital Computer Laboratory, Graduate College, University of Illinois*, Chap. 8, p. 174, Second Edition, April 1958.

² J. E. Robertson, "Theory of Computer Arithmetic Employed in the Design of the New Computer at the University of Illinois," presented at the *University of Michigan Engineering Summer Conference*, "Theory of Computing Machine Design," June 13-17, 1960.

³ G. Metze, "A Study of Parallel One's Complement Arithmetic Units with Separate Carry or Borrow Storage," *Report No. 81, Digital Computer Laboratory, Graduate College, University of Illinois*, Nov. 11, 1957.

⁴ S. Takahasi, "Separate Carry Storage Adders," *Report No. 97, Digital Computer Laboratory, Graduate College, University of Illinois*, March 7, 1960.

⁵ A. Avizienis, "A Study of Redundant Number Representation for Parallel Digital Computers," *Report No. 101, Digital Computer Laboratory, Graduate College, University of Illinois*, May 20, 1960.

number systems; (b) techniques for anticipating carries at higher-order adder positions with combinational logic and carry skip networks;^{6-8, 15} (c) techniques for shortening over-all adder delay by detecting completion of carry propagations rather than always waiting for the "worst-case";^{6, 8-10, 15} (d) techniques employing conditional logic such as conditional sum logic^{11, 12} and conditional carry logic;¹³ and (e) techniques using specialized circuitry for propagating carry information.^{14, 16} Each of these approaches has its own advantages and disadvantages. We are interested in increasing the over-all performance of the arithmetic unit while decreasing its complexity.

This paper describes specialized tunnel-diode circuitry which has demonstrated its ability to propagate carries or borrows with less than a 0.5-nanosecond stage delay and which reduces the over-all complexity of the arithmetic unit as compared with fully transistorized versions operating at the same speeds. In particular, these fully transistorized versions would require involved carry logic to obtain the same speeds. Furthermore, both carries and borrows can be propagated with the tunnel-diode circuitry. This attribute greatly enhances the versatility of the arithmetic unit with regard to the types of arithmetic operations and comparisons available to the programmer.* All the interest-

⁶ O. L. MacSorley, "High Speed Arithmetic in Binary Computers," *Proc. I.R.E.*, Vol. 49, No. 1, p. 67, Jan. 1961.

⁷ A. L. Leiner, J. L. Smith, and A. Weinberger, "System Design of Digital Computer at the National Bureau of Standards," *National Bureau of Standards Circular 591*, Feb. 14, 1958.

⁸ M. Lehman and N. Burla, "Skip Techniques for High-Speed Carry Propagation in Binary Arithmetic Units," *I.R.E. Trans. on Elect. Comp.*, Vol. EC-10, No. 4, p. 691, Dec. 1961.

⁹ B. Gilchrist, L. H. Pomerena, and S. Y. Wong, "Fast Carry Logic for Digital Computers," *I.R.E. Trans. on Elect. Comp.*, Vol. EC-4, p. 133, Dec. 1955.

¹⁰ H. C. Hendrickson, "Fast High-Accuracy Binary Parallel Addition," *I.R.E. Trans. on Elect. Comp.*, Vol. EC-9, No. 4, p. 465, Dec. 1960.

¹¹ J. Sklansky, "Conditional-Sum Addition Logic," *I.R.E. Trans. on Elect. Comp.*, Vol. EC-9, No. 2, p. 226, June 1960.

¹² J. L. Maddox, "Parallel Binary Adder-Subtraction Circuits," U. S. Patent No. 2,954,168, issued September 27, 1960.

¹³ O. J. Bedrij, "Carry-Select Adder," *I.R.E. Trans. on Elect. Comp.*, Vol. EC-11, No. 3, p. 340, June 1962.

¹⁴ F. Slater, "High-Speed Transistorized Adder for A Digital Computer," *I.R.E. Trans. on Elect. Comp.*, Vol. EC-9, No. 4, p. 461, Dec. 1960.

¹⁵ J. Sklansky, "An Evaluation of Several Two Summand Binary Adders," *I.R.E. Trans. on Elect. Comp.*, Vol. EC-9, No. 2, p. 213, June 1960.

¹⁶ T. Motooka and Y. Matsuoka, "Esaki Diode High Speed Carry Network Circuit," proceedings four special conferences, Institute of Electrical Engineers of Japan, April 1961, (In Japanese).

* (A+M), (A-M), (-A+M), (-A-M), (A>M), (M>A) where A and M are the two words, having an arbitrary sign, on which the arithmetic is performed. The comparison operations follow from the (A-M) and (-A+M) operations ("overflow" borrow).

ing logical manipulations are also readily available with this tunnel-diode arithmetic unit. Before describing the performance of a set of tunnel-diode carry generation circuits, the operating principles of the circuits employed will be described.

TUNNEL-DIODE CIRCUIT

Information (e.g., carries and borrows) can be propagated very rapidly from least-significant bit positions to most-significant bit positions of a parallel adder with a string of tunnel-diode OR gates. The simplicity of this tunnel-diode circuitry is easily seen when the information to be propagated is the familiar carry, given by the logical expression,

$$c_{i+1} = a_i m_i + a_i c_i + m_i c_i, \quad (1)$$

where

c_{i+1} = carry into the $(i + 1)$ th bit position from the i th bit position.

a_i, m_i = i th summand bits.

Rearrangement of Equation (1) yields

$$c_{i+1} = (a_i + m_i) (a_i m_i + c_i) \quad (2)$$

which describes a two-input tunnel-diode OR gate with the inputs $[(a_i m_i), (c_i)]$ and with a "controlled" power supply. The controlled power supply for the tunnel-diode OR gate is "on" if $[(a_i + m_i) = 1]$ and "off" if $[(a_i + m_i) = 0]$. Equations for the other three possible arithmetic operations are

$$\begin{aligned} [A-M] : b_{i+1} &= (\bar{a}_i + m_i) (\bar{a}_i m_i + b_i), \\ [-A+M] : b_{i+1} &= (a_i + \bar{m}_i) (a_i \bar{m}_i + b_i), \\ [-A-M] : b_{i+1} &= (\bar{a}_i + \bar{m}_i) (\bar{a}_i \bar{m}_i + b_i), \end{aligned} \quad (3)$$

where b_{i+1} is the borrow from the $(i + 1)$ th bit position.

Figure 1 is a simplified diagram of a tunnel-diode circuit described by Equation (2). The peak in the volt-ampere characteristics for tunnel-diode TD is used as the threshold for the OR function. Rectifier diode D1 ensures directionality of information propagation. Transistors Q1 and Q2 are inverter transistors of standard logic circuits.

Transistor Q1 is "off" when $[(a_i + m_i) = 1]$. Similarly, transistor Q2 is "off" when $[(a_i m_i) = 1]$.*

As shown in the figure, an amplifier with a high-impedance input is connected to tunnel-diode TD. This amplifier senses the voltage state of TD and produces $[c_{i+1}]$ and $[\bar{c}_{i+1}]$ at the required levels for use in

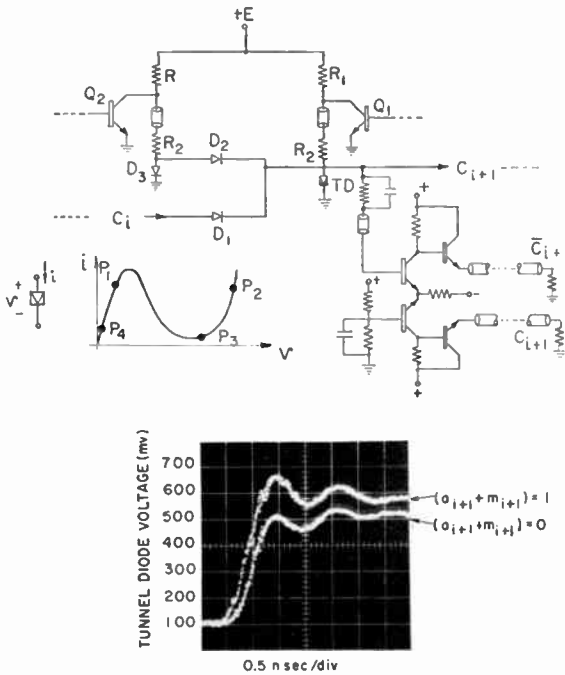


Fig. 1—Tunnel-diode circuit used to propagate carries and borrows in parallel adder.

a standard transistor logic circuit functioning according to the Boolean equation

$$s_{i+1} = a_{i+1} \oplus m_{i+1} \oplus c_{i+1}, \quad (4)$$

where s_{i+1} is the $(i+1)$ th sum bit.† The structure of Equation (4) is independent of the arithmetic operation.

* Logical product and inclusive OR are obtained from the circuitry driving transistors Q1 and Q2.

† Exclusive OR is obtained from Equation (4) by ensuring that $c_{i+1} = 0$ for all i , maintaining the carry string in a "reset" condition.

The operation of the tunnel-diode circuit shown in Figure 1 can be qualitatively explained as follows. When transistor Q1 is "off," the operating point on the volt-ampere characteristic of tunnel-diode TD is P1. If additional current is received through either of the rectifier diodes D1 and D2, tunnel-diode TD will switch to its high-voltage region and the operating point will be either P2 or P3, depending upon the state of $[a_{i+1}, m_{i+1}]$. If $[(a_{i+1} + m_{i+1}) = 1]$, P2 is the stable operating point; otherwise, P3 is the stable operating point.

Typical switching waveforms of the i th tunnel diode are shown in Figure 1. The two waveforms correspond to cases where the operating point in the high-voltage region is either P2 or P3. When P2 is the operating point, the voltage across tunnel-diode TD is 480 mv; for P3 it is 550 mv. The "ringing" in the lower waveform is due to the switching trajectory spiraling in on P3. The "overshoot" in the upper waveform is caused by the switching trajectory intersecting the high-voltage region of tunnel-diode TD at a current level much higher than that of P2.

Resetting tunnel-diode TD in the i th position to the low-voltage region is accomplished by insuring that $[(a_i + m_i)(a_{i-1} + m_{i-1}) = 0]$. When this logical condition exists, P4 is the stable operating point. These bistable tunnel-diode circuits must be reset after every use. The repetition rate for resetting is equal to the rate at which the entire adder subsystem is used. Even for long adders, the maximum rate is generally set by the standard logic circuits represented by transistors Q1 and Q2 in Figure 1.

To summarize, the tunnel-diode circuit described above is a bistable circuit having a fan-out of approximately one. Conventional transistor logic circuits provide a "controlled" power supply, and a transistorized amplifier is used to increase the signal level of the tunnel-diode circuit to that required by other transistor logic circuits. Carries/borrows are sequentially propagated by these tunnel-diode circuits at a very fast rate.

CIRCUIT DESIGN

A carry/borrow string using nine tunnel-diode circuits of the type shown in Figure 1 was constructed using 50-ma gallium-arsenide tunnel diodes for TD. Rectifier diodes D1 and D2 were low-capacitance germanium units. Diode D3 was a gallium-arsenide tunnel rectifier whose injection region served as a voltage clamp on the (a_i, m_i) current source. This clamp serves to prevent twice the normal current from flowing through rectifier diode D1 of the $(i + 1)$ th stage which might otherwise cause the $(i + 1)$ th tunnel-diode TD to switch to its high-voltage

region, even though $[(a_{i+1} + m_{i+1}) = 0]$. The valley capacitance of the gallium-arsenide tunnel diodes was less than 35 picofarads; the string exhibited an average stage delay of 0.86 nanosecond. A second carry/borrow string was constructed using all-germanium tunnel devices.

To minimize undesired feedback signals between stages of the all-germanium carry/borrow string, rectifier diode D1 was actually two germanium tunnel rectifiers in series. This series combination was chosen as the coupling elements so as to obtain a low net shunt capacitance of the composite diode D1 with two tunnel rectifiers having more-reasonable shunt capacitances. For simplicity, rectifier diode D2 was identical to tunnel-rectifier pair D1.*

Because of the realizable current-voltage characteristics of tunnel-rectifier pair D1, a 45-ma peak current was required for germanium tunnel-diode TD. The valley capacitance of TD was less than 12 picofarads. Rectifier diode D3 was replaced by a 15- to 30-ma peak current germanium tunnel diode. Its high-voltage region serves the same function as did the injection region of rectifier diode D3.† In addition, its low-voltage region "clamps" the current through tunnel-rectifier pair D2 to zero when transistor Q2 is saturated. This clamping action simplifies tolerance restrictions on the saturation voltage of transistor Q2.

Tolerance specifications on circuit components for the i th stage were quickly determined by making approximations to the $(i - 1)$ th and $(i + 1)$ th stages. It can be shown that these approximations introduce a considerable safety factor in that the tolerance specifications derived with the aid of these approximations are much tighter than necessary. This simplified design procedure is described as follows.

The $(i + 1)$ th stage is approximated by tunnel-rectifier pair D1 shorted to ground. With $[(a_i + m_i) = 1]$ the minimum resistive characteristics of tunnel-diode D1 is determined. Adequate allowance is made for transient requirements of the current-steering amplifier (3-ma maximum) in that regardless of loading conditions, operating point P3 is never allowed to enter the negative-resistive region of tunnel-diode TD.

The $(i - 1)$ th stage is approximated by tunnel-rectifier pair D1 returned to a voltage source equal to the maximum valley voltage of tunnel-rectifier pair TD. Again with $[(a_i + m_i) = 1]$, the maximum resistive characteristic of tunnel-rectifier pair D1 is determined. Minimum "overdrive"‡ was set at 2.5 ma.

* Hereafter diodes D1 and D2 are tunnel-rectifier pairs.

† Hereafter rectifier diode D3 is replaced by tunnel-diode D3.

‡ "Overdrive" is defined as the difference between the "elevated" static load line and peak current of TD under switching conditions.

Tunnel-rectifier pair D2 has the same volt-ampere characteristics as pair D1 except that there is more latitude in its minimum resistance characteristic. This is because tunnel-diode D3 has a lower valley current, and, in addition, it does not drive a current-steering amplifier.

For the reset operation, the assumption is made that the $(i-1)$ th stage is a current source equal to the maximum possible current through tunnel-rectifier pair D1. As a consequence, the condition $[(a_i + m_i) = 0]$ for all i is established for the reset operation. In addition, transistors Q1 and Q2 must have a saturation voltage less than the minimum valley voltages of tunnel-diodes TD and D3. In practice, only the condition that $[(a_i + m_i) (a_{i-1} + m_{i-1}) = 0]$ need be satisfied to reset the i th tunnel diode.

Tolerance on all power supplies and resistors were ± 3 per cent (worst case). The permissible worst-case peak current variation in tunnel-diode TD was 43 to 47 ma. Peak voltage of tunnel-diode TD was required to be less than 95 mv, with a valley voltage of 375 to 425 mv, and a maximum valley current of 6 ma at 425 mv, all worst-case conditions. The worst-case specifications on tunnel-rectifier pair D1 was: $i \leq 2$ ma at 95 mv, $i \geq 15$ ma at 330 mv, and $21 \text{ ma} \leq i \leq 24$ ma at 425 mv. For tunnel-rectifier pair D2, it was required that $i \leq 3$ ma at 95 mv, $i \geq 15$ ma at 330 mv, and $21 \text{ ma} \leq i \leq 29$ ma at 425 mv. The peak current of tunnel-diode D3 was allowed to vary between 15 and 30 ma. with a maximum valley current of 5 ma at 425 mv, a peak voltage of 50 to 95 mv, and a valley voltage of 375 to 425 mv, all worst case.

Figure 2 is a photograph of the over-all subsystem. Circuit boards that contain AND-OR-NOT logic circuits that serve as the power supplies for the tunnel-diode circuitry are located behind the main panel. These logic circuits have a worst-case stage delay of 5 nanoseconds. Smaller circuit boards, as indicated in the figure, contain the current-steering amplifiers. The four transistors and the majority of the passive components for this circuitry are contained in the low silhouette TO-15 can.

Figure 3 is a close-up view of one of the tunnel-diode circuits. Sub-miniature coaxial cable is used to interconnect all transistor circuitry with all the tunnel-diode circuitry.

PERFORMANCE

The average stage delay for the tunnel-diode circuits was under 0.5 nanosecond. Typical waveforms of five successive carry ripples are shown in Figure 4. A small variation in average stage delay as a

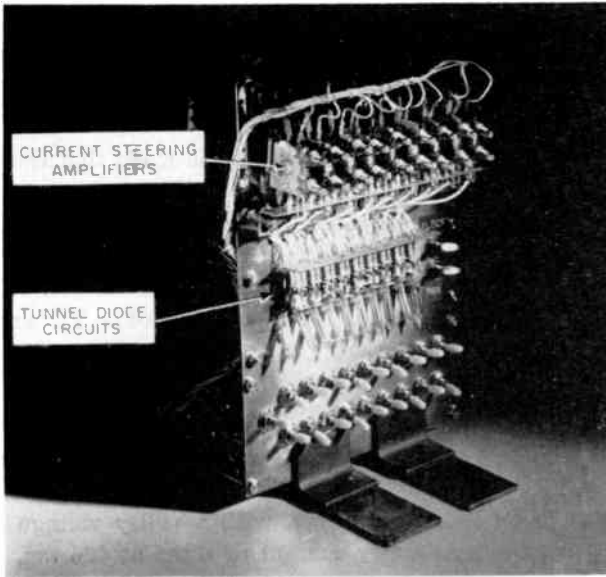


Fig. 2—Nine-stage tunnel-diode carry/borrow string.

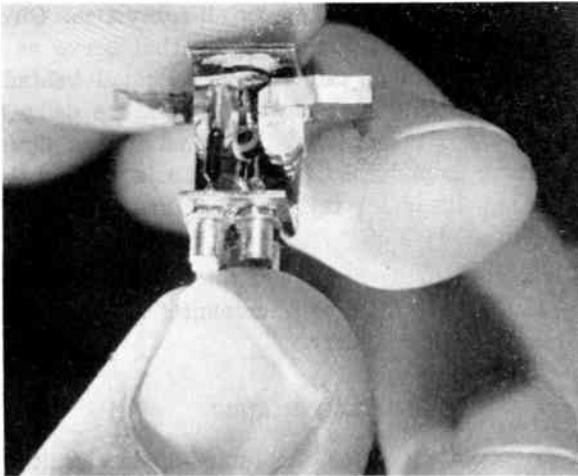


Fig. 3—Close-up view of one of the tunnel-diode circuits.

function of power-supply voltage E (see Figure 1) is to be expected since the current level of P1 (I_{P1}) directly influences the proportion of the switching current (approximately $I_{P1} - I_{P3}$) available to charge shunt capacitances of the tunnel diodes. For this subsystem, the average stage delay varied between 0.37 and 0.30 nanosecond for the permissible worst-case tolerance variation in E . Complete operation ceased for $E < 5.0$ volts and $E > 5.7$ volts ($R_1 + R_2 = 128$ ohms). Operation was unreliable for $E > 5.6$ volts. This unreliable operation was caused by an occasional triggering of the $(i - 1)$ th stage when $[(a_{i-1} + m_{i-1}) (a_i m_i) = 1]$. This triggering was a result of feedback coming

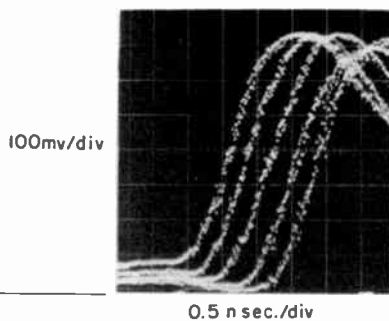


Fig. 4—Waveforms of five successive carry ripples. Average stage delay ≈ 0.32 nanosecond.

through the shunt capacitance of tunnel-rectifier pair D1. For this nine-stage subsystem, the shunt capacitance of D1 was less than 1.8 picofarads. It should be noted that each tunnel-rectifier of the pair has a shunt capacitance of less than 3.6 picofarads. Reliable operation can be extended all the way to 5.7 volts if lower-capacitance tunnel rectifiers are employed.

The transistor amplifier used to sense voltage states of the tunnel diodes exhibited a maximum output rise (and fall) for c_{i+1} (and \bar{c}_{i+1}) of 4 nanoseconds. The amplifiers have a maximum "wait" time between the *start* of the change of state of tunnel-diode TD and the *start* of the change of c_{i+1} of 2.7 nanosecond. Typical waveforms for this transistor amplifiers are shown in Figure 5.

The total "wait" time, T_w , for generation of a set of carries for n bits would be the sum of

- (1) stage delay of the transistor power-supply circuits (defined as the time between the 50 per cent point on the input to the 50 per cent point on the output),

- (2) one-half the rise time of the transistor power-supply circuit represented by transistor Q2 in Figure 1,
- (3) average stage delay of the tunnel-diode circuits times n ,
- (4) wait time plus one-half the rise time of output amplifier for \bar{c}_{n-1} .

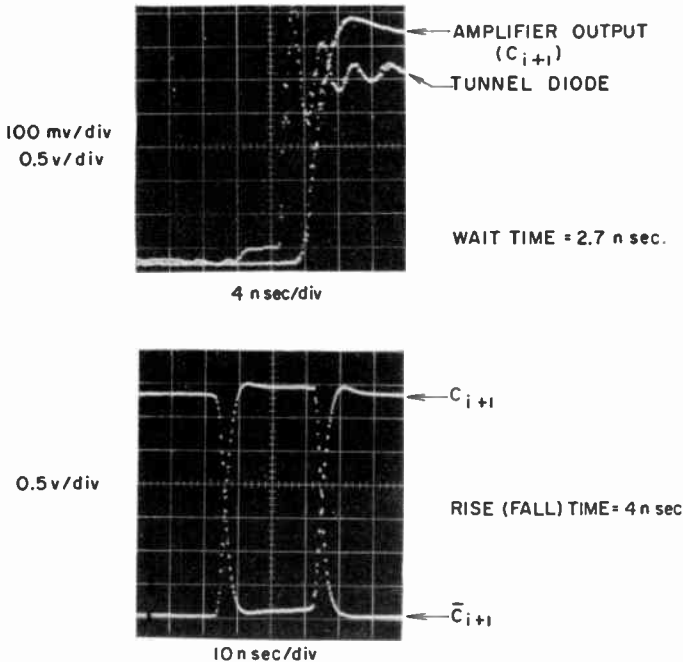


Fig. 5—Typical waveforms of current-steering amplifier.

For the subsystem discussed here,

$$T_w = (5.0 + 2.0 + 0.37n + 4.7) \text{ nanosecond.}$$

and for an n of 50, T_w equals 30.2 nanosecond. T_w , of course, does not include cable delays.

CONCLUSION

Sets of carries and borrows can be generated with minimum equipment and with a minimum of wait time using tunnel diodes in relatively straight forward circuits. We have optimized a balance between sequential and parallel processing so that performance is increased while complexity is decreased. This general philosophy is applicable in other subsystems.

COMPARATIVE STUDY OF LOW-VHF, HIGH-VHF, AND UHF TELEVISION BROADCASTING IN THE NEW YORK CITY AREA

BY

DONALD W. PETERSON

RCA Missile and Surface Radar Division,
Moorestown, N. J.

Summary—In 1961, the Federal Communications Commission placed a UHF system in operation in New York City for an extensive study aimed at providing a quantitative measure of the comparative merit of VHF and UHF television transmission in large cities. A comparison between the FCC UHF (channel 31) transmission from the Empire State Building and existing VHF transmissions has also been made by RCA. A comparative evaluation of picture degradation from multipath propagation and of the availability of useful levels of signal strength in highly built-up parts of Manhattan were the principal objects of study. This was supplemented with similar comparisons in other areas where there was less variability. Surveys of comparative field strength were performed along the smoothest and the roughest available radial profiles.

INTRODUCTION

A SUBSTANTIAL PART of the UHF television spectrum (470-890 mc) remains unused in the United States.¹ Technical differences between VHF and UHF system performance are partially responsible for this situation.

The most conspicuous of these differences, and one which favors the VHF end of the spectrum, is that shadow loss due to hills increases with frequency. Another difference, less commonly observed in operating systems, is the apparent theoretical advantage of UHF propagation over very smooth terrain. When the terrain is smooth enough to produce interference lobing, the field strength (for a given radiated power) at normal receiving antenna heights increases with frequency throughout a considerable distance range. There are, however, fundamental receiving antenna problems which tend to adversely affect performance of all systems in cluttered surroundings. Also, a number of state-of-the-art differences in r-f hardware exist and currently are important factors in relative system performance over the spectrum. The most serious of these is the substantial difference in receiver

¹ *Television Factbook*, Addenda of January 6, 1962 shows five times as many VHF stations in operation with only about one sixth as many channels as there are for UHF; No. 32, *Television Digest*, Triangle Publications, Inc., Radnor, Pa., 1962.

noise figure, which favors the lower end of the television spectrum. In addition, galactic noise is received at a high enough level to establish a limitation substantially higher than the thermal noise level for the lowest VHF channels. UHF system noise performance could eventually surpass low VHF performance in view of this fact, although the necessity for low receiver cost makes this seem unlikely. Finally, in practice, much higher gain transmitting antennas are used for UHF than for VHF. Adoption of this expedient, which is necessary for UHF systems, has objectionable consequences, particularly in hilly or rising terrain.

A long series of studies of the propagation problems and extensive advances of the hardware art culminated in the Television Allocations Study Organization (TASO) studies reported in 1959.² This large cooperative undertaking of government and industry answered most of the questions about frequency dependence.

One problem area was slighted, however, because of the costliness of an effective study. Up to 1962 there had been no comprehensive comparison of VHF and UHF television in a highly built-up city. In view of the dominant part that large cities, and New York City in particular, play in American television, this remaining problem was serious enough to merit study.

FEDERAL COMMUNICATIONS COMMISSION NEW YORK UHF PROJECT

The Federal Communications Commission (FCC) obtained from the 86th Congress a two-million-dollar appropriation for the necessary instrumentation, field testing, and data analysis to study large-city television problems. The FCC conducted a large-scale field survey in the New York City area^{3,4} during late 1961 and 1962.

A transmitter was leased by the FCC, installed on the 80th floor of the Empire State Building, and operated by the City of New York as channel 31 (572-578 mc). A specially developed omnidirectional antenna was interspersed between layers of the channel 2 antenna on the tower above the Empire State Building. A private organization was engaged to do the field testing using commercial receivers and a specially developed portable all-channel field-strength meter. The UHF broadcasting system, with the call letters WUHF, was put into operation in November 1961, thus affording an opportunity to perform comparative studies of UHF and VHF stations in and around the city.

² *Television Allocations Study Organization Report: "Engineering Aspects of Television Allocations,"* March 1959.

³ A. G. Skrivseth, "New York UHF-TV Project of the FCC," *Trans. I.R.E. PGB*, Vol. 7, No. 4, p. 24, Dec. 1961.

⁴ A. G. Skrivseth, "Early Returns from WUHF," *I.R.E. Convention Record*, Part 7, p. 101, 1962.

RCA UHF PROJECT

In view of the availability of the UHF signals, an RCA field project in the New York City area was planned late in 1960 in the belief that the knowledge gained could supplement the output of the FCC project. Figure 1 is a map of New York City showing the various areas involved. The purpose of the RCA project was to study propagation in the clutter of highly built-up portions of the city—the large-building areas. It was to determine the frequency dependence of the picture degradation resulting from multipath propagation and the transmission loss in highly built-up and variable areas such as those east and west of Central Park in Manhattan. The degradation of color pictures from multipath propagation was of particular interest.

The UHF transmissions from the Empire State Building provided an opportunity to examine frequency dependence in an entire service area under true broadcasting conditions. With more radiated power and better receivers and field strength meters available than for earlier New York surveys, radial surveys outside the city could be carried out more completely than before.

The problems of the comparative study can be divided into two categories: (1) smooth-terrain problems and (2) rough-terrain problems. Broadly speaking there are two basic kinds of propagation problems in both categories. First, both buildings and hills cause multipath propagation with resultant picture degradation. Second, they produce distorted field distributions and shadow loss, both of which tend to reduce the space median of antenna terminal voltages. (It is assumed here that UHF antennas of interest have aperture dimensions in the order of several wavelengths.) Besides acting as reflectors, buildings also introduce attenuation, since propagation must sometimes be through walls. In a smooth-terrain, built-up city area, the receiving antennas are figuratively immersed in a sea of clutter, with little or no possibility of using antenna directivity or gain in a predictable way, if the building heights are variable. In the rural hilly-terrain situation, the propagation effects may be qualitatively understood by inspection of the surroundings. The consequences of terrain shadowing may be dominant. While all kinds of situations are of interest, it was found expedient to study clutter effects in smooth terrain, and rough-terrain effects with clutter eliminated.

Smooth-Terrain Problems

The clutter of New York City ranges from the extreme variation of building sizes of Manhattan, illustrated in Figure 2, to the slight



Fig. 1—Map of the New York City area.

variation of two-story row houses in Queens and Brooklyn. The situations studied in New York City are shown in Table I. In all of these situations it was necessary to determine both the multipath picture degradation and the receiver terminal voltage.

The distance of the "fringe area" in residential sections was determined. Since here we were not concerned with multipath degradation, it was necessary to measure only field strength above roof-top level. A radial line along the south shore of Long Island was chosen for a survey over exceptionally smooth terrain with suburban clutter. The useful range of the fringe area, particularly for UHF, depends upon the receiving antenna gain which can be effectively employed; thus effective receiving-antenna gain in clutter is of interest.

Table I—Clutter situations studied in New York City.

Location	Roof	Room	Street	Character of Sample	Type of Sampling
Manhattan	x	x		Extremely varied building sizes	Random
Queens	x	x		Moderately varied building sizes	Random
Queens		x	x	Six story apartments	Random
Queens			x	Two story row houses	Periodic
Queens			x	Two story single houses	Periodic

Rough-Terrain Problems

The extent to which rough-terrain problems can be studied in the New York area is quite limited. The two Watchung ranges in New Jersey afford what is probably the best available topographic situation for studying terrain effects. The shadow loss from these ranges was too great to enable complete measurement of field strength with the radiated power and instrumentation available for the 1948 tests.⁵ It was therefore desired to include a survey along a radial line through the Watchungs. The topography is relatively simple, and the mountain ranges are only 14 to 15.5 miles from the Empire State Building.

CONDITIONS OF THE FIELD TEST

Low VHF channel 2 (54-60 mc) and high VHF channel 7 (174-180

⁵G. H. Brown, J. Epstein and D. W. Peterson, "Comparative Propagation Measurements; Television Transmitters at 67.25, 288, 510, and 910 Megacycles," *RCA Review*, Vol. IX, No. 2, p. 177, June 1948.



Fig. 2—Manhattan, illustrating the degree of clutter. The view is looking north across Central Park, the northern boundary of which is 110th street. The Hudson River is seen at the upper left.

mc) stations were chosen by the FCC as the most suitable broadcasting systems for comparison with the channel-31 system; the same channels were also used for the RCA comparison. Within a radius of about two miles, all three transmitting plants delivered field strengths which were usually excessive for standard receivers and transmission lines. It was quite usual for the stray pick-up of a standard receiver to exceed the signal level from the antenna. As a consequence, antenna orientation was relatively ineffective in reducing multipath degradation. Special receiver shielding and transmission line shielding was found to be necessary to avoid stray pick-up, and was employed successfully. Color programming was available from the channel 4 (66-72 mc) station directly, and via channel 31. Therefore, these channels were used for color comparisons.

It was necessary to use regular program material for subjective evaluations of picture quality. This meant that the evaluator could not know the picture quality as transmitted. In fact, the variation in quality of transmitted pictures was great enough to have a significant effect on the observations. Experience with subjective evaluation in Manhattan, where picture quality is notoriously poor, led to a recognition of further problems:

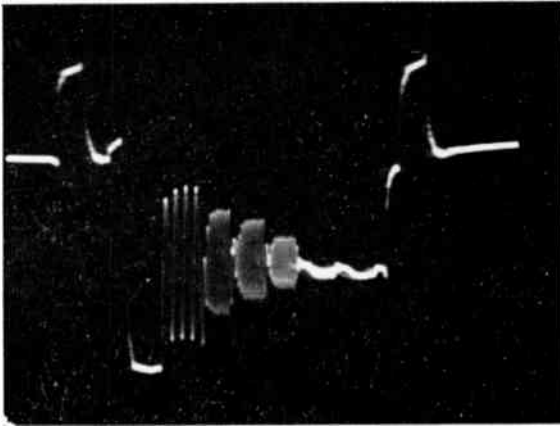
- (1) If the picture defect consisted of lack of resolution, there was a marked tendency for picture quality judgments to depend upon the amount of information in the picture. For example, a close-up of a person might appear to have satisfactory resolution while printed matter in a commercial might not be legible or a crowd scene might be quite unsatisfactory.
- (2) If the picture defect consisted of ghost images, these were found to be quite objectionable in some scenes and not even noticeable in others under identical receiving conditions.
- (3) It was often not at all obvious just what was wrong with poor pictures.

It was concluded that a picture evaluator in the field could probably benefit by the use of special test waveforms viewed on an oscilloscope.

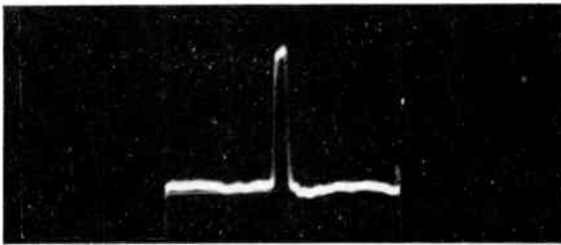
TEST SIGNALS

The difficulty of making reliable subjective evaluations was substantially alleviated by employing two kinds of test signals. The first of these, a part of the standard synchronizing waveform known as the equalizing pulse, is a two microsecond pulse which proved to be useful

in observing multipath echo waveforms. The second test signal used is a succession of video modulating bursts ranging from 0.5 to 3.58 mc/sec and occurring along a picture line. Since this multiburst is put on only one or two picture lines during regular broadcasting, it must be observed with a line-selector oscilloscope. Both test-signal waveforms are directly related to picture quality. Their value increased as the picture evaluator gained experience using them.



(a)



(b)

Fig. 3—Test waveforms: (a) multiburst and (b) two-microsecond pulse.

Both the equalizing pulse and the multiburst test signals were displayed on an oscilloscope and photographed as a part of most of the RCA field observations made in New York City. Their use eliminated most of the doubts experienced in picture evaluation. Photographs of the test waveforms are shown in Figure 3.

TRANSMITTING AND RECEIVING ANTENNAS

The transmitting antenna elevations on Empire State Building are

shown in Figure 4. The transmitting antenna azimuth patterns are shown in Figure 5. The geographical orientations of the channels 2, 4, and 7 patterns are known and hence could be taken into account in computing theoretical field strengths. The orientation of the channel 31 pattern was not known so there is an approximate $+4$ to -8 decibels

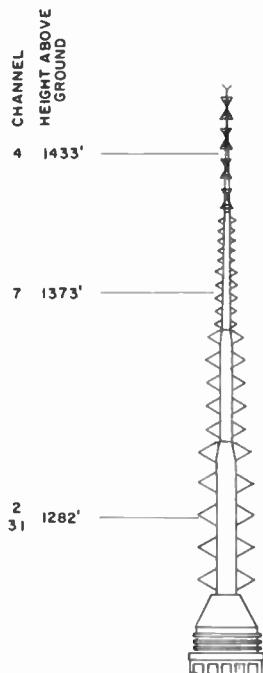


Fig. 4—Empire State Building antenna tower.

uncertainty in all UHF computations of theoretical field strength. To put this another way, the radiated power probably lies between 4 decibels above and 8 decibels below the nominal (average) value and varies with azimuth angle in an unpredictable manner.

The elevation patterns of the transmitting antennas are shown in Figure 6. It should be noted that the VHF patterns have deeper minima than the channel-31 patterns from the pattern maximum down to -20° . The portions of the service area served by the elevation pattern minima may be seen by reference to Figure 7. These minima serve distances of about 1.25, 0.8, and 1.2 miles for channels 2, 4, and 7, respectively. The UHF elevation pattern has been shaped to yield constant field strength with distance over "average" terrain for the

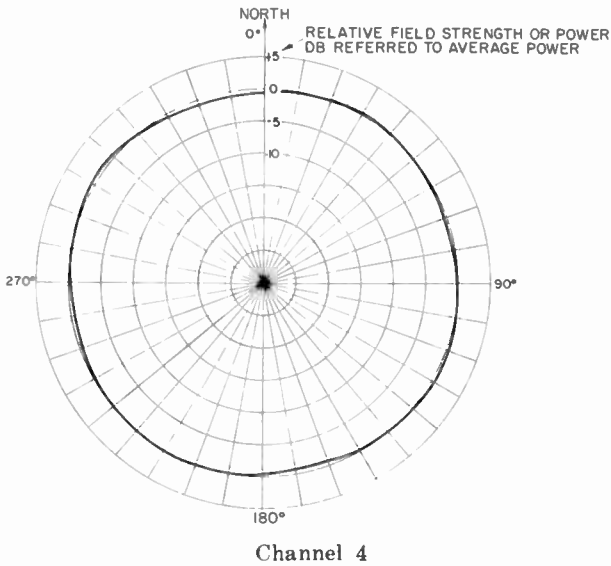
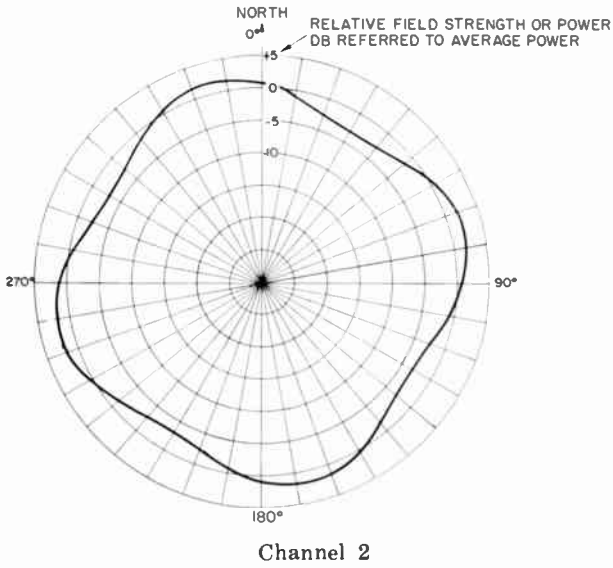
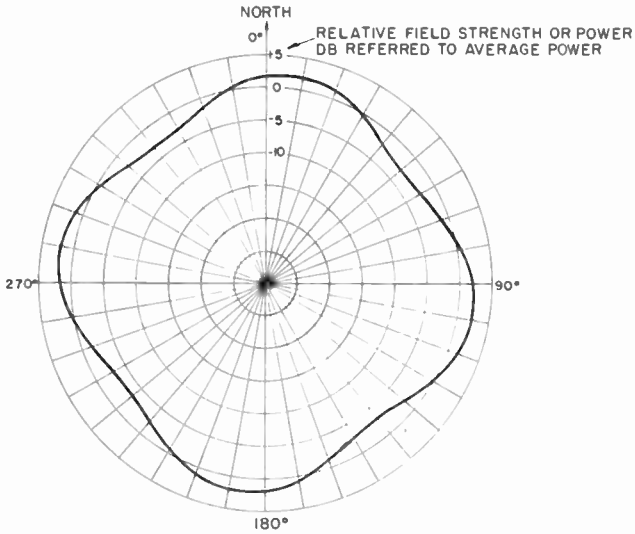
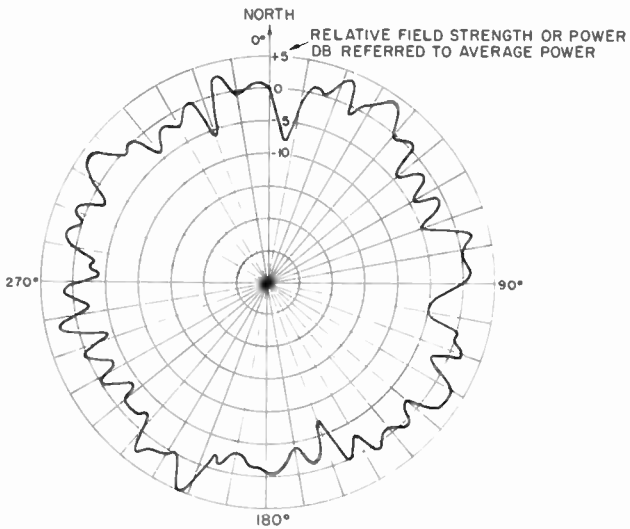


Fig. 5—Transmitting antenna azimuth patterns for channels 2 and 4.



Channel 7



Channel 31

Fig. 5 (cont.)—Transmitting antenna azimuth patterns for channels 7 and 31.

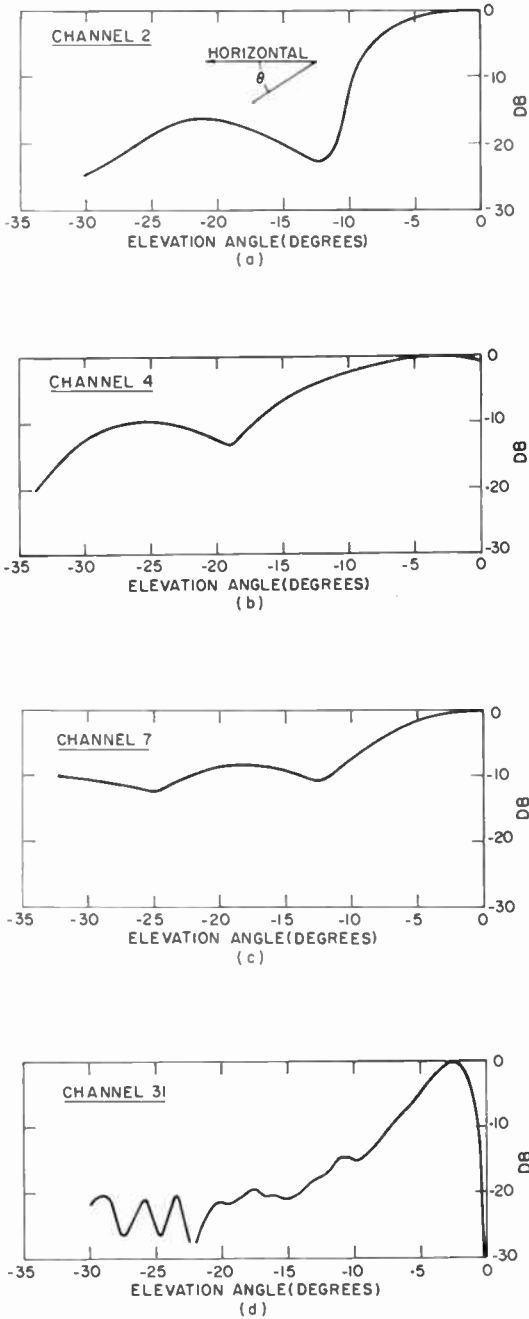


Fig. 6—Transmitting antenna elevation patterns for channels 2, 4, 7 and 31.

FCC F(50,50) propagation curves.⁶ Because of the necessity of using high UHF antenna gain, the pattern drops rapidly from a maximum at -2.5° as zero elevation angle is approached. This, it will be seen later, has important consequences in hilly and rising terrain.

The outdoor receiving-antenna azimuth patterns are shown in Figure 8. The antennas used were chosen as approximately encompassing the practical range of usable physical sizes. Simplicity of structure and clean patterns were influencing factors in the specific

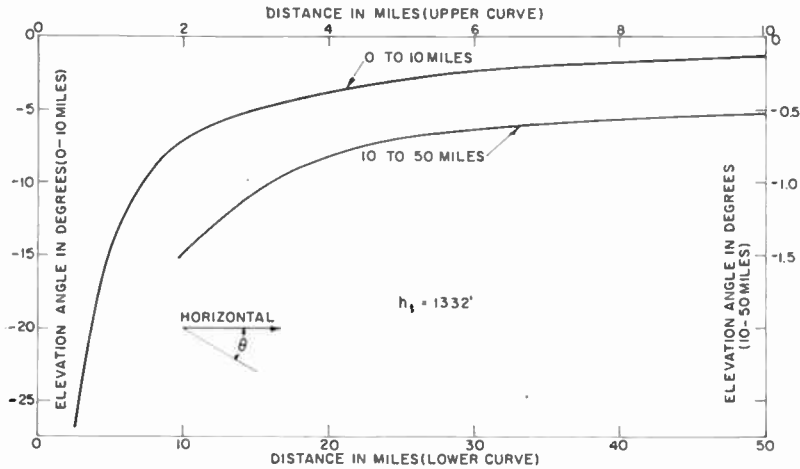


Fig. 7—Elevation angle over smooth spherical earth.

choices. A large and a small antenna were used for each frequency. VHF antennas are in such wide use as to establish the norm for size. On this basis a commercial all-channel unidirectional VHF antenna was chosen for the large VHF antenna. The small VHF antennas were single-channel dipoles with a parasitic reflector. The small unidirectional UHF antenna was a corner reflector type, and the large one was a 6-foot paraboloid. The unidirectional receiving antenna gains are shown in Table II.

The VHF unidirectional and the UHF corner-reflector antennas have similar patterns. The VHF unidirectional and the UHF paraboloid antennas are comparable in physical size and mechanical complexity.

Indoor receiving antennas consisted of rabbit-ear dipoles for channels 2, 4, and 7 and the corner reflector and a dipole with reflector antenna for channel 31.

⁶ Sixth Report and Order of the FCC (52-294) published by *TV Digest*, April 1952. A revision of the VHF propagation curves was recommended to the FCC by the Radio Propagation Advisory Committee.

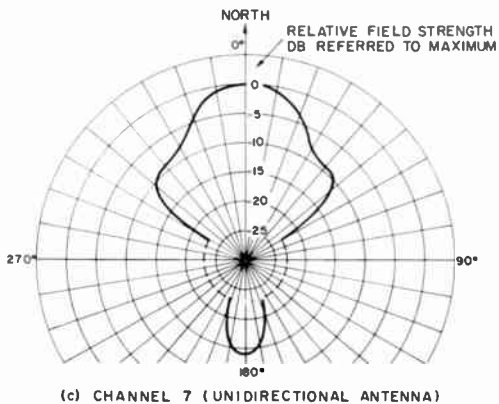
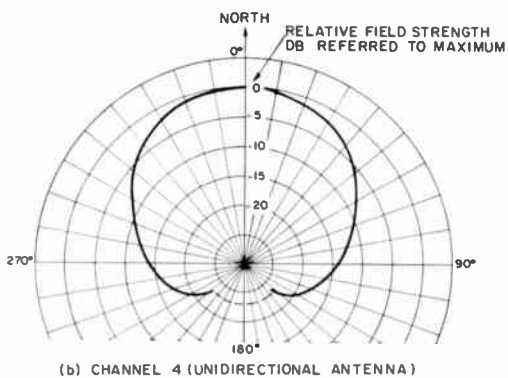
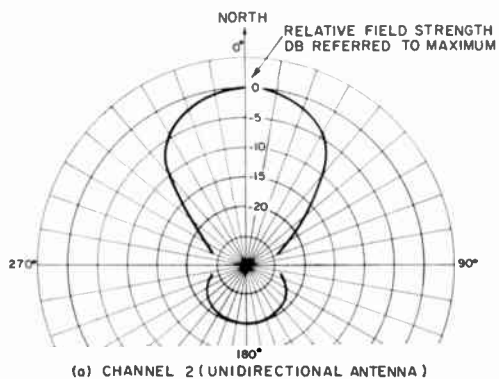
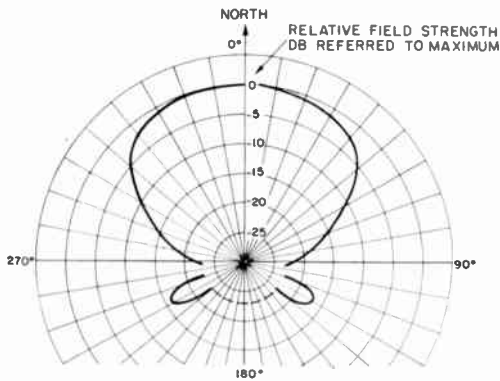


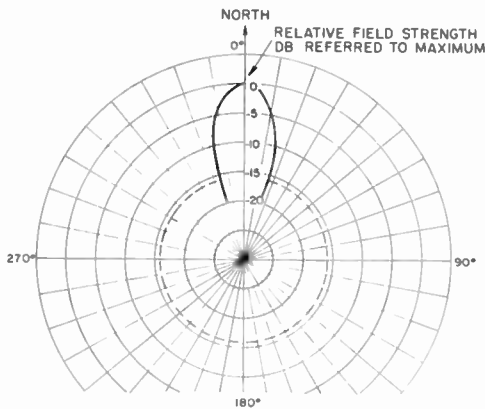
Fig. 8—Receiving antenna azimuth patterns for channels 2, 4, and 7.

Table II—Receiving antenna gains (db referred to $\lambda/2$ dipole for each respective frequency).

Antenna	Channel			
	2	4	7	31
Unidirectional VHF	5	4	8	
Corner Reflector				7.7
Paraboloid				13



(d) CHANNEL 31 (CORNER REFLECTOR ANTENNA)



(e) CHANNEL 31 (PARABOLOID ANTENNA)

Fig. 8 (cont.)—Receiving antenna azimuth patterns for channel 31.

MANHATTAN FIELD TEST

A VHF-UHF comparison of television reception in highly built-up Manhattan is by its very nature a statistical problem. The topography of most of the island is a much less significant factor than the man-made features. The photograph in Figure 2 shows part of the area and suggests by the wide variation of building heights and their random distribution that reception will be extremely varied.

Both indoor and roof-top reception are of interest. The best way to learn the statistics of reception under the exceedingly varied conditions of Manhattan is by measurement in a random selection of receiving locations in buildings and on rooftops. This could be on the basis

Table III—Picture ratings (based on multipath degradation).

Rating	Description
1	Excellent; no multipath degradation
2	Fine; negligibly small degradation
3	Passable; moderate degradation
4	Marginal; objectional degradation
5	Inferior; lowest class of usable picture
6	Unusable

of a rigorously random sampling process with the attendant practical problem that some of the apartment dwellers so chosen would not care to cooperate with the experiment. The method used instead was to choose the area of Manhattan where building heights are extremely varied and then deliberately choose available test locations with studied randomness.

The method of test location choice was recognized to lack mathematical rigor. It was felt, however, that any significant frequency-dependent differences would be discovered by the field test. There could then remain a problem in determining the degree of significance of the differences, since the sampling was not rigorously random. On the other hand, if no differences were uncovered, a more rigorous sampling process would likewise probably not reveal a difference. It fortunately turned out that frequency-dependent differences were so small that there was no need for going beyond the original sampling.

Multipath degradation was evaluated in terms of TASO subjective ratings.² The meanings of the ratings are shown in Table III. The ratings were based on apparent picture quality tempered by knowledge



Fig. 9—Manhattan location sampling.

of the received test waveforms. In all cases the waveforms included the two-microsecond pulse, and in most cases also included the multi-burst test waveform for comparisons of color on channels 4 and 31. The Manhattan ratings for the locations of Figure 9 are shown in Table IV. The subjective evaluation data for Manhattan is based on a sampling of 239 locations. There were from two to four locations per building. The absence of frequency dependence is readily apparent. Roof reception about one grade better than indoor reception is quite consistent throughout the data. Color picture ratings are about half a grade poorer than monochrome ratings. A laboratory comparison⁷ of monochrome and color-television delayed-image effects made in 1953 showed a similar tendency.

Table IV—Subjective multipath picture ratings for Manhattan.

Receiver type	Location	Median Ratings		
		Low VHF	High VHF	UHF
Monochrome	Indoor	3.8	3.7	3.8
	Roof	2.7	2.4	2.7
Color	Indoor	4.3		4.4
	Roof	3.1		3.2

Reception is generally poor in most of Manhattan below 110th Street because of the varied building heights and the low angle of arrival. By far the most serious problem is the multipath degradation. There are installation problems which often fail to get deserved attention because customers are unwilling to stand the expense. If the best quality possible is to be accomplished in an installation, there must be roof-top exploration which will not necessarily be fruitful. Since receivers high in tall buildings and within about two miles from the transmitter are exposed to unusually high field strengths, there are receiver and cable shielding inadequacies apparent in common installation practice. Even the best installation work is often undone by echoes resulting from new building construction.

Field-strength and terminal-voltage data for Manhattan are shown in Figure 10 as a function of distance. It is noteworthy that on all

⁷ G. Fredendall, "A Comparison of Monochrome and Color Television With Reference to Susceptibility to Various Types of Interference," *RCA Review*, Vol. XIV, No. 3, p. 341-358, Sept. 1953.

Table V—Receiver noise figures.

Channel	Noise Figure (db referred to 1 μ v)
2	5
4	5
7	5
31	10

frequencies the terminal voltage available from rooftop antennas was adequate to over-ride thermal and galactic noise, as well as most man-made interference. UHF terminal voltages indoors were sometimes too low to over-ride thermal noise. When this occurred, VHF pictures usually suffered very severe multipath degradation.

Receiver noise figures are shown in Table V. A satisfactory picture with respect to noise will be obtained with a signal-to-noise ratio of 30 decibels. The required terminal voltages for good commercial receivers are shown in Table VI.

A statistical analysis of the Manhattan data, made without regard for distance, is shown in Figure 11. The median terminal voltages are shown in Table VII.

MISCELLANEOUS OBSERVATIONS IN MANHATTAN

Several potential problems were examined qualitatively during the field tests. Picture degradation from man-made interference was found to occur infrequently in Manhattan and Queens. Evidently field strengths were high enough to over-ride interference on all frequencies most of the time. There were occasional objectionable picture disturbances from moving about the room when indoor antennas were used. Little or no frequency dependence was noted in this effect. With indoor antennas, there was on rare occasions objectionable distortion of sound

Table VI—Terminal voltages required for 30 db signal-to-noise ratio.

Channel	Noise Figure, db	Terminal Voltage
2	5	35.7
4	5	35.7
7	5	35.7
31	10	40.7

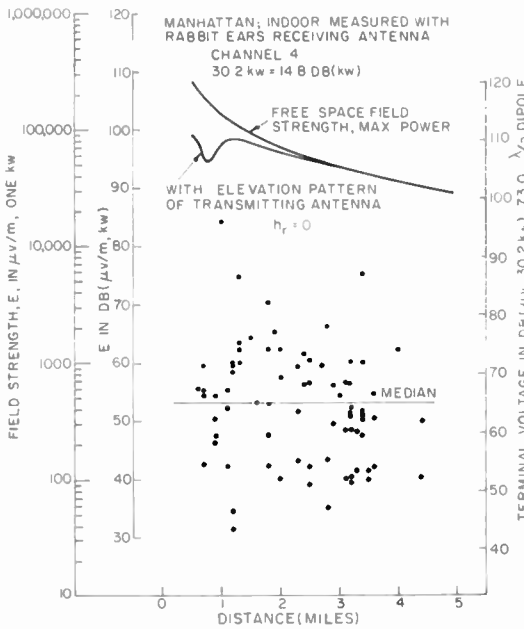
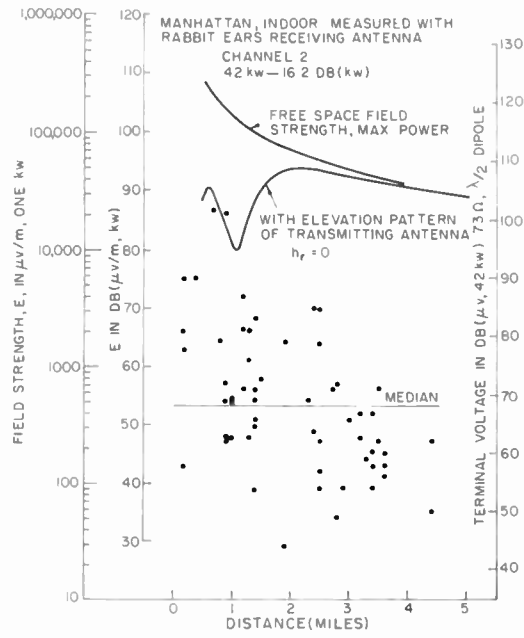


Fig. 10—Field-strength data (indoor) for channels 2 and 4.

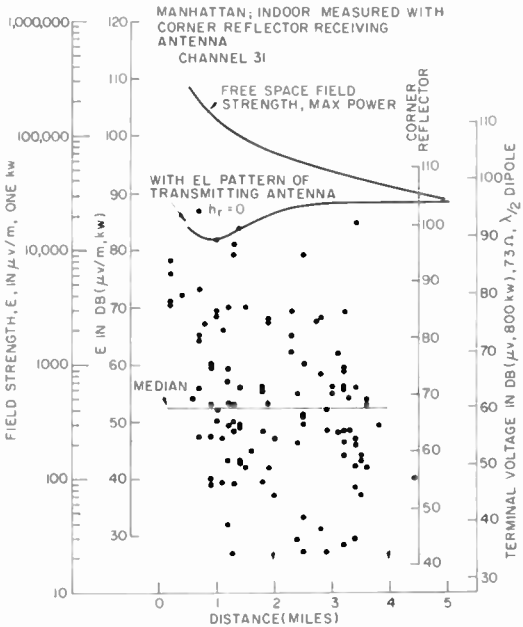
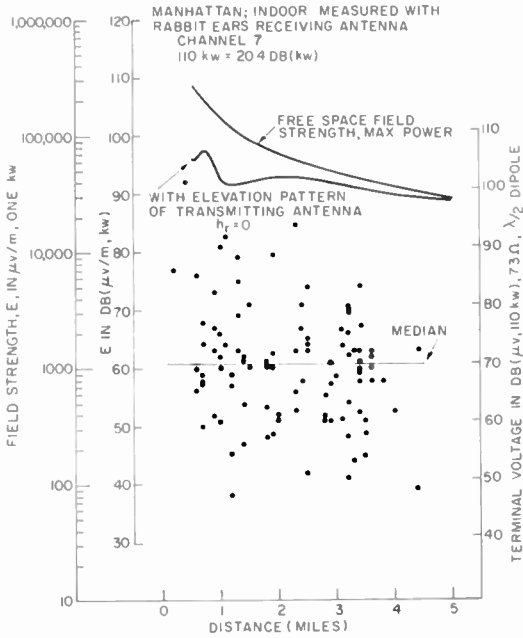


Fig. 10 (cont.)—Field-strength data (indoor) for channels 7 and 31.

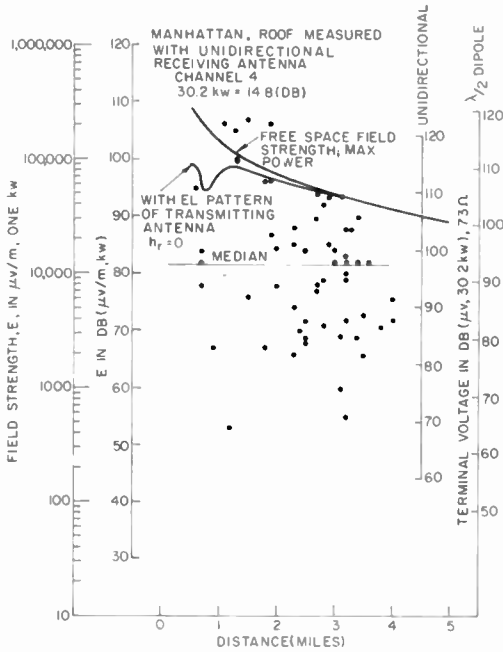
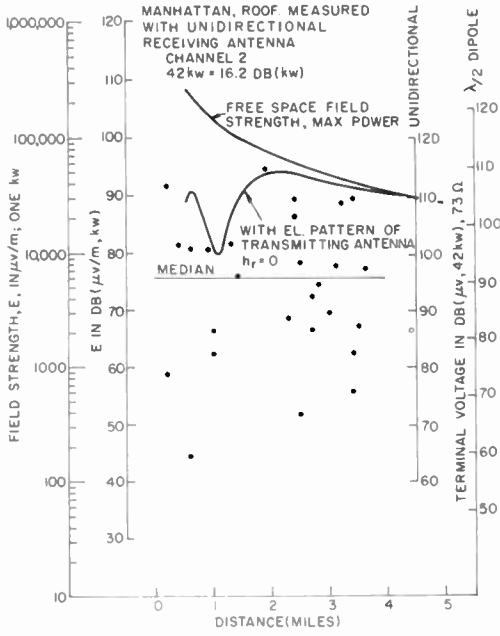


Fig. 10 (cont.)—Field-strength data (roof) for channels 2 and 4.

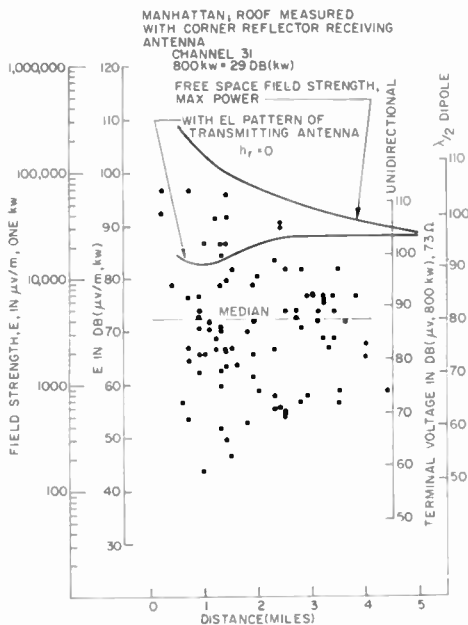
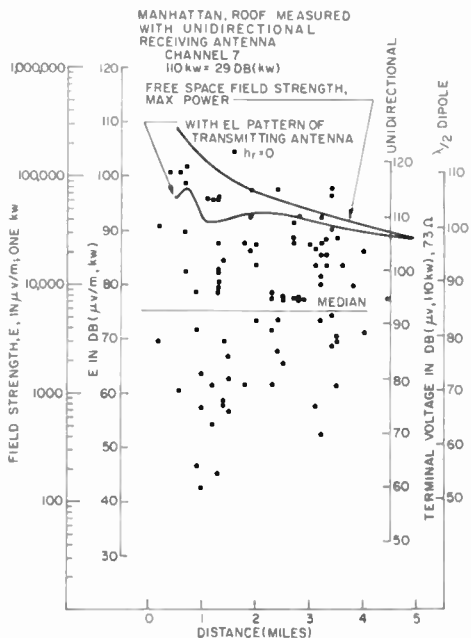


Fig. 10 (cont.)—Field-strength data (roof) for channels 7 and 31.

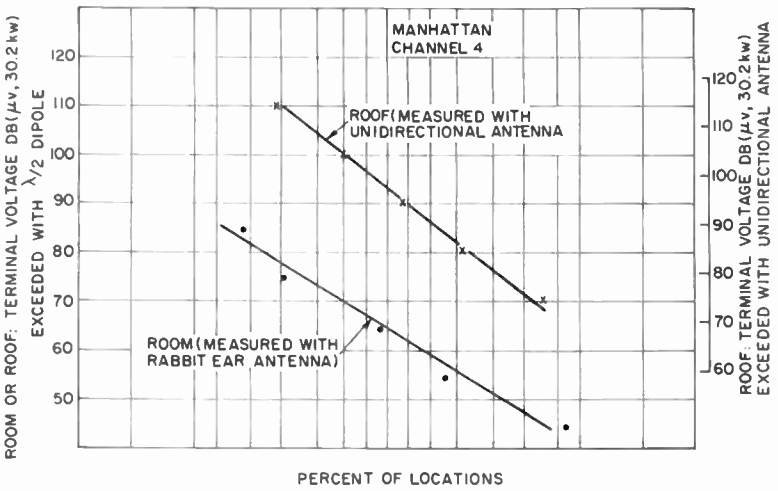
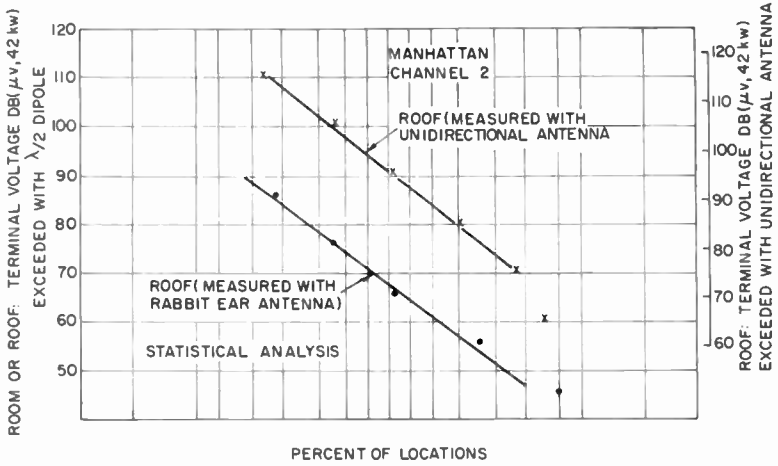


Fig. 11—Manhattan statistical analysis for channels 2 and 4.

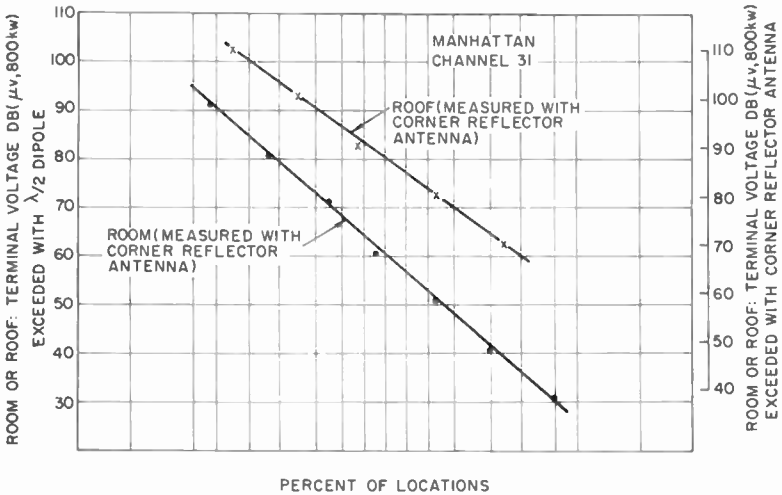
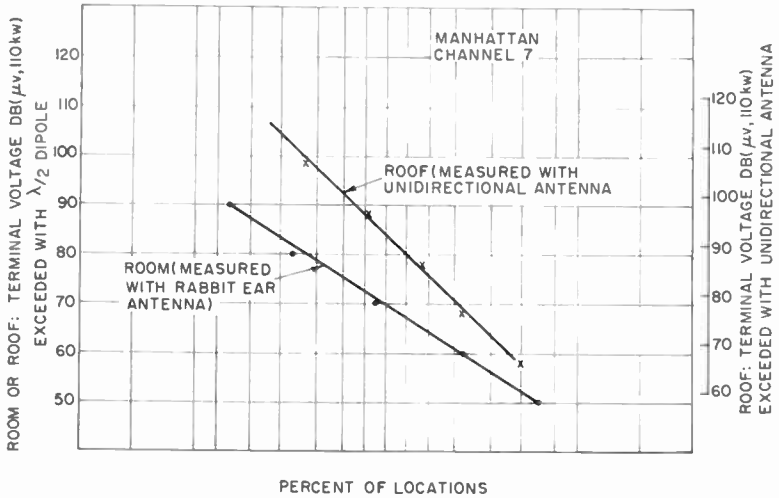


Fig. 11 (cont.)—Manhattan statistical analysis for channels 7 and 31.

from severe multipath propagation. This distortion also was independent of frequency.

On Manhattan rooftops (in the highly built-up smooth terrain below 110th Street) UHF improvement from use of the highly directional paraboloid antenna was usually demonstrable. However, orientation was so excessively critical, because of extreme field distortion, as to cast doubt upon recommending general use of high-gain UHF re-

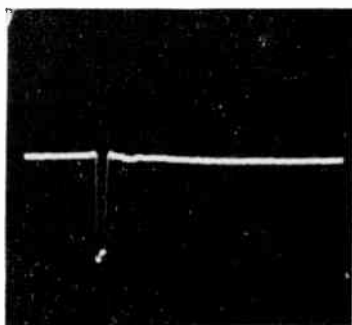
Table VII—Terminal voltage statistics (actual power across 73 ohms).

Channel	Roof		Indoor		Average Distance (miles)
	Antenna	Terminal Voltage Median (db referred to 1 μ v)	Antenna	Terminal Voltage Median (db referred to 1 μ v)	
Manhattan					
2	VHF	96	R.E.	68	2.5
4	VHF	97.5	R.E.	65	
7	VHF	92	R.E.	70	
31	C.R.	87.5	C.R.	67.5	
Forest Hills					
4	VHF	80	R.E.	56	7.3
7	VHF	81	R.E.	59	
31	C.R.	81	C.R.	60	
Queens (6 story)					
4	No roof data		R.E.	56	5.2
7			R.E.	65	
31			C.R.	69	

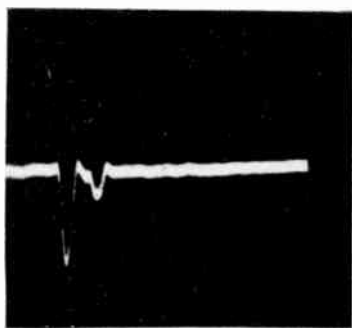
VHF = unidirectional VHF; C.R. = corner reflector;
R.E. = "rabbit-ear" dipole.

ceiving antennas. The broad-beam unidirectional antennas were quite satisfactory from an orientation standpoint. Use of antennas with poorer patterns than these can hardly be justified for Manhattan roofs.

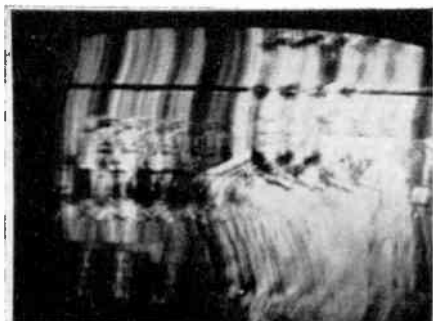
The character of the picture degradation resulting from multipath propagation is apparent from the kinescope photographs of Figure 12. Almost all Manhattan pictures in the area sampled suffered from low resolution, sometimes as low as the resolution of a 0.5-mc system. Discrete ghost images with objectionable intensity also were seen quite



(a)



(b)



(c)

Fig. 12—Range of picture quality in Manhattan. Picture (b) is closest to typical quality.

commonly. Typically, the principal ghost images had time delays up to about two microseconds, although there were cases with substantial echo voltages with delays up to at least a full picture line or 63 microseconds as in Figure 13. The test waveform data in Figure 12 illustrates the supplementary value to the picture evaluator of seeing the distortion of constant test signals which are common to all channels being compared.

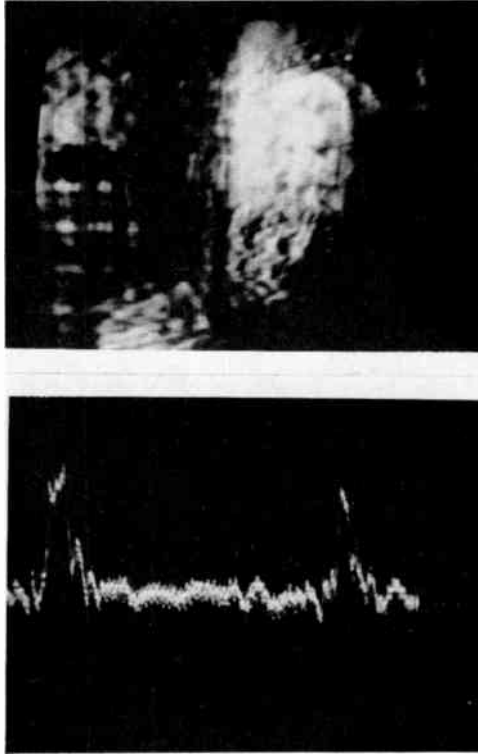


Fig. 13—Unusually long echo delay.

OBSERVATIONS IN QUEENS AND BROOKLYN

The areas chosen for measuring multipath degradation from buildings included the entire range of building sizes and varieties to be found in the flat portions of the city, such as most of Queens and Brooklyn. The subjective ratings are given in Table VIII. Multipath degradation was reduced in a consistent fashion as buildings became smaller until with two-story buildings reception was rated "fine" on

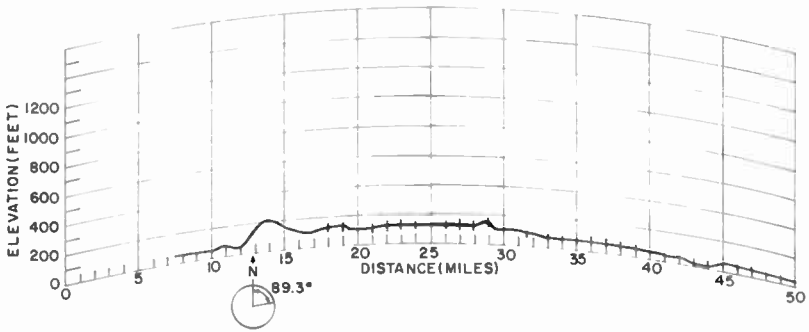


Fig. 14—Elevation profile, east radial.

all frequencies. Since each of these sets of data represents a small range of distances, the terminal voltages can be given in terms of the statistical data shown in Table VII.

FIELD STRENGTH IN SMOOTH-TERRAIN CITY AREAS

An eastward radial line near the south shore of Long Island was chosen for a survey of field strength. Most of the radial passes through cities with one- and two-story single dwellings. The topographic profile shown in Figure 14 indicates the measuring locations. This radial comes about as close to fitting smooth, spherical-earth propagation conditions as any densely populated area can. It is therefore interesting to compare measured field strength with smooth spherical-earth theory. Both measured data and theoretical curves are shown in Figure 15.

Table VIII—Subjective multipath picture ratings (monochrome).

Location	Number of Samples	Median Ratings		
		Low VHF	High VHF	UHF
Forest Hills—indoor	30	3.2	3.3	3.3
Forest Hills—roof	15	2.7	2.6	2.5
Queens, 6-story apartment, indoor	22	2.5	2.4	2.8
Queens, 6-story apartment, street	12	2.6	2.5	2.7
2-story row houses, street	7	2	2	2
2-story single houses, street	6	2.5	2.5	2.5

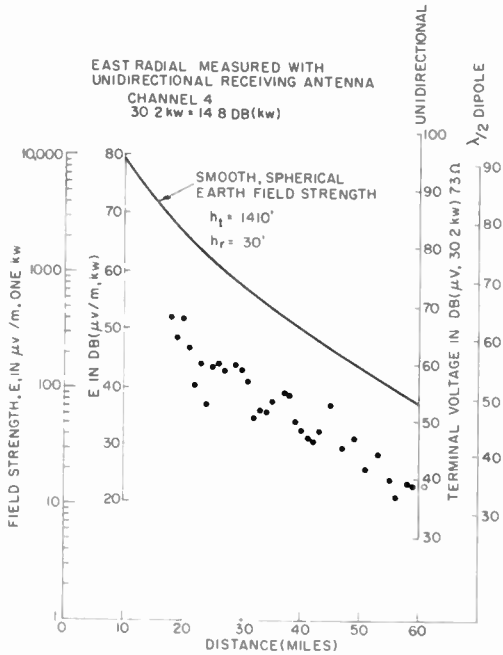
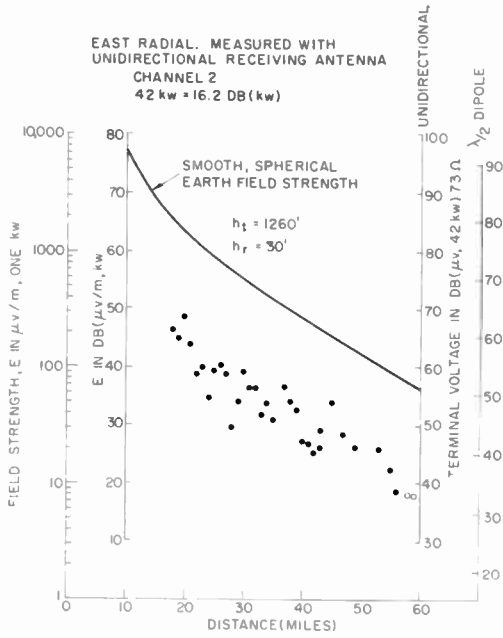


Fig. 15—East radial field-strength data for channels 2 and 4.

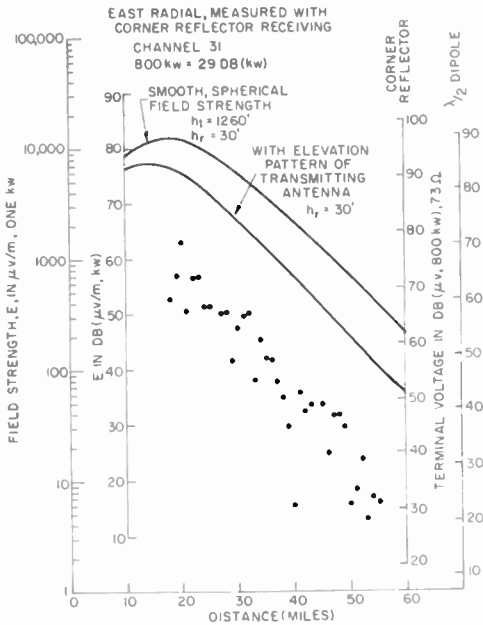
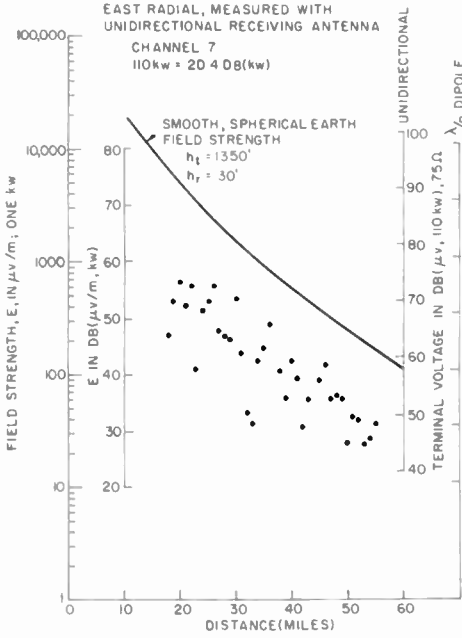


Fig. 15—East radial field-strength data for channels 7 and 31.

It is apparent that the theory bears a useful relationship to the measured data, since the theoretical curve and the average of field-strength data have the same slope for each respective frequency. There is an average departure in measured field strength below the theoretical curves which probably can be ascribed to clutter loss—the average reduction of apparent field strength resulting from local shadowing and field distortion. This kind of loss is always in evidence around buildings and trees as a consequence of multiple reflections and shadowing.

From the data of Table VIII, picture degradation from multipath effects was known to be negligible under the conditions of this radial

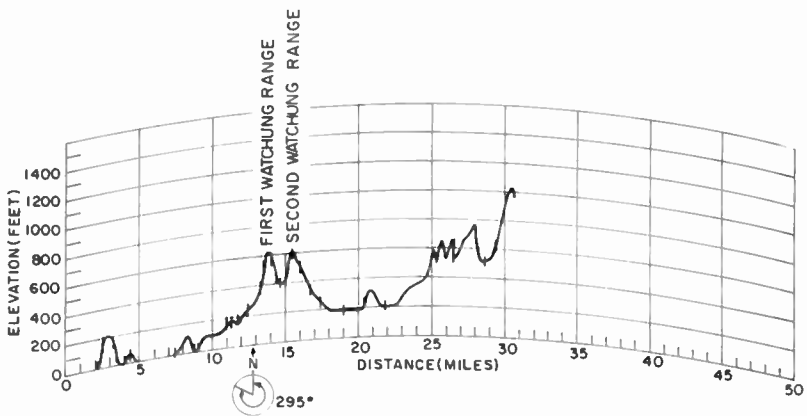


Fig. 16—Elevation profile, west radial.

survey. Therefore, picture observation was deemed unnecessary, and only field strength was measured. The unidirectional VHF antenna and the corner-reflector UHF antenna were used at about the same heights above the street as antennas on the rooftops in the respective areas (about 30 feet).

RECEPTION IN ROUGH TERRAIN

A westward radial line through northern New Jersey was chosen for observing rough-terrain effects. Local clutter was avoided in order that topographic effects would predominate. The topographic profile is shown in Figure 16, again with measuring locations indicated. Field strength was measured at a height of 30 feet with the unidirectional VHF antenna and the paraboloid UHF antenna. Pictures were observed wherever possible. The measured field strengths are shown in Figure 17.

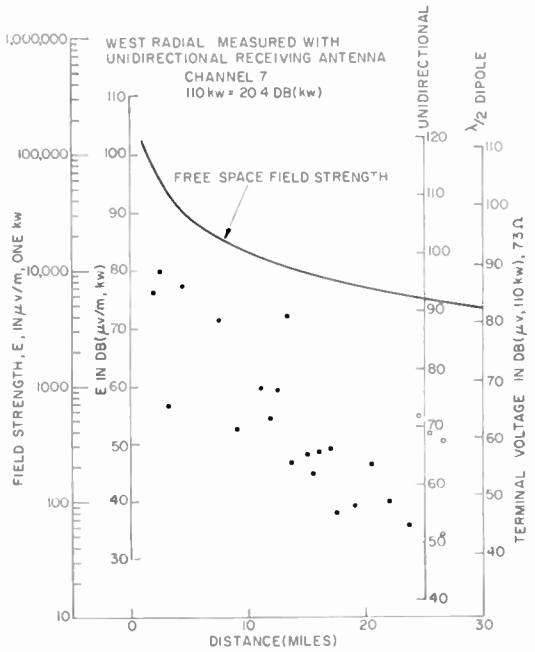
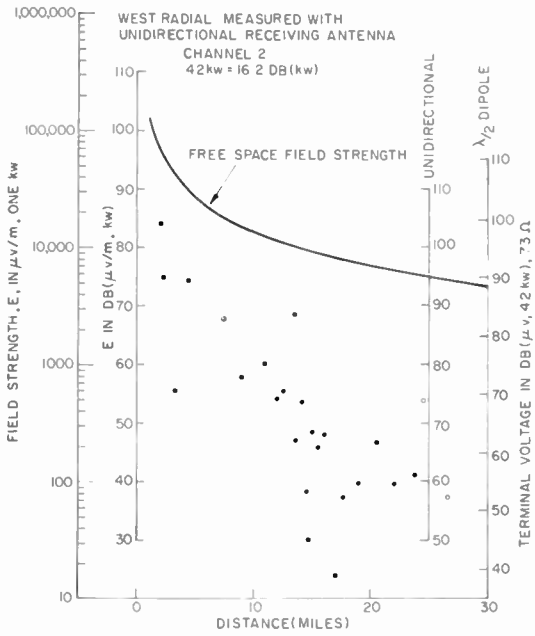


Fig. 17—West radial field strength measured with unidirectional receiving antenna for channels 2 and 7.

From 14 miles and beyond, the UHF field strength was usually too low for direct picture observations. The direct and the mountain-reflected signals were measured with the paraboloid antenna by use of the equalizing pulse. The time separation between direct and reflected pulses thus afforded made it possible to separate the direct and reflected signals for measurement. At a distance of 15 miles, in a shadowed valley between the two Watchung ranges, the UHF reflected

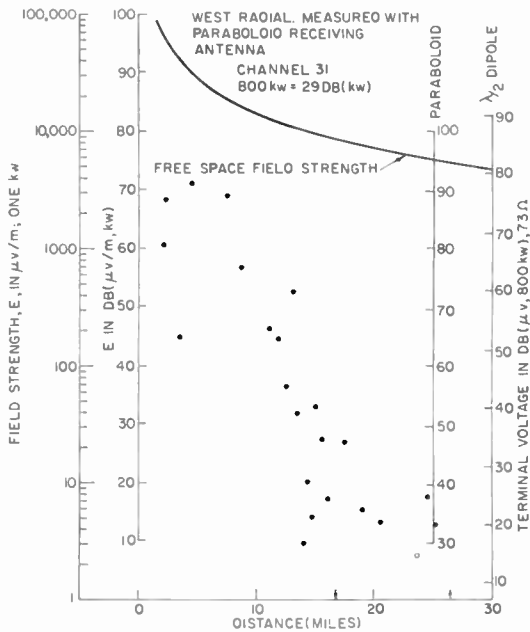


Fig. 17 (cont.)—West radial field strength measured with paraboloid antenna for channel 31.

signal was comparable in magnitude to the direct signal. This means that there would be multipath degradation if the signal level were high enough for picture observation, unless better receiving antennas become available.

Similar pulse measurements for channels 2 and 7, where direct picture observation was possible, corroborated the conclusions. On the basis of the pulse measurements very little multipath degradation was expected and, in fact, very little was seen in the VHF pictures.

Because of the transmitting-antenna azimuth pattern uncertainty of +4 to -8 decibels for channel 31 and the rapid variation of elevation pattern with angle, no attempt was made to extract shadow losses from the measured data. This seriously limited the usefulness of the UHF field-strength data obtainable in rough terrain.

The UHF elevation-pattern problem alluded to earlier is illustrated in Figure 18. In the vicinity of 0° elevation angle, the channel-31 relative field is seen to be substantially lower than the channel-2 relative field as a result of elevation-pattern differences. Over smooth terrain with constant elevation, this difference is relatively unobjectionable. If there are hills (or a gradual rise away from the transmitting antenna) of the same order of magnitude as the transmitting antenna height, the pattern difference has serious consequences, as illustrated in Figure 19. The antenna elevation patterns are superimposed on spherical-earth coordinate paper. Because the elevation scale is exaggerated relative to the distance scale, the angle scale is distorted. However, propagation rays appear as straight lines. In the example shown, a 500-foot hillcrest at 17 miles receives maximum radiated power from the broad channel-2 elevation pattern. The narrower channel-31 pattern is down 10 decibels at the same crest. In addition, the channel-31 transmission will suffer greater diffraction loss than the lower-frequency channel-2 transmission.

UHF RECEIVING-ANTENNA EFFECTIVE GAIN

High receiving-antenna gain is possible with physically realizable antenna sizes; it is particularly desirable for UHF. The receiver terminal voltage for a given field strength is inversely proportional to frequency when $\lambda/2$ dipoles are used. Since a UHF $\lambda/2$ dipole is physically much smaller than a low-VHF $\lambda/2$ dipole, it is reasonable to use an array of dipoles (or the equivalent) for UHF reception. Since large-aperture antennas depend upon a uniform field distribution for gain, their effectiveness will probably be reduced in cluttered surroundings.

An experiment was performed on Long Island to compare the effective gain of a corner reflector (5-square-foot aperture) and a paraboloid (31-square-foot aperture). As a practical matter, installation technicians cannot be expected to explore in height above rooftops. Therefore a fixed height (10 feet) above average roof level was used for the comparison. The measurements were made in the street where fields are probably no less uniform than above rooftops.

The measured free-space gain of the paraboloid and the corner-reflector antennas are, respectively, 13 and 7.7 decibels referred to a $\lambda/2$ dipole. Thus, in a uniform field, the paraboloid gain is 5.3 decibels higher than the corner-reflector gain. The measured median gain of paraboloid over corner reflector antenna in cluttered surroundings was 2.3 decibels. This means that high gain UHF receiving antennas may in fact be expected to have reduced effectiveness in cluttered surroundings.

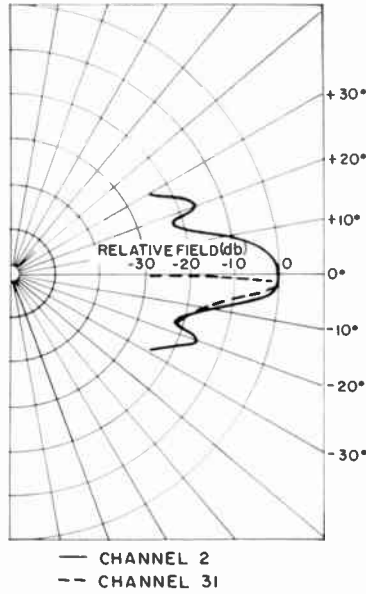


Fig. 18—Elevation patterns, channels 2 and 31.

CONCLUSIONS

In Manhattan below 110th Street, a smooth-terrain extremely built-up area, there was no frequency dependence apparent in the subjective picture ratings based on multipath degradation. Rooftop reception was of poor quality, and the multipath degradation was highly

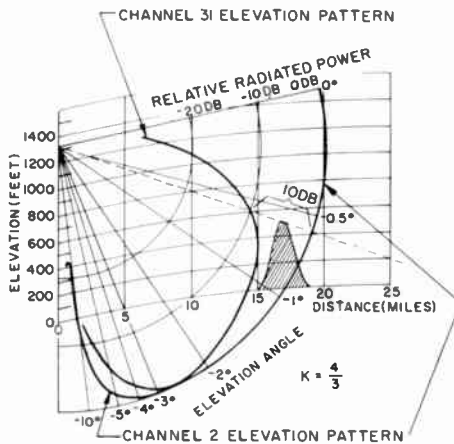


Fig. 19—Elevation patterns superimposed on smooth, spherical-earth coordinates.

unpredictable for specific locations even in most line-of-sight locations. Indoor reception was very poor as a result of high direct-path attenuation and the consequent multipath degradation. Color pictures in Manhattan below 110th Street were rated even poorer on the basis of multipath degradation than monochrome pictures.

In a six-story apartment area in smooth terrain, the multipath degradation was only moderate even with indoor antennas. In two-story-dwelling areas the degradation was very slight. Again there was no frequency dependence.

The median terminal voltage with outdoor receiving antennas was adequate on all frequencies in the multipath-troubled part of Manhattan. In smooth terrain the useful distance ranges for residential areas were about 55 miles on channel 2, 60 miles on channel 4, over 60 miles on channel 7, and 48 miles on channel 31. This was based on actual average radiated powers on the elevation pattern maxima of 42, 30.2, 110, and 800 kilowatts for channels 2, 4, 7, and 31, respectively. The present state-of-the-art noise figures from Table V were assumed. These are 5, 5, 5, and 10 decibels for the respective channels.

The west radial illustrates the rough-terrain problems of UHF television. With loss both from shadowing and from the narrowness of the transmitting-antenna elevation pattern, the field strengths were far below useful level at all distances beyond 14 miles except on line-of-sight crests. Approximately twice this range was satisfactorily served by the VHF systems. There was evidence in hilly terrain of multipath degradation more severe on the UHF channel 31 than on the lower frequency channels.

The high-gain receiving antennas which are needed for UHF use in rough terrain or for extending the fringe-area range in smooth terrain fail to realize their free-space gain by a substantial margin. In areas with building heights as variable as Manhattan below 110th Street, high-gain UHF receiving antennas are moderately effective in reducing multipath degradation, but their orientation is excessively critical.

ACKNOWLEDGMENT

A group of RCA Service Company engineers performed the field measurements. Special test signals were furnished by the Columbia Broadcasting System (channel 2), the National Broadcasting Company (channel 4), the American Broadcasting Company (channel 7), and WPIX Inc. (channel 11). The fullest cooperation was enjoyed from the operating staff of the channel 31 station, WUHF, the Federal Communications Commission engineering staff, and the several RCA Service Company branches in New York City.

It is convenient to transform the circuit of Figure 1 to its series equivalent shown in Figure 2, where the following relations apply:

$$r_e = \frac{r}{1 + Q^2}, \quad Q = \frac{r}{X}, \quad X = \frac{X_b X_c}{X_b + X_c}, \quad (1)$$

$$X_e = \frac{Q^2}{1 + Q^2} X. \quad (2)$$

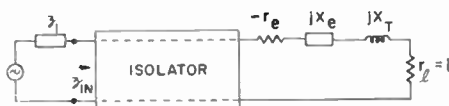


Fig. 2—Series equivalent circuit of Figure 1.

If $Q^2 \gg 1$, the above equations reduce to

$$r_e \cong \frac{r}{Q^2}, \quad (1a)$$

$$X_e \cong X. \quad (1b)$$

Equation (1a) demonstrates that a high-impedance diode may be used to generate the required low impedance. Also, the variation of r_e with Q aids in deactivating the diode off resonance.

The available power gain of the device with $z_1 = 1$ is given by

$$A = \frac{1}{\left(1 - \frac{r_e}{2}\right)^2 + \left(\frac{X_e + X_l}{2}\right)^2}. \quad (3)$$

The gain reaches its maximum value at a frequency slightly off resonance, which condition is defined by $X_e + X_l = 0$.

STABILITY

Stability requires that the Laplace-transformed equations describing the system be free of roots in the right half s plane. A rigorous

approach to the circuit of Figure 1, however, is complicated by the nonreciprocal nature of the isolator. Consequently, an approximate analysis is used. The experimental results given later bear out the adequacy of the analysis.

An unstable amplifier with no input voltage applied exhibits either a growing exponential or growing sinusoidal waveform at all points in the circuit. Unless Q is very small, the first type of instability will not be observed, since the two reactances shunting the negative resistance contribute large additive positive damping along the positive real axis of the s plane. Hence, only the second type of instability leading to distorted sinusoids is troublesome. If the harmonic content of the oscillation is not excessive, an application of Kirchoff's law leads to the conclusion that the loop impedance at any point in the circuit is nearly zero at the fundamental frequency. A vanishing loop impedance is impossible, however, if the real part of the input impedance is positive, for then the loop impedance $z_1 + z_{in}$ seen at the input terminals will have a positive real part. Consequently, it is necessary to demonstrate only that z_{in} has a positive real part at all frequencies, ω , to ensure unconditional stability. This condition should be satisfied for all possible average values of the nonlinear resistance, r . If biasing at the point of inflection is assumed, only values of r greater than the minimum need be checked. This, in essence, is a check for large-signal oscillations (or alternatively, for roots off the $j\omega$ axis in the right half s plane). z_{in} and the input reflection coefficient, Γ_{in} are related by

$$\Gamma_{in} = \frac{z_{in} - 1}{z_{in} + 1} = \frac{r_{in} - 1 + jX_{in}}{r_{in} + 1 + jX_{in}}. \quad (4)$$

It is noted that the conditions $r_{in} > 0$ and $|\Gamma_{in}|^2 < 1$ are equivalent. Consequently, the criterion reduces to $|\Gamma_{in}|^2 < 1$ or, in terms of decibels, $P_1 = 10 \log_{10} |\Gamma_{in}|^2 < 0$. P_1 is made up of two components: the power reflected at the diode, P_D , and that lost in the ferrite, P_F . The latter quantity is the sum of forward and reverse losses in the isolator. Finally, then, the criterion for unconditional stability may be expressed as

$$P_D < P_F \text{ for all } \omega. \quad (5)$$

P_F is obtained experimentally, while P_D is easily shown to be

$$P_D = 10 \log_{10} \frac{1}{1 + \frac{4(1 + Q^2 - r)}{(r + QX_t)^2 - X_t^2}}. \quad (6)$$

It is seen from Figure 1 that if $X_b = \infty$, $z_{in} \rightarrow -r + 1 < 0$ as $\omega \rightarrow 0$, since low-frequency ferrite absorption is negligible. Equation (5) will then be violated. Therefore, X_b must be chosen to effectively short-circuit the diode at low frequencies, while permitting high gain in the passband.

In the following analysis, X_b and X_t are assumed to be ideal inductances. If, at frequencies much below diode cutoff, this is not the case, instabilities not predicted by the theory may result. For a given diode, X_b determines r_e at a specified frequency, and X_t is adjusted to produce the desired resonance. The three reactances produce two resonances. It is assumed that the region of high gain is near the upper resonant frequency, ω_0 , i.e., $r_e \cong 2$ at $\omega = \omega_0$. In the following equations, which are derived in a straight-forward manner, $\rho = \omega/\omega_0$, $\omega_1 =$ the frequency at which X has a pole, $a = \omega_0/\omega_1$, and $Q_0 = Q$ at ω_0 .

$$Q = \frac{\left(a^2 \rho - \frac{1}{\rho} \right) Q_0}{a^2 - 1}, \quad (7)$$

$$X_t = \frac{-rQ_0\rho}{1 + Q_0^2}. \quad (8)$$

Equations (7) and (8) were evaluated for $a = 1.3$, $r = 8.5$, $Q_0 = -2$ (this gives 20 decibels maximum gain) and substituted in Equation (6). The result is shown in Figure 3, which also includes P_P for a typical broad-band isolator. Note that Equation (5) is satisfied for all ω . It may be demonstrated that Equation (5) is satisfied even more easily for $r > 8.5$. One may expect, therefore, that the amplifier is unconditionally stable.

EXPERIMENTAL RESULTS

A 0.5-ma diode, its tuning element, and bias coil were mounted at the end of a Sperry D44L4 isolator which provides significant isolation over a 25 per cent bandwidth. It should be noted that isolators with bandwidths up to an octave are available. With diode and inductances chosen to approximate the values of parameters given above, the am-

plifier was tuned to 1040 mc where it exhibited a 3-decibel bandwidth of 40 mc and a maximum gain of 20 decibels. It was verified that the amplifier was indeed unconditionally stable. The use of a broader band isolator (or circulator) and multiple-tuning techniques would, in theory, provide a bandwidth increase of nearly an order of magnitude.

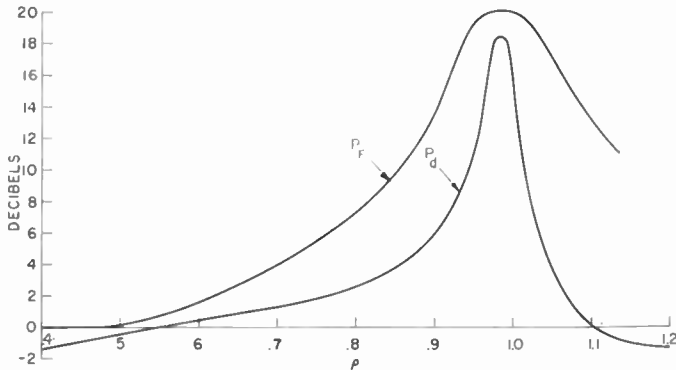


Fig. 3—Characteristics of isolator and diode circuit.

WIDE-BAND AMPLIFICATION

In both the one-port and two-port amplifiers, effective nonreciprocity must be provided over a bandwidth considerably in excess of the amplifier bandwidth if unconditional stability is to be guaranteed. Though this excess may be narrowed by the use of more-sophisticated stabilizing circuits (e.g., multiple-tuned circuits) to achieve truly wide bandwidths, means of stabilization other than or in addition to nonreciprocity, must be employed.

Attention naturally focuses on the effect of distributing the tunnel diodes. One means of doing this is by cascading stages and providing isolation between them. However, the degree to which the gain-bandwidth product may be increased in this manner is limited. Also, the performance of the multistage amplifier is limited, ultimately, by the nonideal nature of the isolators.

Another means of distributing the gain is by incorporating the diodes in a broadband structure, thereby modifying the propagating characteristics. The concept of a distributed negative-resistance transmission line has previously held interest for engineers. An amplifier

containing distributed varactors⁴ is known to result, under proper conditions, in greatly increased bandwidths. In the following, some of the properties of the distributed tunnel-diode line are discussed; particular attention is focused on the unique stability problems associated with it.

Consider the amplifier of Figure 4 where a transmission line is evenly loaded with diodes spaced considerably closer than the quarter wavelength corresponding to the diode cutoff frequency, so that the assumption of a continuous admittance distribution is valid. The inductance and capacitance represent the distributed parameters of the line, and y_a is a distributed stabilizing admittance which, for the time being, will be ignored. The equivalent circuit is probably best realized

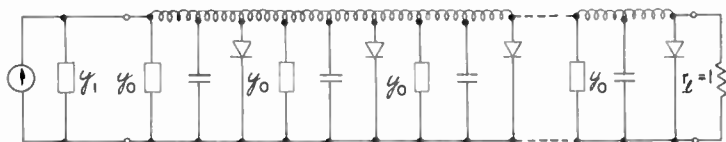


Fig. 4—Distributed tunnel diode amplifier.

with a microstrip structure, the strip separation of which is equal to the height of the diode package. Other broad-band structures have their own specific advantages.

The noise performance of the tunnel-diode line has been independently explored by Chang⁵ and Hines.⁶ They found the noise figure to be comparable to that of the analogous lumped amplifier. Some characteristics of a similar structure were discussed by Hines.⁶ Attention is now turned to the properties of gain, gain stability, bandwidth, and stability with respect to spurious oscillations. In the following, L , C , and $-G$, represent the per-unit-length inductance, capacitance, and conductance (C also includes the diode capacitance). The relations are given in terms of the normalized complex frequency, $s = (C/G)S$, and

⁴ L. A. Blackwell and K. L. Kotzebue, *Semiconductor Diode Parametric Amplifiers*, p. 85, Prentice-Hall, Inc., Englewood Cliffs, New Jersey, 1961.

⁵ K. K. N. Chang, "Theory of a Negative-Resistance Transmission Line Amplifier with Distributed Noise Generators," *Jour. Appl. Phys.*, Vol. 31, No. 5, p. 871, May 1960.

⁶ M. E. Hines, "High-Frequency Negative-Resistance Circuit Principles for Esaki Diode Applications," *Bell System Tech. Jour.*, Vol. 39, No. 3, p. 477, May 1960.

normalized conductance, $g = G/G_0$, $G_0 = \sqrt{C/L}$. The diode inductance and positive resistance is neglected on the basis that since the gain per diode will be very low, the diodes used will be of high junction impedance.

$$\gamma = \text{propagation constant} = \alpha + j\beta = \sqrt{(-G + SC)SL} = g\sqrt{(s-1)s}, \quad (9)$$

y_c = normalized characteristic admittance

$$= \frac{1}{G_0} \sqrt{\frac{-G + SC}{SL}} = \sqrt{\frac{s-1}{s}}. \quad (10)$$

The performance at real frequencies is found by letting $s = j\rho$. For the present, only the nature of γ and y_c in the pass band of the amplifier, which is defined as $\rho \gg 1$, is of concern. Equations (9) and (10) show that

$$\gamma \cong \frac{-g}{2} + jg\rho, \quad (9a)$$

$$y_c \cong 1. \quad (10a)$$

Assuming the device to be terminated at each end in a normalized resistance of unity, which condition will result in maximum power output, the available power gain is

$$A = e^{-2\alpha l} = e^{g_l} = e^{g_t}, \quad (11)$$

$$= 4.3 g_t \text{ decibels} \quad (11a)$$

where l is the length of the line and $g_t = gl$, the total normalized negative conductance.

An important feature of the distributed line is its superior gain stability. One measure of this is the ratio of the fractional change of the gain to that of the diode negative resistance (or conductance) which, for the lumped amplifier previously considered is, from Equations (1), (1a), and (3),

$$\left| \frac{\frac{dA}{A}}{\frac{dr}{r}} \right| \cong 2A^{1/2}. \quad (12)$$

Equation (12) assumes high gain ($r_0 \cong 2$) and operation at resonance. For the distributed circuit of Figure 4, Equation (11) gives

$$\left| \begin{array}{c} \frac{dA}{A} \\ \frac{dr}{r} \end{array} \right| = \frac{dA}{A} = \ln A. \quad (13)$$

For a power gain of 30 decibels ($A = 1000$), Equations (12) and (13) demonstrate that the distributed amplifier is more than nine times less gain sensitive than the lumped amplifier. Therefore, the gain variations resulting from fluctuations of temperature, bias supply, or a change of diodes, will be diminished. Now, attention is turned to the matter of bandwidth. At lower frequencies, where $\rho \gg 1$ is violated, the gain is less than that indicated by Equation (11). This leads to a lower 3-decibel bandwidth frequency, ρ_1 , which corresponds to an actual angular frequency $\omega_1 = (G/C)\rho_1$. It is seen that in principle ω_1 can be lowered as much as desired for the same maximum gain by making G smaller and l correspondingly larger; i.e., by using an infinite length of line and perturbing it with an infinitesimal G , the bandwidth can be extended to d-c. However, the precise relation for ω_1 will not be derived since this is materially affected by the stabilizing admittance, y_0 .

The upper limit on bandwidth is determined by the diode cutoff frequency rather than by any resonant characteristic of the system. The device, therefore, can be made to exhibit the exceedingly large bandwidths characteristic of traveling-wave systems.

STABILITY OF THE DISTRIBUTED TUNNEL-DIODE AMPLIFIER

It has been shown that the distributed tunnel-diode line appreciably outstrips the lumped amplifier as regards the gain-bandwidth product and gain stability. The practical significance of the device, however, ultimately rests on its stability performance. Again, the goal is unconditional stability. A one-port circuit is unconditionally stable *if and only if the real part of the normalized input admittance is positive over the entire right half of the s plane*. (The circuit of Figure 4 qualifies as one-port since the load is assumed invariant.) This is not, in general, the simplest criterion for unconditional stability, but it is the most convenient for present purposes.

Returning to the lumped amplifier, it is seen from Equation (3)

and Figure 2 that since $r_e \cong 2$ in the pass band, the criterion for unconditional stability cannot be satisfied without the isolator. This, however, is not true for the distributed line, since Equation (10a) indicates that the input conductance is positive in the pass band and, in fact, for all s such that $|s| \gg 1$. Put in another way, no oscillation can occur in the pass band if at least one end is well terminated, since any spurious currents or voltages will travel smoothly toward the well-terminated end (either directly or by reflection from the other end) and will be absorbed. Regenerative action in the pass band is, therefore, impossible. If the load does not present a good constant match in the pass band, it should be isolated from the line so that Equation (10a) is still valid. The importance of a proper termination at the output increases with increasing gain.

It is interesting to note that if the line contains both series and shunt negative components, $-R$ and $-G$, Equation (10a) is precisely valid at all s if $L/R = C/G$. If the series negative resistance is also provided by tunnel diodes, however, the line will be unstable. The instability results from the increase in nonlinear R with signal level which causes the gain to run away.

Returning to the structure of Figure 4, it has been shown that the line is stable in the pass band. Attention now turns to the lower frequencies (or, more precisely, the region of the s plane near the origin). It can be seen from Figure 4 that if $y_a = 0$, the amplifier input admittance at $s = 0$, which is a point of entrance to the right half plane, is $y_{in} = 1 - g_t$. This value is negative if the gain is greater than 4.3 decibels. Clearly, then, some form of stabilization is required to satisfy the criterion for unconditional stability.

In the lumped amplifier (Figure 1) it was possible to insure against low-frequency instabilities by shunting the active element with a single stabilizing impedance. Since the transmission-line amplifier may be approximated by a lumped circuit at low frequencies, it seems reasonable to determine whether or not it too can be stabilized with a single element. Consider the amplifier shunted at its input by a stabilizing admittance, y_b , with which it is hoped the new input admittance, $y'_{in} = y_b + y_{in}$, can be made to satisfy the criterion. It is easily shown that along the real axis ($s = \sigma$) y_{in} takes the form

$$y_{in} = \frac{1 + \sqrt{\frac{\sigma - 1}{\sigma}} \tanh g_t \sqrt{(\sigma - 1)\sigma}}{1 + \sqrt{\frac{\sigma}{\sigma - 1}} \tanh g_t \sqrt{(\sigma - 1)\sigma}} \quad (14)$$

Equation (14) indicates that for $\sigma > 1$, $y_{in} > 0$, and this range is passive even if no stabilizing admittance is used. For $0 < \sigma < 1$, Equation (14) is conveniently rewritten as

$$y_{in} = \frac{1 - \sqrt{\frac{1-\sigma}{\sigma}} \tan g_l \sqrt{(1-\sigma)\sigma}}{1 + \sqrt{\frac{\sigma}{1-\sigma}} \tan g_l \sqrt{(1-\sigma)\sigma}}. \quad (14a)$$

From Equation (14a) it is seen that for reasonable gain there are poles of y_{in} along $0 < \sigma < 1$, the number of poles depending on g_l . Points may therefore be found along the σ axis, near the poles, where y_{in} is real, negative, and indefinitely large. The same must be true, then, of y_{in}' . Similar conclusions result if one attempts to relocate the stabilizing admittance. Consequently, the criterion for unconditional stability can not be met with a single stabilizing element. Unconditional stability can be assured only if the stabilization is distributed along with the negative conductance, as in Figure 4. The stabilizing admittance, y_a , must be such as to deactivate the line for small $|s|$ while leaving it undisturbed in the pass band. Clearly, a high-pass admittance (such as a lossy coil) is called for. Sharper cutoff admittances may be used in order not to infringe appreciably on the gain at the low end of the pass band. Hence, by distributing the stabilization as well as the active elements, unconditionally stable, wide-band tunnel-diode amplification is made possible.

ACKNOWLEDGMENTS

The author wishes to acknowledge helpful discussions with K. K. N. Chang, R. Braden and R. Hughes relating to this work.

SCALE-MODEL INVESTIGATIONS OF ELECTROMAGNETIC WAVE PROPAGATION OVER NATURAL OBSTACLES*

BY

M. P. BACHYNSKI

RCA Victor Research Laboratories
Montreal, Canada

Summary—Scale-model techniques have been developed whereby the effect of natural obstacles on the propagation of electromagnetic waves over the surface of the earth can be investigated within the laboratory. The major advantage of the scale-model laboratory experiments has been the ease with which control can be exercised over the pertinent parameters. As a result, the influence of critical factors could be specifically ascertained.

The influence of obstacle shape (crest and profile) and the effect of the orientation of the radiated electromagnetic fields (angles of incidence and polarization) on the received power, as well as various cross-polarization phenomena have been experimentally determined. Comparisons of diffraction by knife edge, wedge, cylindrical and conical obstacles have been made. For obstacles with sharp crests (e.g., knife edges) there is little distinction between vertically and horizontally polarized fields measured at some distance from the obstacle. Profound polarization effects occur for obstacles with large smooth crests, with vertically polarized fields producing more power at the receiver in all cases. The effect of oblique incidence of electromagnetic energy on an obstacle is equivalent to changing its radius of curvature. Some measurements on the effects of ground reflections, rough diffracting surfaces and surface conductivity have also been made.

Finally, a considerable bibliography on theories of diffraction of electromagnetic waves by various obstacles and on field measurements of "obstacle gain" is included.

INTRODUCTION

NUMEROUS DIFFICULTIES are encountered in carrying out full-scale experiments on electromagnetic wave propagation over natural obstacles. The greatest difficulty is that it is virtually impossible to vary the most important parameters such as the size, shape, and location of the obstacle. The topography and electrical constants are fixed for a given terrain and cannot be altered. The only variable which can be changed systematically with relative

* This work has been supported by the Air Force Cambridge Research Center under Contract AF19(604)-3049 and by the RCA Victor Research Laboratories, Montreal.

ease is the height of the terminal antennas. In addition, the establishment of suitable experimental transmitter-receiver stations is extremely costly and is usually never attempted except for actual "site testing" of questionable propagation paths. In general, great effort is devoted to avoid routes which may cause difficulty, and some general "rules of thumb" based on past experience have evolved on the effect of natural obstacles on wave propagation. Finally, random features of the terrain and atmosphere may contribute effects which are difficult to evaluate.

In order to formulate a proper theory of the propagation of electromagnetic waves over natural obstacles, controlled experimental conditions are required both to guide the theoretical approach and to test the theoretical predictions. Scale-model experiments conducted within the laboratory are particularly suitable for the measurement and evaluation of specific critical factors. The major advantage of the scale-model techniques is the ease with which control can be exercised over the pertinent parameters such as the obstacle shape, geometry of the propagation link, frequency, polarization, and antenna directivity. Furthermore, model experiments are relatively inexpensive. In general, the geometries associated with model propagation links are more severe (i.e., come closer to violating the theoretical assumptions) than those encountered in the field. Consequently, theoretical predications satisfying model measurements should be even more applicable to idealized full-scale situations. Although the effects of certain parameters such as surface roughness and electrical properties of the obstacle can not be directly scaled, experiments to determine limiting effects of these variations can be readily performed and the bounds ascertained within which practical cases will occur.

This paper presents a summary of scale-model measurements which have been made in order to study the effect of obstacle shape (crest and profile) and the effect of the orientation of the radiated electromagnetic fields (angles of incidence and polarization) on the power received behind a dominant obstacle. Comparisons of diffraction by knife edge, wedge, cylindrical and conical obstacles are shown, as well as some measurements on the effects of ground reflections, rough diffracting surfaces and surface conductivity on electromagnetic wave propagation. Comparison of the model measurements with predictions of theories based on simplified concepts are made, and satisfactory agreement obtained. In addition, a considerable bibliography on theories of diffraction of electromagnetic waves by various obstacles and on field measurements behind dominant natural obstacles (obstacle gain) is included.

SCALE-MODEL TECHNIQUES

Investigations of diffraction by various obstacles (knife edges, wedges, cylinders, cones) have been carried out on perfectly conducting models using k-band (24,000 mc) frequencies. A schematic of the general experimental arrangement is shown in Figure 1a. A 2K33 klystron was used as the source of r-f energy. The transmitted signal, modulated at 1000 cps, was crystal detected and the rectified signal fed directly into an automatic recorder. Small horns with very similar patterns in both the E and H planes of polarization were used for the transmitting and receiving antennas. The measurements obtained with the receiving horn were checked against those obtained with a dipole and found to be identical for most of the range of scattering angles investigated in these experiments. In regions where this is not the case, experimentally determined correction factors for the illumination were applied when comparing theory with measurements. In some cases in order to eliminate the effect of transmitting and receiving antenna patterns on measurements of the power variation with lateral position of the obstacle, the obstacle was scanned across fixed transmitter-receiver sites. In the other measurements, the receiving antenna was moved. The motion of the receiver probe was directly coupled to the chart drive of the recorder so that scans of received power against probe position could be directly obtained. A picture of a typical experimental set-up is shown in Figure 1b.

Measurements on a rectangular diffracting knife edge served as a comparison for the results obtained experimentally for the other obstacles. The knife edges consisted of aluminum sheet 1/16 inch thick, sharpened at the edges; the wedges were also of aluminum sheet, while the half cylinders were constructed from thin, conducting aluminum foil, sufficiently reinforced to form smooth, cylindrical surfaces. Care was taken to make the knife edge and cylindrical surfaces sufficiently long so that end effects were negligible.

The major parameters of interest in the study of electromagnetic wave propagation over natural obstacles are shown in Figure 1c. These include the apex angle (ϕ) of the obstacle as viewed from the receiving site looking towards the transmitter, the scattering angle (ψ), the angle of obliqueness (ξ), the slant half-angle of the obstacle (τ) as well as the radius of curvature of the obstacle at the point of incidence (a_e), and the transmitter and receiver distances to the obstacle (d_1 and d_2 , respectively). The incident wave is characterized by its wavelength (λ) and by the polarization of the electromagnetic fields. In addition, consideration must be given to the conductivity and roughness of the

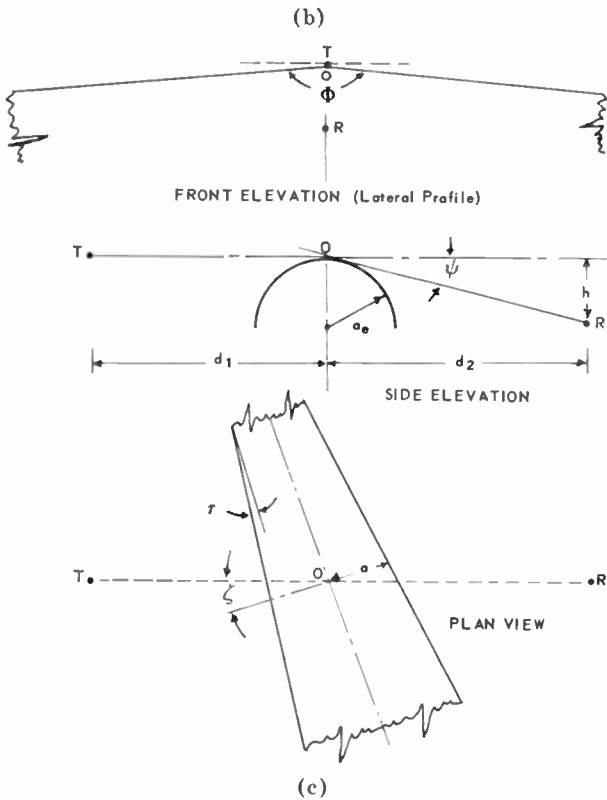
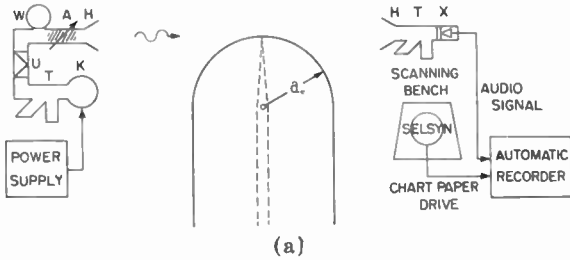


Fig. 1—(a) Schematic diagram of the experimental arrangement (A = attenuator, H = transmitting horn, K = klystron, T = E-H tuner, U = isolator, W = wavemeter, X = crystal detector); (b) scale model experimental arrangement; and (c) geometrical parameters of interest.

surface of the diffracting obstacle and to the nature of the intervening surface between the obstacle and the transmitter, receiver locations.

EXPERIMENTAL INVESTIGATIONS

Lateral Profile Effect

In practice, when it is desired to compute the field diffracted by a dominant obstacle, the obstacle is replaced (in the mathematical sense) by a rectangular knife edge of equivalent height, and since the theory of knife-edge diffraction is well established the computations can be carried through. Thus, scale-model measurements of diffraction by rectangular knife edges serve as a calibration of the experimental techniques and can be used as normalizing values for other shaped obstacles. If the knife-edge profile is not a straight line, then the computations are not straightforward. Furthermore, obstacles encountered under natural conditions have lateral profiles which are far from linear. It is thus of interest to investigate the dependence of the diffracted electromagnetic fields on the lateral profile of the diffracting obstacle.

Experimental studies on the effect of the profile of a dominant obstacle on the diffraction of electromagnetic waves have been conducted using scale-model techniques. In order to eliminate the effect of the crest of the obstacle and hence simplify comparison with theory, knife-edge (zero radius of curvature of the crest) obstacles were used in the investigations.

The variation of diffracted power behind symmetrical triangular knife-edge obstacles with included angle for various scattering angles is shown in Figure 2. In all these measurements, the geometry was such that a straight line from transmitter to receiver would intersect the obstacle on the line which bisects the apex angle. At grazing incidence ($\psi = 0^\circ$) the received power depends only on the included angle of the obstacle. For receiver positions in the shadow region, the diffracted power increases as the included angle of the obstacle decreases. For semicircular knife-edge obstacles, the diffracted power corresponds closely to that behind a rectangular knife-edge (apex angle = 180°) even for the smallest radius of curvature (42.3λ) measured. For the knife-edge obstacle there appears to be little difference in the far-field diffracted power between vertically polarized and horizontally polarized incident fields.

In Figure 3 the variation of diffracted power with scattering angle is shown for differently shaped knife-edge obstacles. Comparison with a rectangular knife edge (180° apex angle) is made, and the enhance-

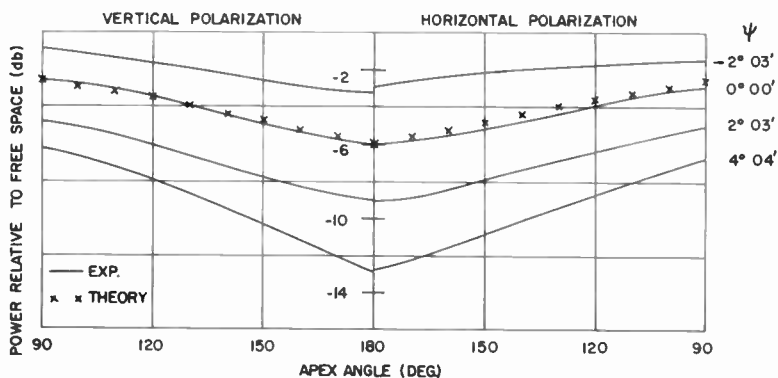


Fig. 2—Power behind triangular knife-edge as function of apex angle of triangle. The points are theoretical calculations. (Transmitter-receiver located directly in line with apex, $d_1 = 150\lambda$, $d_2 = 113\lambda$, $\lambda = 1.25$ cm, $\psi =$ scattering angle.)

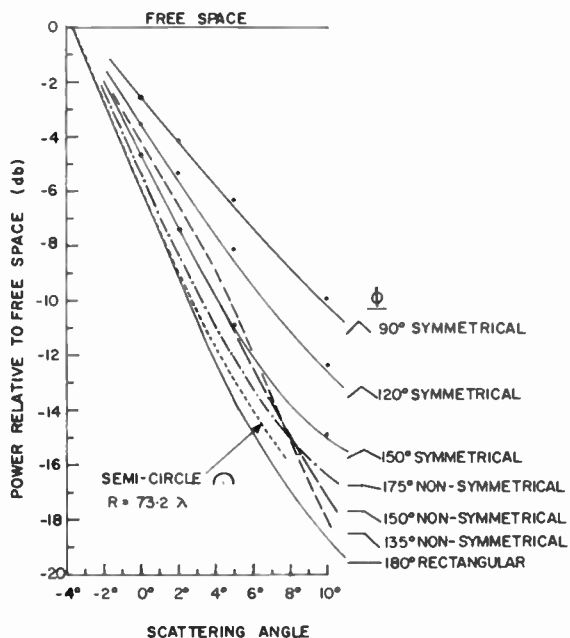


Fig. 3—Power variation with scattering angle (ψ) behind knife-edge obstacles of various shape ($d_1 = 150\lambda$, $d_2 = 113\lambda$, $\lambda = 1.25$ cm.). The points are theoretical calculations.

ment of power resulting from the smaller obstruction presented by a triangular obstacle is apparent. The semicircular obstacle, on the other hand, behaves very nearly like the rectangular knife edge.

A series of measurements on the power distribution behind various knife-edge obstacles indicate positions of power enhancement and also regions of very little power. Figure 4a illustrates the diffracted power

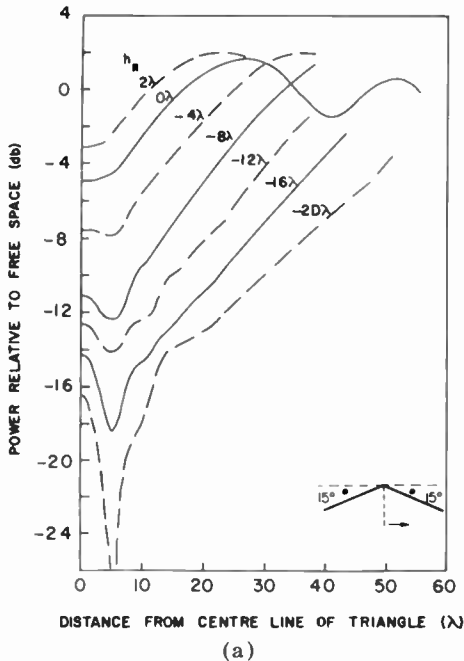


Fig. 4—Power distribution behind knife-edge obstacles ($d_1 = 150\lambda$, $d_2 = 113\lambda$, $\lambda = 1.25$ cm, $h_r =$ receiver position below grazing point, scatter angle $\psi = \tan^{-1}(h_r/113\lambda)$): (a) symmetrical knife edge (horizontal polarization).

behind a symmetrically orientated knife-edge obstacle as function of lateral displacement of the transmitter-receiver from the center line of the obstacle. Of importance is the maximum of power located directly behind the apex of the edge and the extremely sharp and deep minima which occur with lateral displacement especially for the larger scattering angles. This suggests that very "unfavorable" site locations are possible such that when the geometry of the transmission paths locates the receiving terminal in a minimum of the power distribution, low signal strength and rapid fading can result. This occurs even for very modest deviations of the triangular shape from an included angle of 180° as seen from the measurements on the triangular edge of 15°

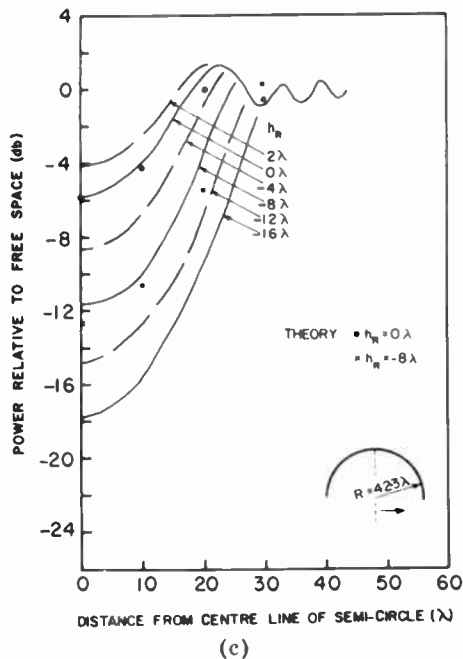
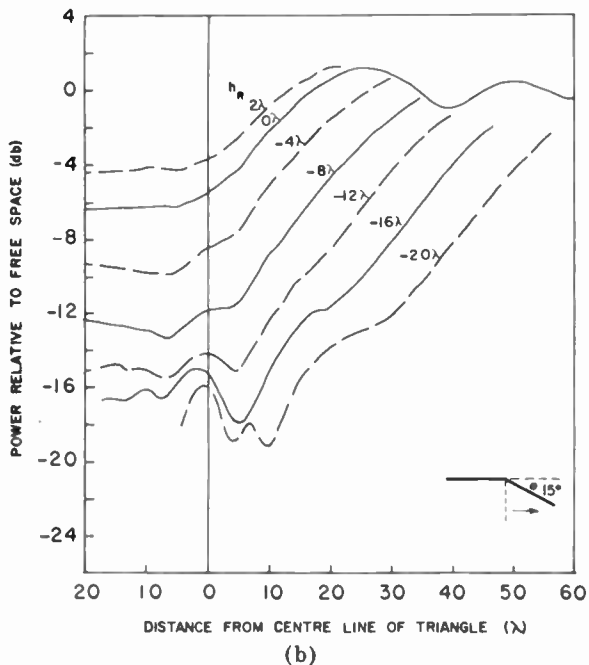


Fig. 4 (cont.)—(b) nonsymmetrical knife edge (vertical polarization), and (c) semicircular knife edge (horizontal polarization).

deviation. For nonsymmetrical obstacles (see Figure 4b) this effect is not quite as pronounced, but does still occur at larger scattering angles. The power diffracted behind a semicircular knife edge (Figure 4c) does not show maxima and minima with lateral displacement, but only a monotonic change. In all cases (both triangular and semicircular knife-edge obstacles) there appears to be little difference in the far-field diffracted power for either vertically or horizontally polarized incident waves.

A comparison of the measured distribution of diffracted electromagnetic energy behind triangular (both symmetrical and nonsymmetrical) knife edges and semicircular knife edges reveals some important practical features. In contrast to the case of a horizontal obstacle, where the received power is independent of lateral position behind the obstacle (except for the distance factor), the profile of the obstacle determines the optimum receiving site, and relatively small changes in receiver position can result in substantial changes in received power.

The Crest Effect

Obstacles occurring in nature do not have crests that have a zero radius of curvature, i.e., they cannot be approximated by knife edges. Thus, the effects of the crests of the obstacle may contribute significantly to the power at the receiving terminal.

Scale-model measurements have been conducted on wedges, circular cylinders and half-cones (i.e., cylinders with uniformly varying radius of curvature) in order to determine the influence of the crest on electromagnetic wave propagation over dominant, natural obstacles.

The effect of the crest is to introduce a profound difference in the power received for incident vertical polarization relative to that received for incident horizontally polarized waves. A plot of received power versus scattering angle is shown in Figure 5 for both polarizations and for wedge angles ranging from 175° to 90° . Mean values of the power are shown. The variations of power for wedges have a strong oscillatory behavior as illustrated in the figure. The undulations are due to the reflections from the wedge faces. The field strengths are greater for vertically polarized waves than for horizontally polarized waves. The signal is strongest for vertical polarization at large wedge angles, while the opposite is true for horizontal polarization. For small wedge angles the effects due to the two polarizations approach each other. Figure 6 shows this effect more vividly; here the received power at grazing (zero scattering angle) is plotted against wedge angle.

The effect of a smooth crest of an obstacle on the diffracted field as determined by the power measured behind a conducting cylindrical mountain of $ka = 239$ ($k = 2\pi/\lambda$, $a =$ crest radius) is shown in Figures 7a and 7b. A large difference exists between the two polarizations,

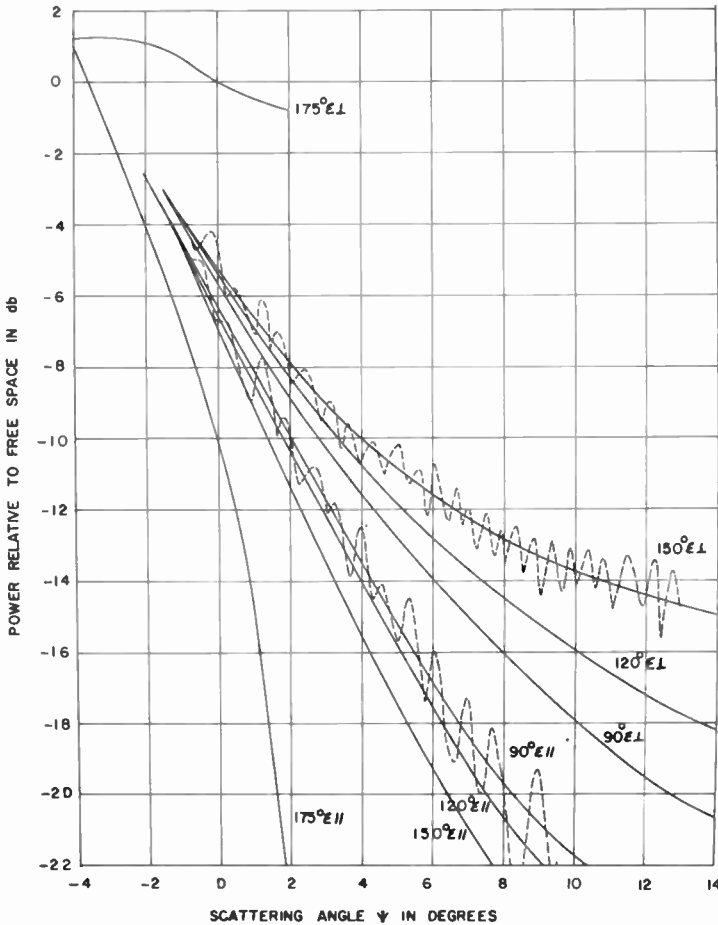


Fig. 5—Power variation with scattering angle (ψ) behind a perfectly conducting wedge. The full lines represent mean values of the power only. The dotted lines represent the actual variation of power ($d_1 = 150\lambda$, $d_2 = 113\lambda$, $\lambda = 1.25$ cm, $\epsilon_v =$ vertical polarization, $\epsilon_h =$ horizontal polarization).

particularly when the mountain is approached. For vertical polarization the field is much stronger than for horizontal polarization. This halo effect is a function of radius of curvature of the crest (in terms of λ) and polarization as is shown in the next measurements (Figure 8) performed with a series of cylindrical mountains of different radii.

For vertical polarization the received power increases with ka , while the reverse is true for horizontal polarization. In addition, the slope of the power variation with scattering (diffraction) angle is essentially the same as for knife edge in the case of vertical polarization, but becomes steeper with increasing ka for horizontal polarization. Thus the region behind the mountain is "brighter" than that behind a knife edge in the case of vertical polarization and "darker" than behind a knife edge for horizontal polarization.

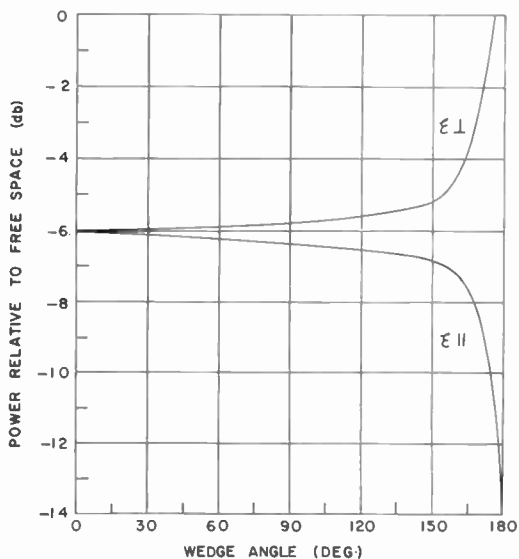
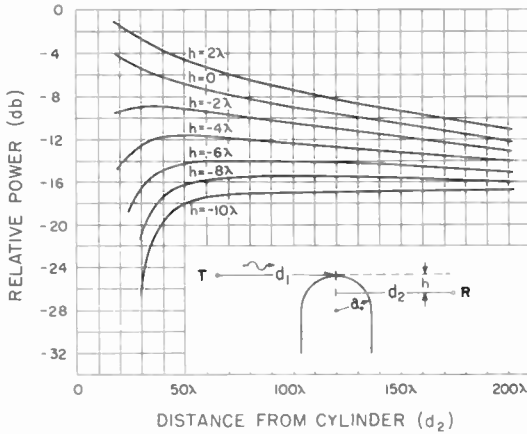


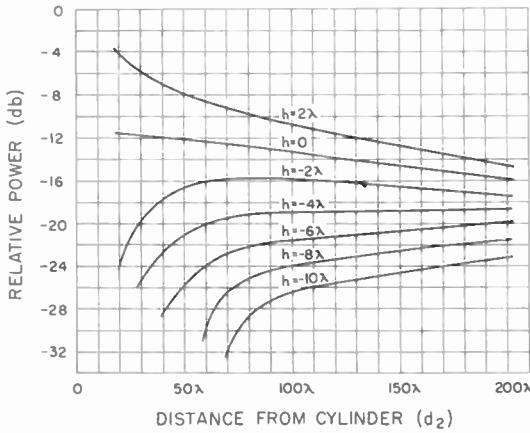
Fig. 6—Variation of power diffracted at grazing incidence ($\psi = 0$) by a perfectly conducting wedge with wedge angle (ϕ).

Figure 9 shows the variation of power behind a conical mountain (half-cylinder with varying radius of curvature) with scattering angle as a function of radius of curvature. The behavior is very similar to that of a cylindrical mountain. Again the received power for vertical polarization increases with increasing radius of curvature, while the reverse is true for horizontal polarization. The variation is smooth, monotonic with no undulations as in the case of wedges. In addition, the slope of the power variation with scattering (diffraction) angle becomes steeper with increasing curvature for horizontal polarization and remains essentially the same as for a knife edge in the case of vertical polarization. The power behind a conducting conical mountain as function of radius of curvature for normally incident electromagnetic waves at the grazing angle is shown in Figure 10. A large differ-

ence between the two polarizations exists with the vertically polarized field which increases with radius of curvature being much stronger than the horizontally polarized field which decreases with radius of curvature.



(a)



(b)

Fig. 7—Power distribution behind a cylindrical mountain ($ka = 239$, $d_1 = 150\lambda$) (a) for vertical polarization and (b) for horizontal polarization.

Oblique Incidence

Of common occurrence in radio engineering is the situation where an obstruction lies at an oblique angle across the path between transmitting and receiving stations. Model measurements have been used to investigate the propagation of electromagnetic energy at oblique

incidence over smooth, perfectly conducting cylindrical obstacles of both uniform and linearly varying radius of curvature.

Measurements of diffracted power as function of angle of obliqueness could be performed by rotating the model about a vertical axis in the vertical plane containing the fixed receiver-transmitter positions and passing through the axis of the model. In this manner, ka_e values

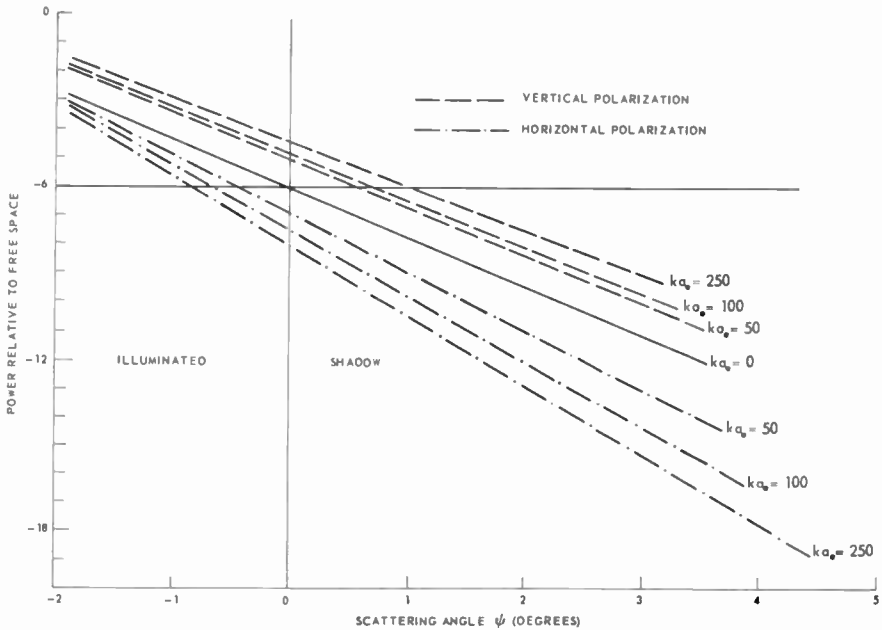


Fig. 8—Variation of power in the far-field behind a cylindrical mountain with scattering angle ψ as function of polarization and radius of curvature (ka).

greater than 2000 could be obtained where a_e is the effective radius of curvature of the obstacle. The sizes of the models permitted investigations for angles of obliqueness of up to 60° from the normal before end effects became important. In addition, power measurements behind obstacles for scattering angle of up to 12° were made.

The power variation at different receiver heights with angle of obliqueness (ζ) is shown in Figure 11 (cylindrical obstacles of uniform radius of curvature) and Figure 12 (cylindrical obstacles of linearly varying radius of curvature).

For vertical polarization, the diffracted power in the receiving space varies with angle of obliqueness such that in the illuminated

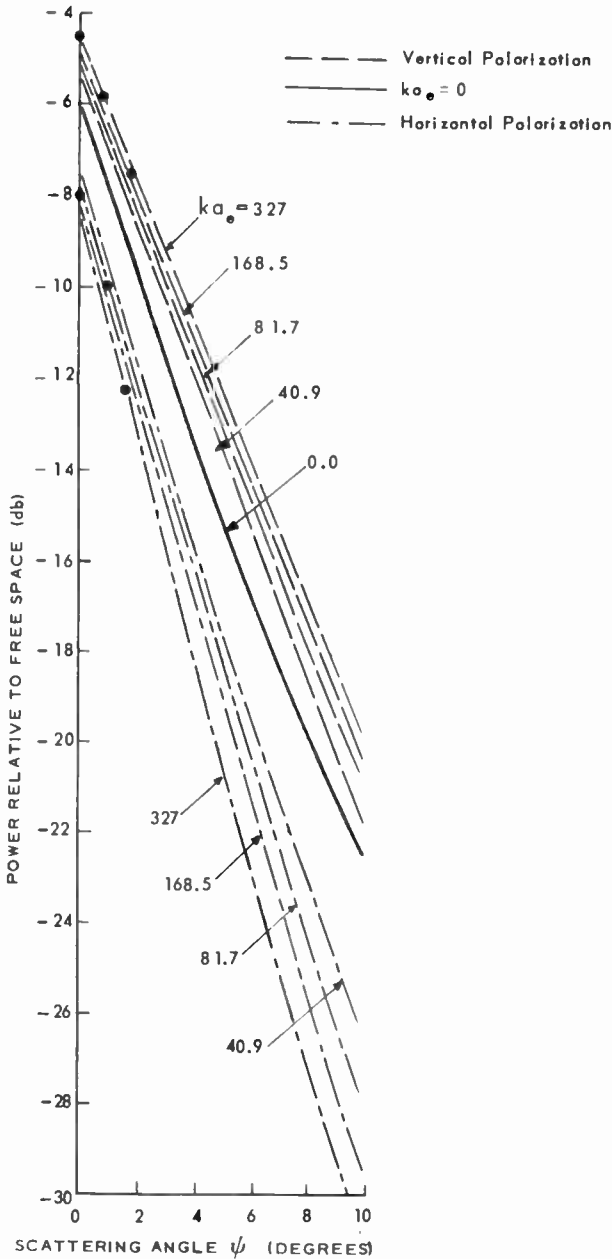


Fig. 9—Variation of power behind a conical mountain with scattering angle as a function of radius of curvature ($d_1 = 150\lambda$, $d_2 = 113\lambda$, $\psi_{ec} = \psi \cos \tau \cos \zeta$; $a_c = a/\cos \tau = 15^\circ$, $\zeta = 0^\circ$). Theoretical points are for $ka_e = 239$.

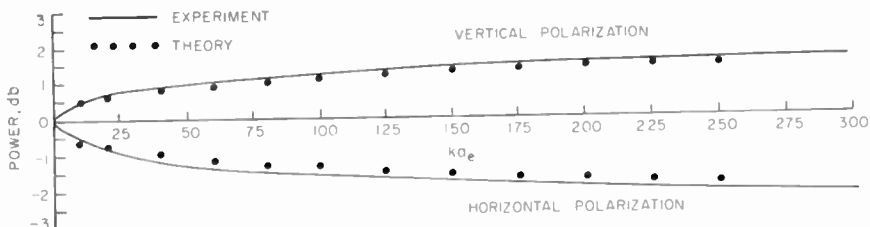


Fig. 10—Variation of power behind a conical mountain at grazing incidence with radius of curvature of the obstacle in the vertical plane containing the transmitting and receiving terminals. ($d_1 = 150\lambda$, $d_2 = 113\lambda$, $\psi = 0^\circ$, $\lambda = 1.252$ cm.).

region ($\psi_{sc} < 0$), the diffracted power increases with angle of obliqueness and increasing radius of curvature. Small values of radius of curvature show little variation with angle of obliqueness. In the “halo” region ($\psi_{sc} \sim 0-5^\circ$) the power increases with increasing angle of obliqueness and increasing radius of curvature. In the shadow region ($\psi_{sc} > 5^\circ$) the power deep in the shadow depends on the value of ka_e . For small ka_e values, the power continues to increase with increasing angles of obliqueness while for large values of ka_e the diffracted power decreases with angle of obliqueness. Alternate regions are possible where the diffracted power is independent of angle of obliqueness.

For horizontally polarized waves incident on the obstacles, the

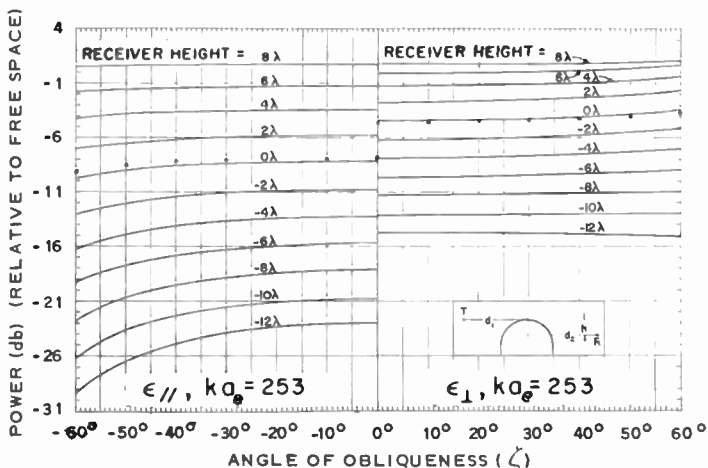


Fig. 11—Power variation with angle of obliqueness for a smooth, perfectly conducting cylindrical obstacle of constant radius of curvature for both horizontal polarization (ϵ_{\parallel}) and vertical polarization (ϵ_{\perp}). ($d_1 = 150\lambda$, $d_2 = 113\lambda$, $\lambda = 1.25$ cm.).

diffracted power behavior is nearly constant with angle of obliqueness in the illuminated region, showing only a small increase at large values of radius of curvature and large oblique angles. In the "halo" region the diffracted power decreases with increasing angle of obliqueness and increasing ka_e values. In the shadow region the power decreases rapidly with angle of obliqueness and increasing effective radius.

Behind a knife edge obstruction ($ka_e = 0$) the diffracted power is independent of both the angle of obliqueness of the incident energy and of polarization.

Comparison of the data for obstacles of constant radius and varying radius of curvature shows that the diffracted power variation with angle of obliqueness is indeed similar provided their effective radii of

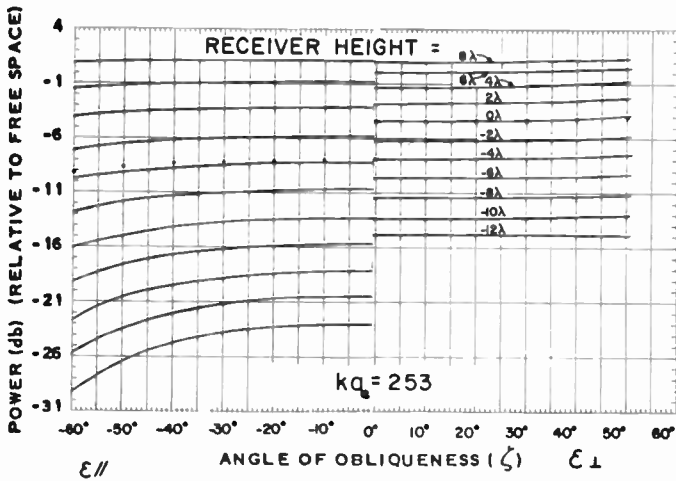


Fig. 12—Power variation with angle of obliqueness for a smooth, perfectly conducting cylindrical obstacle of uniformly varying radius of curvature (15° half cone angle) ($d_1 = 150\lambda$, $d_2 = 113\lambda$, $\lambda = 1.25$ cm).

curvature (a_e) are the same. In all cases the horizontally polarized field results in the diffracted power in the halo and shadow regions being considerably less than for a knife-edge obstruction. The vertically polarized energy, on the other hand, is greater than the values for a knife-edge obstacle in the halo region but can be less than the knife-edge values deep in the shadow region.

The variation of the diffracted power with scattering angle is shown for normal incidence ($\psi = 0^\circ$) and an angle of obliqueness of 60° for obstacles of constant radius in Figure 13a and for obstacles of varying radius of curvature in Figure 13b.

In the illuminated region, the horizontally polarized energy is considerably greater than the vertically polarized energy. The power for a knife-edge obstruction is intermediate to the values for the two polarizations. The effect of oblique incidence is small for either polarization.

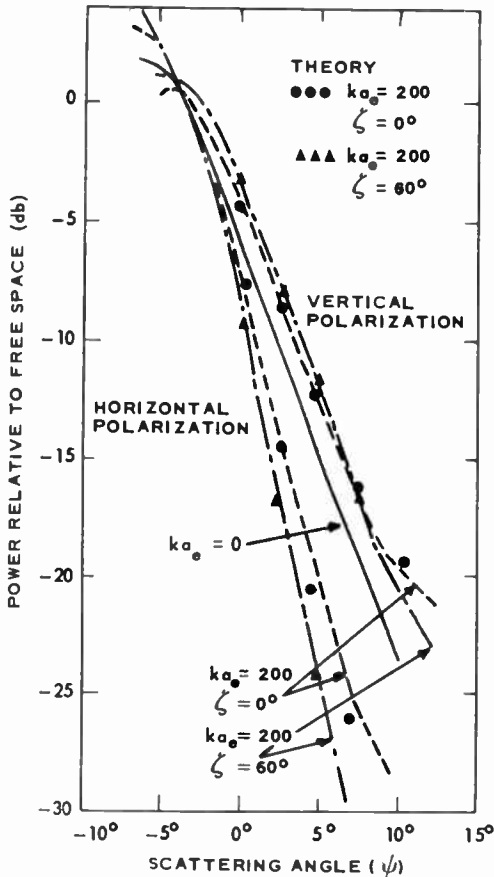


Fig. 13a—Variation of diffracted power with scattering angle for angles of incidence of 0° and 60° . (Obstacles of constant radius of curvature) ($d_1 = 150\lambda$, $d_2 = 113\lambda$, $\lambda = 1.25$ cm.).

For small scattering angles, the diffracted power for vertical polarization is greater at oblique angles, while the reverse is true for horizontal polarization. Comparison with theory shows satisfactory agreement.

At large scattering angles, the vertically polarized energy decreases with angle of obliqueness and becomes *less* than for normal incidence.

The horizontally polarized energy, however, continues to decrease more rapidly with angle of obliqueness. This behavior for large ka_c values has been predicted for normal incidence in earlier publications but not verified experimentally.

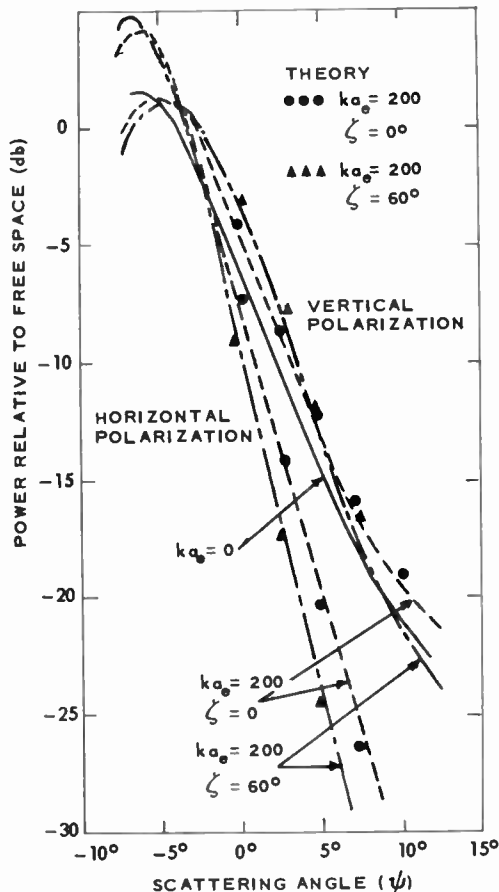


Fig. 13b—Variation of diffracted power with scattering angle for angles of incidence of 0° and 60° (obstacles of uniformly varying radius of curvature: 15° —half cone angle). ($d_1 = 150\lambda$, $d_2 = 113\lambda$, $\lambda = 1.25$ cm.)

Ground Reflections

Thus far only the effects due to the obstacle profile and the crest of the obstacle have been considered. If the intervening terrain between the obstacle and the receiver-transmitter is smooth, then ground reflections will occur and these reflections must be considered in addition to the direct radiation. The ground reflections are taken into

account by considering the reflections to originate from virtual images of the terminal antennas located the same distances below the reflecting surface that the real antennas are located above the reflecting surface. As a result there are four possible paths—direct transmitter to receiver, one reflection on receiver side, one reflection on transmitter side, and a reflection on each side of the path—by means of which energy from the transmitter reaches the receiver. The effect of the

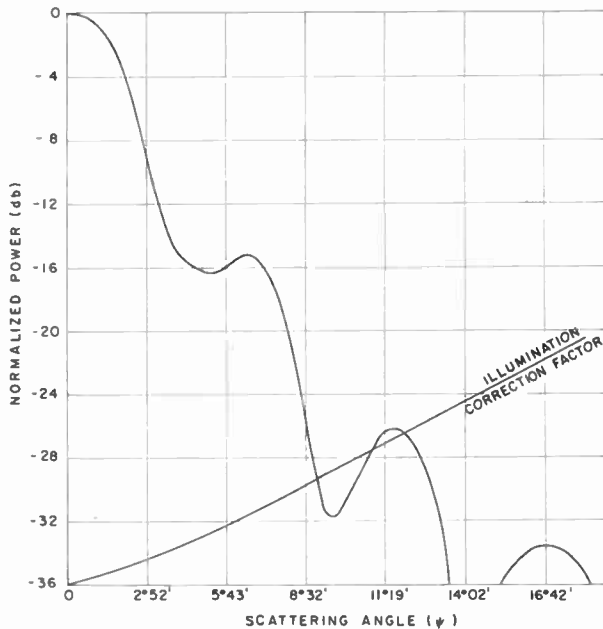


Fig. 14a—Variation of received power with scattering angle for a knife edge obstacle including ground reflections on both sides of the obstacle ($d_1 = d_2 = 100$ cm, horizontal polarization, T, R heights above reflecting plane = 7.92 cm, $\lambda = 1.25$ cm). (To obtain variation for omnidirectional antennas add the illumination correction factor to the measured values).

obstacle on each of these radiations must be considered and the resultant appropriately summed at the receiving terminal in order to determine the diffracted power.

These effects can be demonstrated using model techniques. Figure 14 shows plots of received power versus scattering angle for propagation models which include the effect of earth reflections. In each case the geometry of the transmission link is the same. Figure 14a shows the undulations in received power which depend upon the path geometry (obstacle height, transmitter and receiver distances and position above ground, as well as frequency and polarization) for the case of a

rectangular knife-edge obstacle. Positions occur where the energy in the diffracted field can be either much greater or much less than the corresponding field of a knife-edge obstacle without the effect of ground reflections. The maximum positions correspond to regions where "obstacle gain" can be achieved by a suitable choice of the transmission link. A change in the polarization of the electromagnetic field from horizontal to vertical polarization would interchange the positions of

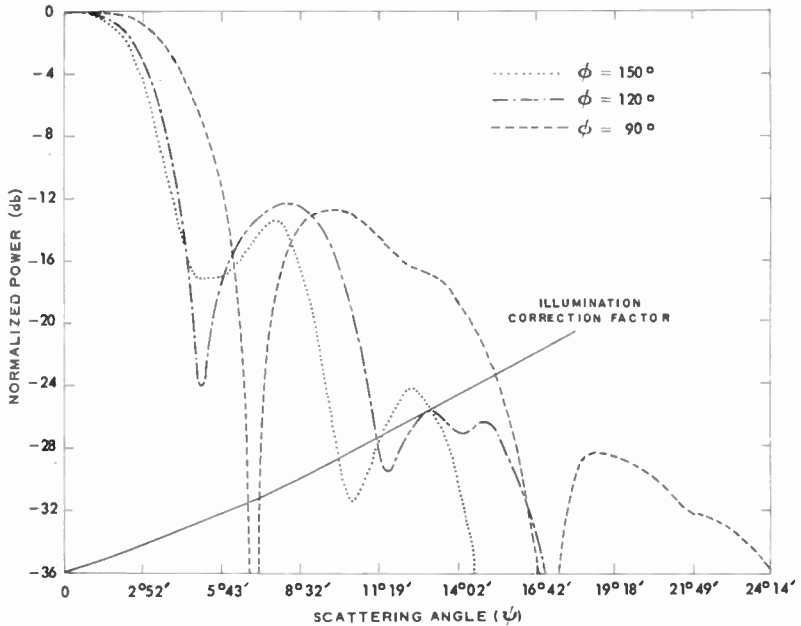


Fig. 14b—Variation of receiver power with scattering angle for a triangular knife-edge obstacle including ground reflections on both sides of the obstacle (horizontal polarization).

the maxima and minima. The effect of the lateral profile (Figure 14b) is, surprisingly enough, to increase the depth of the minima of diffracted power, although the average power level (as expected) is increased. An unfortunate location of transmitting and receiving antennas would correspond to a geometry such that the received power would be a minimum. This could indeed be small when ground reflections are adequate to give a situation as illustrated by the model measurements. The effect of ground reflections as well as reflections off the surface of a wedge-shaped dominant obstacle are shown in Figure 14c. Note the sharp, highly repetitive oscillations within the envelope of

the general behavior induced by the multiple reflections off the wedge. Sharp "pockets" of 15 decibels less power than the median value occur. These can also be the cause of considerable fading, since the path would be sensitive to variations in atmospheric refractivity and to frequency, this latter controlling the bandwidth that can be uniformly transmitted. Note also the large differences in power which exist between the minimum and maximum of the field distributions and which can be utilized by proper siting.

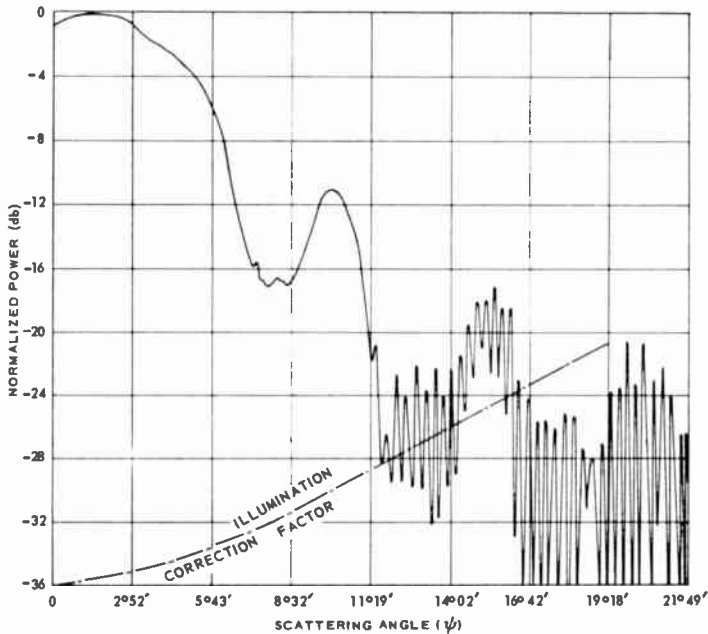


Fig. 14c—Variation of received power with scattering angle for a wedge shaped obstacle ($\phi = 55^\circ$) including ground reflections on both sides of the obstacle (vertical polarization).

The effect of ground reflections when the dominant obstacle has a large smooth crest (shown in Figure 14d) is more like that for a rectangular knife edge, although the locations of the maxima and minima regions of power would be somewhat displaced even for the same polarization. (Note that the experimental results shown in Figure 14 have been obtained using slightly directive antennas. To convert to power received using omnidirectional antennas add the experimentally determined "illumination" correction curve plotted on the same figure to the values of the measured power.)

Rough Surfaces

Obstacles occurring in nature have irregular contours and surfaces which for the most part may be considered as "rough" insofar as electromagnetic wave propagation is concerned. These surface irregularities fluctuate both in location and with time (season). The major difficulty in considering the effect of surface roughness has been the inability to establish the relationship of the important parameters

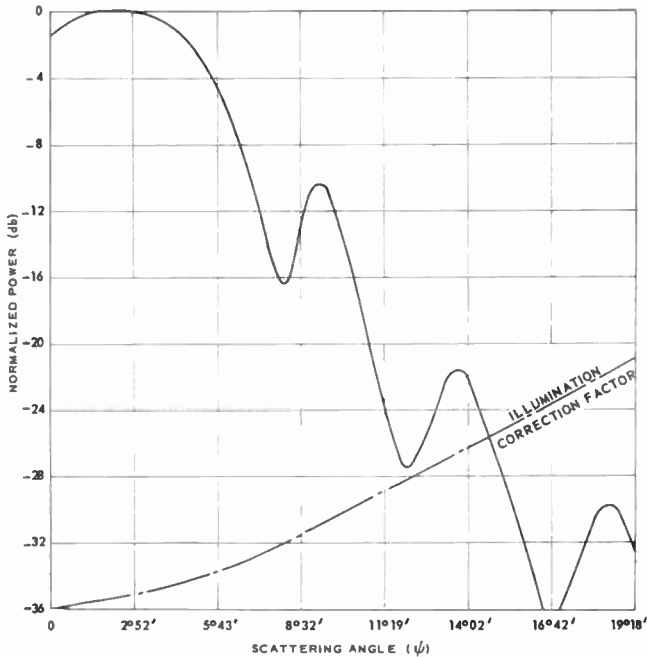


Fig. 14d—Variation of received power with scattering angle for a cylindrical obstacle ($ka = 239$) including ground reflections on both sides of the obstacle (vertical polarization).

with the practical terrain profiles, principally because of the vast and random fluctuations of these quantities. Furthermore, the theoretical approaches are limited by the simplifying assumptions which have to be introduced in order to be able to obtain a solution at all.

Model experiments can be employed to illustrate some of the effects which rough surfaces can have on electromagnetic wave propagation over natural obstacles. As an example, Figure 15 shows a comparison of the experimentally determined variation of diffracted power with scattering angle for a dominant cylindrical conducting obstacle whose

crest is rough with that for an obstacle of the same radius of curvature, but whose crest is smooth. Because of the difficulty of explicitly defining parameters of roughness, the results should be considered as qualitative. However, the important consideration is the influence of the rough surface on the diffracted power. The variation is opposite for the two polarizations. For vertically polarized incident fields the

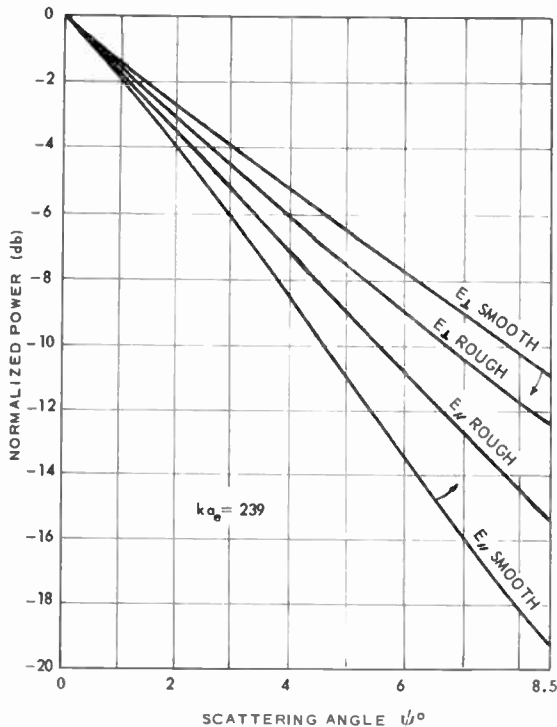


Fig. 15—Comparison of variation of received power with scattering angle for smooth and rough cylindrical obstacles.

diffracted energy decreases with roughness of the diffracting surface, while for horizontally polarized incident fields the diffracted energy *increases* with surface roughness. The variations of diffracted power for a smooth obstacle are thus the extremes that can be obtained for an obstacle of a given radius of curvature, with horizontal polarization providing the minimum value and vertical polarization the maximum value.

Depolarization

In the far field, the signal diffracted by a knife-edge obstacle is

independent of the polarization of the electromagnetic fields incident upon the obstacle. Polarization effects do, however, predominate at relatively short distances (measured in wavelengths) from the diffracting edge. Figure 16 shows the ratio between the diffracted power measured behind a rectangular knife edge for an incident field whose electric vector is orientated normal to the edge and that when the electric vector of the incident field is parallel to the edge. Near the edge there is a very strong dependence on polarization of the incident field; this field decreases with increasing distance from the edge.

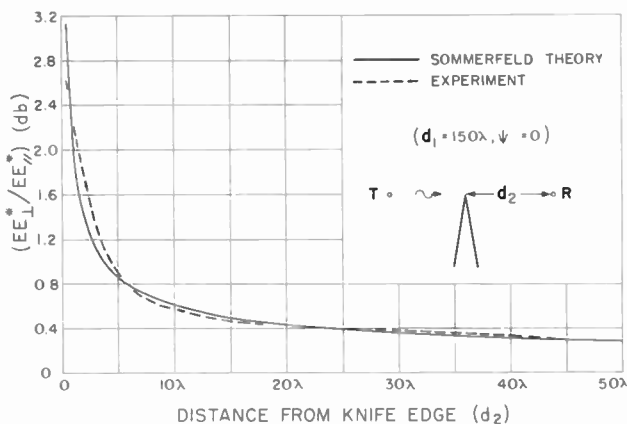


Fig. 16—Ratio of power behind a knife edge at grazing incidence when the incident electric field is normal to the edge to power when the incident field is parallel to the edge.

This suggests that since the diffraction coefficients (which determine the amount by which the electric vector perpendicular to and parallel to an edge are reduced upon diffraction) are different for electric fields incident normal to or parallel to the diffracting edge, then for the incident electric field orientated at an angle (other than zero or 90°) to the diffracted edge, diffracted fields polarized normally to the incident fields will exist.

In the far field of a diffracted signal, the amount of this cross-polarized energy is usually immeasurable. However, near the obstacle, and in particular if the obstacle has sharp edges and is of finite conductivity, notable amounts of cross-polarized energy may be found.

For a rectangular knife edge, if the incident field is oriented either along or normal to the edge, then no cross-polarized effects occur. If this is not the case then cross-polarized fields exist. Figure 17 shows the components of power measured near a triangular edge for fields

polarized in the same direction as the incident fields and for the fields polarized normally to the incident fields. The cross-polarized power is surprisingly strong, being approximately 12 decibels below the normal field components. Since bodies with smooth crests show differences in the diffracted fields which depend on the polarization of the incident fields, cross-polarized energy will be present when the surface of the

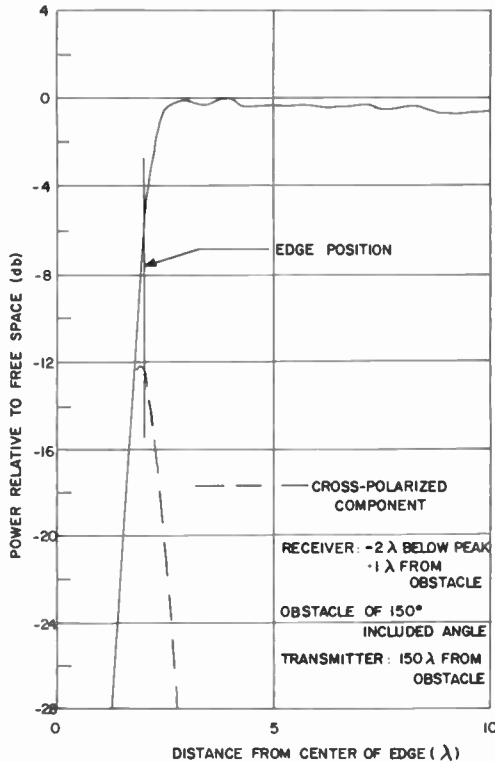


Fig. 17—Normally polarized and cross-polarized power received near a triangularly shaped knife edge.

diffracting obstacle is oriented in a direction which is not either parallel or perpendicular to the electric vector of the incident field.

These cross-polarized fields can be of influence on passive repeaters, for example, located on sharp, natural ridges.

Surface Conductivity

Considerable interest exists in the problem of propagation of electromagnetic waves over a "mixed" path composed of several regions

of different conductivity (e.g., sea and land). In particular a "recovery effect" of the electromagnetic field is found for vertically polarized incident radiation as the region of low conductivity changes to one of greater conductivity. Close comparison of the experimental findings with theory is hampered by the difficulty of controlling the important parameters. Furthermore, much of the theoretical work has been confined to the case of low frequencies (1 mc and lower) and vertical polarization.

Preliminary scale-model laboratory experiments have been made above a plane surface exhibiting a sharp change in electrical properties. The measurements were performed at a frequency of 24,000 mc for both vertical and horizontal polarization. For vertical polarization (see Figure 18a), a recovery effect of the electric field similar to that reported in the literature (see bibliography) when transition is made from a region of low conductivity to one of high conductivity was found. The rate of change and degree of this effect varied markedly with position of the transmitter-receiver above the surface. For horizontal polarization (Figure 18b) the measurements were found also to be affected by this transition of surface electrical properties, but the trend of behavior was totally different from that for vertically polarized waves.

No attempt was made to correlate these preliminary measurements quantitatively with any of the present theories. However, for vertical polarization there exists qualitative agreement, and it appears that the scale-model techniques are especially adaptable for a systematic study of such surface effects, in particular since it would be possible to measure the phase of the electromagnetic fields as well as the amplitude.

Path Reciprocity

The reciprocity theorem applies to diffraction paths, as confirmed by measurements not included in this paper.

THEORETICAL CONSIDERATIONS

Comparisons of the experimental model measurements with prediction of theories based on simplified concepts have been made and satisfactory agreement obtained. The derivation of these theories is based on a generalized concept of the Green's function and on the use of corrective factors from rigorous diffraction theory. The received power is described in terms of a "knife-edge" contribution due to the projected outline of the obstacle and, in the case of obstacles with

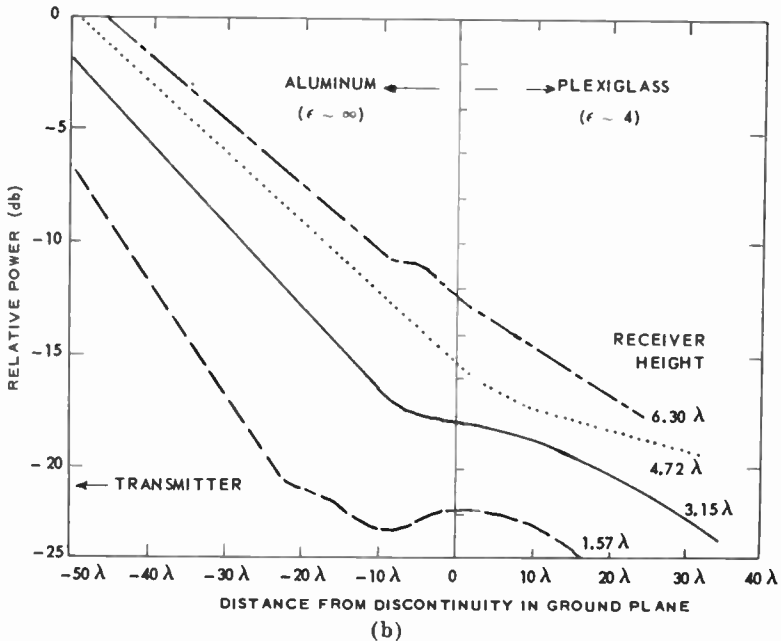
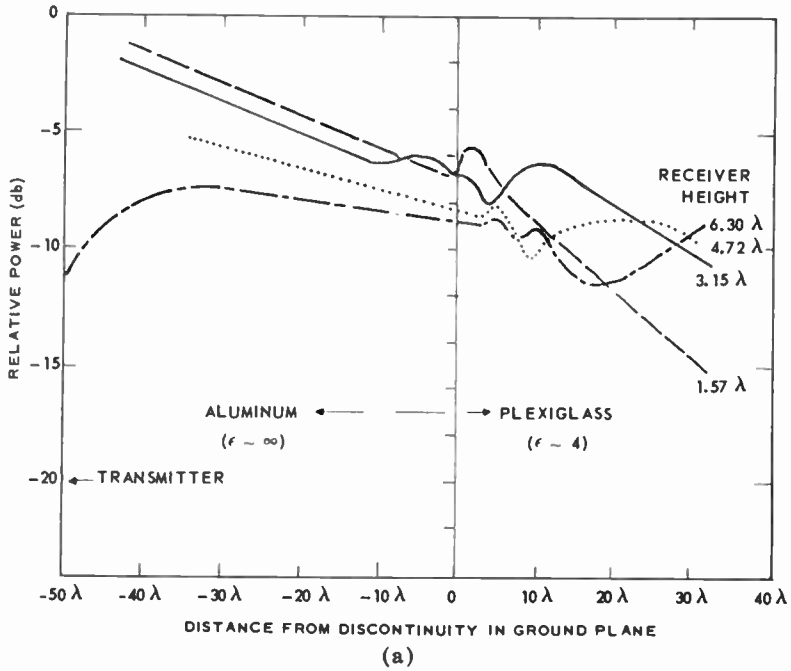


Fig. 18—Variation of received field with distance from transmitter. Transmitter located on smooth plane surface with abrupt change in conductivity at a distance 65λ from discontinuity. Transmitter height 1.18λ ; (a) vertical polarization and (b) horizontal polarization.

smooth surfaces, in terms of "halo" contributions resulting from the crest of the obstacle. Such an approach can be generalized to include oblique incidence of the radiation and surfaces of conical shape. We shall outline only the qualitative, general features of such an approach and the reader is referred elsewhere^{1,40,52,66} for details.

Knife-Edge Theory

The classical treatment of diffraction by a knife-edge obstacle starts from the Huygens-Kirchhoff diffraction integral, namely,

$$\mu(p) = -\frac{1}{4\pi} \iint_S \left\{ \frac{e^{-jkr}}{r} \frac{\partial \psi_0}{\partial n} - \psi_0 \frac{\partial}{\partial n} \left(\frac{e^{-jkr}}{r} \right) \right\} da,$$

where $\mu(p)$ is the value of the field (E or H) at the field point p , S is the surface of integration, ψ_0 is the source function, \vec{n} is the outward unit normal to S , and r is the distance from point p to any part of S . For the far-field, the integral reduces to

$$\frac{\mu(p)}{\mu_0} = \frac{jk}{4\pi} \iint_S \frac{e^{-jk(r+l)}}{rR} (\cos\theta - \cos\theta_1) da,$$

where μ_0 is the strength of the source, R is the distance from the source to the point of integration on S , and θ , θ_1 are the angles of incidence. The major difficulty is thus the evaluation of the above integral over the appropriate surface S . S is the surface through which the radiation must pass, i.e., the area in the plane of the knife edge but not contained by the edge.

Rectangular knife edge

For the case of a rectangular knife edge, the integration is particularly simple and the results readily expressed in terms of Fresnel integrals.

Triangular knife edge

The evaluation of the diffraction integral for a triangular knife edge is more involved. However, by an appropriate subdivision of the area of the triangle⁵² it is possible to evaluate the integrals by standard techniques as before. In general, the same is true for a semicircular edge although the resulting functions¹ will not be the Fresnel integrals.

Halo or Crest Effect

For obstacles with smooth crests, in addition to the direct radiation which reaches the receiver (and which is exactly the same as for a knife-edge obstacle), there are three other paths that also contribute to the received field and that depend on reflection from the crest of the obstacle. The received power can thus be expressed as a knife-edge term E_{kc} (due to the sharp-edged plane substitute of the obstacle) and halo terms which represent the additional "crest effect" or radiation due to smooth surface of the obstacle. It is thus possible to write

$$E_{\text{total}} = E_{kc} + \rho_1 E_2 + \rho_2 E_3 + \rho_1 \rho_2 E_4$$

where the ρ 's correspond to a factor which indicates change of phase and/or intensity upon reflection, and E corresponds to the electric field for each of the contributing paths.

The evaluation of the knife-edge term is carried out as before. Each of the remaining terms can be similarly evaluated, taking into account the appropriate path length and also two other important considerations. These are

1. The divergence factor, which accounts for the reduction in intensity of a beam of radiation upon reflection from a curved surface due to the energy being spread over a wider angle.
2. The fact that, as shown by recent developments in electromagnetic theory,^{31,32} the geometric optics field must be multiplied by a slowly varying factor to obtain the real field in the penumbra zone for obstacles of large radius of curvature. No correction is required for horizontal polarization because geometric optics and Fock's theory predict a vanishing field near the surface. For vertical polarization, geometric optics predicts twice the incident field, whereas Fock's theory predicts 1.4 times the incident field. Hence the required correction factor is 0.7. Strictly speaking, this factor is not a constant but depends on the location of the point of the surface where the reflection takes place. It has been shown that the agreement between theory and experiment can be slightly improved by calculating the halo terms with a varying correction factor.¹⁶

The inclusion of the halo effects in addition to the knife-edge term permits the diffracted field due to cylindrical obstacles to be evaluated.

These same concepts can be extended to include conical obstacles and to radiation at an oblique angle. In general, the results for diffraction by cylindrical obstacles at normal incidence are applicable to conical obstacles at oblique incidence provided the scattering angle is given by

$$\psi_{sc} = \psi \cos \zeta \cos \tau,$$

and the radius of curvature by

$$a_e = \frac{a}{\cos^2 \zeta \cos \tau},$$

where τ is the cone half-angle, ζ the angle of obliqueness, and ψ, a are the scattering angle and radius of curvature for normal incidence.

In a similar manner ground reflections can be taken into account by considering the contributions to the total field from the reflected fields.^{45,69}

In the case where polarization effects occur, the two polarizations encompass the extremes in the behavior of the received fields. Since for conducting obstacles the field is zero at the surface for horizontal polarization, this polarization exhibits the least received signal in the shadow region. The converse is true for vertical polarization. The effects of surface roughness, imperfect conductivity, and the like found in a full-scale propagation link tend to make the values of received power fall between the idealized situations for the two polarizations. Thus model experiments illustrate very closely the behavior and the range of various parameters to be met with in practice.

Other Theoretical Approaches

A considerable amount of theoretical work has been devoted to the investigation of electromagnetic wave propagation over various obstacles. A considerable number of important references are cited in the following bibliography. In addition a number of field measurements dealing principally with "obstacle gain" are also indicated.

In the application of a given theory to practical computations, care must be exercised in ascertaining the limits of validity of the theory before wholesale and indiscriminate use is made of it. In addition, considerable discrepancies exist in the difficulty of numerically evaluating the different theories. In this regard a strong need exists for the numerical values to be put into the form of easy-to-use charts and nomographs.

As demonstrated, the use of scale-model measurements to ascertain the influence of important parameters in order to test the theoretical

predictions is of immense value. A number of effects which cannot be demonstrated by theory without a considerable computational effort are readily observed from the model experiments. In this way model measurements complement the fund of information provided by theory and field trials.

ACKNOWLEDGMENTS

Many of the ideas for the model measurements stemmed from numerous fruitful discussions with Dr. H. E. J. Neugebauer, while a number of the measurements shown were performed by Mr. M. G. Kingsmill, to both of whom the author is greatly indebted.

BIBLIOGRAPHY

Lateral Profile

1. M. P. Bachynski and M. G. Kingsmill, "Effect of Obstacle Profile on Knife-Edge Diffraction," *Trans. I.R.E.*, Vol. AP-10, p. 201, March (1962).
2. S. Matsuo, "The Method of Calculating VHF Field Intensity and Research on its Variation," Electrical Comm. Lab., Tokyo, Japan, Rep. No. 621.29.001.6 (047.3), (1950).

Crest Effect

Knife Edge

Since the classical theory of diffraction by a knife-edge is well known, the following list is confined to considerations of more difficult situations such as thick edges, multiple diffracting edges and techniques for simplifying computation.

3. L. J. Anderson and L. G. Trolese, "Simplified Method for Computing Knife-Edge Diffraction in the Shadow Regions," *Trans. I.R.E.*, Vol. AP-6, p. 281, July (1958).
4. M. G. Cheney and R. B. Watson, "On the Diffraction of e.m. Waves by Two Conducting Half-Planes," *Jour. Appl. Phys.*, Vol. 22, p. 675 (1951).
5. B. N. Harden, "Diffraction of e.m. Waves by Two Parallel Half-Planes," *Proc. I.E.E.*, Part III, Vol. 100, p. 348 (1953).
6. D. S. Jones, "Diffraction by a Thick Semi-Infinite Plate," *Proc. Roy. Soc.*, Vol. 217A, p. 153 (1953).
7. L. A. Vainstein, "On the Theory of Diffraction by Two Parallel Half-Planes," *IAN (Ser. Fiz.)*, Vol. 12, p. 166 (1948).

8. J. R. Wait, "Wave Propagation Around a Curved Boundary Which Contains an Obstacle," *Can. Jour. Phys.*, Vol. 40, p. 1010 (1962).
9. W. E. Williams, "Diffraction by Two Parallel Planes of Finite Length," *Proc. Cambridge Phil. Soc.*, Vol. 50, Pt. 2, p. 390 (1954).

Wedges

10. T. J. Bromwich, "Diffraction of Waves by a Wedge," *Proc. London Math. Soc.*, Series 2, Vol. 14, p. 450 (1915).
11. H. Carslaw, "Diffraction by a Wedge of any Angle," *Proc. London Math. Soc.*, Vol. 18, p. 291 (1918).
12. W. W. Grannemann and R. B. Watson, "Diffraction of E.M. Waves by a Metallic Wedge of Acute and Dehdral Angle," *Jour. Appl. Phys.*, Vol. 26, p. 392, April (1955).
13. V. A. Il'in, "Diffraction of E.M. Waves at a Non-ideally Conducting Wedge and Problem of Coastal Refraction," *Compt. Rend. Acad. Sc. (USSR)*, Vol. 99, p. 47, Nov. (1954).
14. W. H. Jackson, "On the Diffraction of Light Produced by an Opaque Prism of Finite Angles," *Proc. London Math. Soc.*, Series 2, Vol. 1, p. 393 (1903-04).
15. D. S. Jones and F. B. Pidduck, "Diffraction by Metallic Wedges at Large Angles," *Quart. Jour. Math.*, Oxford, p. 420, Sept. (1950).
16. J. B. Keller and A. Blank, "Diffraction and Reflection of Pulses by Wedges and Corners," *Comm. Pure Appl. Math.*, Vol. 4, p. 75, June (1951).
17. J. B. Keller and A. Kay, "Diffraction of an Arbitrary Pulse by a Wedge," *Jour. Appl. Phys.*, Vol. 23, p. 1267 (1952).
18. H. M. MacDonald, *Electric Waves*, Cambridge Univ. Press, pp. 186-198 (1902).
19. H. M. MacDonald, "A Class of Diffraction Problems," *Proc. London Math. Soc.*, Series 2, Vol. 14, p. 410 (1915).
20. H. M. MacDonald, *Electromagnetism*, G. Bell, London, pp. 79-85 (1934).
21. Y. Nomura, "On the Diffraction of Electric Waves by a Perfectly Reflecting Wedge," *Sci. Rep. Tohoku Univ.* 1, 2B, pp. 1-23 (1951).
22. F. Oberhettinger, "Diffraction of Waves by a Wedge," *Comm. Pure Appl. Math.*, Vol. 7, p. 551 (1954).
23. F. Oberhettinger, "On Asymptotic Series for Functions Occurring in the Theory of Diffraction by Wedges," *Jour. Math. Phys.*, Vol. 34, p. 245, Jan. (1956).

24. F. Oberhettinger, "On the Diffraction and Reflection of Waves and Pulses by Wedges and Cones," *NBS Jour. Res.*, Vol. 61, p. 343 (1958).
25. A. Sommerfeld, "Mathematische Theorie der Diffraction," *Mathematische Annalen*, Vol. 47, p. 317 (1896).
26. R. B. Watson and C. W. Horton, "On the Diffraction of a Radar Wave by a Conducting Wedge," *Jour. Appl. Phys.*, Vol. 21, p. 802 (1950).
27. W. E. Williams, "Diffraction of an E-Polarized Planewave by an Imperfectly Conducting Wedge," *Proc. Roy. Soc.*, Vol. 252A, p. 376, Sept. (1959).

Cylinders

Included are only the more recent references which contribute to the understanding of electromagnetic wave propagation over natural obstacles.

28. A. W. Adey, "Diffraction of Microwaves by Long Metal Cylinders," *Can. Jour. Phys.*, Vol. 33, p. 407, Aug. (1955).
29. E. L. Burshtein and L. S. Solovev, "Diffraction of a Finite Beam of E-M Waves by a Cylindrical Obstacle," *Compt. Rend. Acad. Sci. (USSR)*, Vol. 109, p. 473, July (1956).
30. J. H. Crysdale, "Comparison of Some Experimental Terrain Diffraction Losses with Predictions Based on Rices' Theory for Diffraction by a Parabolic Cylinder," *Trans. I.R.E.*, Vol. AP-6, p. 293, July (1958).
31. V. Fock, "The Distribution of Currents Induced by a Plane Wave on the Surface of a Conductor," *Jour. Phys. (USSR)*, Vol. 10, p. 130, Feb. (1946).
32. V. Fock, "The Field of a Plane Wave Near the Surface of a Conducting Body," *Jour. Phys. (USSR)*, Vol. 10, p. 399 (1946).
33. V. Fock and A. A. Fedorov, "Diffraction of a Plane Wave by a Perfectly Conducting Paraboloid of Rotation," *Zh. Tech. Fiz.*, Vol. 28, p. 2548, Nov. (1958).
34. F. G. Friedlander, "Diffraction of Pulses by a Circular Cylinder," *Comm. Pure Appl. Math.*, Vol. 7, p. 705, Nov. (1954).
35. K. Furtusu, "On the Theory of Diffraction of E-M Waves by Mountains," *Jour. Phys. Soc. (Japan)*, Vol. 8, p. 500 (1953).
36. A. S. Goriainov, "Diffraction of Plane Electromagnetic Waves on a Conducting Cylinder," *Radio tekhnika i Elektronika*, Vol. 3, p. 603, May (1958).
37. J. B. Keller, "Diffraction by a Convex Cylinder," *Trans. I.R.E.*, Vol. AP-4, p. 312, July (1956).

38. J. B. Keller, "Geometrical Theory of Diffraction," *Jour. Opt. Soc. Am.*, Vol. 52, p. 116 (1962).
39. D. E. Kerr, *Propagation of Short Radio Waves*, p. 96, McGraw-Hill Book Co., New York, 1st Edition (1951).
40. H. E. J. Neugebauer and M. P. Bachynski, "Diffraction by Smooth Cylindrical Mountains," *Proc. I.R.E.*, Vol. 46, No. 9, p. 1619, Sept. (1958).
41. Y. Nomura, "On the Propagation of Electric Waves Behind a Mountain," *Sci. Rep. Res. Inst.*, Tohoku Univ., Ser. B, Vol. 3, p. 115, March (1952).
42. Y. Nomura, "On the Method of Estimating Electric Field Intensity in VHF Propagation in Mountainous Regions," *Sci. Rep. Res. Inst.*, Tohoku Univ., Ser. B, Vol. 6, p. 157 (1955).
43. K. A. Norton, P. L. Rice, and L. E. Vogler, "The Use of Angular Distance in Estimating Transmission Loss and Finding Range for Propagation Through a Turbulent Atmosphere over Irregular Terrain," *Proc. I.R.E.*, Vol. 43, p. 1488, Oct. (1955).
44. S. O. Rice, "Diffraction of Plane Radio Waves by a Parabolic Cylinder," *Bell Syst. Tech. Jour.*, Vol. 33, p. 417, March (1954).
45. I. P. Shkarofsky, H. E. J. Neugebauer, and M. P. Bachynski, "Effect of Mountains with Smooth Crests on Wave Propagation," *Trans. I.R.E.*, Vol. AP-6, No. 4, p. 341, Oct. (1958).
46. I. P. Shkarofsky, M. P. Bachynski, and H. E. J. Neugebauer, "Electromagnetic Wave Propagation Over Mountains," *Can. I.R.E. Conv. Rec.*, Oct. (1958).
47. J. R. Wait and A. M. Conda, "Diffraction of Electromagnetic Waves by Smooth Obstacles for Grazing Angles," *N.B.S. Jour. Res. IV*, Vol. 63, p. 181, Sept.-Oct. (1959).
48. J. R. Wait, *Electromagnetic Radiation from Cylindrical Structures*, Pergamon Press, N.Y. (1959).

Cones

49. L. B. Felsen, "Backscattering from Wide-Angle and Narrow-Angle Cones," *Jour. Appl. Phys.*, Vol. 26, p. 138, Feb. (1955).
50. L. B. Felsen, "Plane-Wave Scattering by Small-Angle Cones," *Trans. I.R.E.*, Vol. AP-5, p. 121, Jan. (1957).
51. L. B. Felsen, "Asymptotic Expansion of the Diffracted Wave for a Semi-infinite Cone," *Trans. I.R.E.*, Vol. AP-5, p. 402, Oct. (1957).
52. H. E. J. Neugebauer and M. P. Bachynski, "Diffraction by

Smooth Conical Obstacles," *N.B.S. Jour. Res.*, Vol. 64D, p. 317, July-Aug. (1960).

53. F. M. Weiner, "Diffraction by Cones," *Jour. Acous. Soc. Am.*, Vol. 20, p. 367 (1948).

Spheres

Much of the development of radio propagation over the surface of the earth is contained in Bremmer's book (see below). Listed are some further important contributions.

54. H. Bremmer, *Terrestrial Radio Waves*, Elsevier Publishing Co., N.Y., N.Y. (1948).
55. K. Bullington, "Propagation of VHF and SHF Waves Beyond the Horizon," *Proc. I.R.E.*, Vol. 38, p. 1221, Oct. (1950).
56. C. R. Burrows and M. C. Gray, "The Effects of the Earth's Curvature on Ground Wave Propagation," *Proc. I.R.E.*, Vol. 29, p. 16, Jan. (1941).
57. C. Domb and M. H. L. Pryce, "The Calculation of Field Strengths Over a Spherical Earth," *Jour. I.E.E.*, Part III, Vol. 94, p. 325, Sept. (1947).
58. V. A. Fock, "Diffraction of Radio Waves Around the Earth's Surface," *Academy of Sciences, USSR* (1946).
59. V. A. Fock, "Fresnel Diffraction from Convex Bodies," *Uspekhi Fiz. Nauk.*, Vol. 43, p. 587 (1951).
60. K. Furutsu, "On the Multiple Diffraction of E-M Waves by Spherical Mountains," *Jour. Radio Res. Labs, Japan*, Vol. 3, p. 331, Oct. (1956).
61. R. N. Ghose and W. G. Albright, "VHF Field Intensities in the Diffraction Zone," *Trans. I.R.E.*, Vol. AP-2, p. 35, Jan. (1954).
62. A. I. Kalinin, "Calculation of the Field Strengths in Shadow and Half-Shadow Regions in the Case of Ultra Short Waves Traveling Along a Smooth Spherical Surface of the Earth," *Radio-technica* (Moscow), Vol. 11, p. 43, June (1956).
63. K. A. Norton, "The Calculation of Ground-Wave Field Intensity Over a Finitely Conducting Spherical Earth," *Proc. I.R.E.*, Vol. 29, p. 623, Dec. (1941).
64. L. E. Vogler, "Smooth Earth Diffraction Calculations for Horizontal Polarization," *N.B.S. Jour. Res.*, Vol. 65D, p. 397, July-Aug. (1961).
65. L. C. Walters and J. R. Johler, "On the Diffraction of Spherical Radio Waves by a Finitely Conducting Spherical Earth," *N.B.S. Jour. Res.*, Vol. 66D, p. 101, Jan.-Feb. (1962).

Oblique Incidence

66. M. P. Bachynski, "Propagation at Oblique Incidence Over Cylindrical Obstacles," *N.B.S. Jour. Res.*, Vol. 64D, p. 311, July-Aug. (1960).
67. J. R. Wait, "Scattering of a Plane Wave from a Circular Dielectric Cylinder at Oblique Incidence," *Can. Jour. Phys.*, Vol. 33, p. 189, May (1955).

Ground Reflections

68. K. Bullington, "Reflection Coefficient of Irregular Terrain," *Proc. I.R.E.*, Vol. 42, p. 1258, Aug. (1954).
69. J. C. Schelling, C. R. Burrows, and E. B. Ferrell, "Ultra-Short Wave Propagation," *Proc. I.R.E.*, Vol. 21, p. 427, March (1933).

Rough Surfaces

For an extensive list of references of work prior to 1959 see:

70. M. P. Bachynski, "Microwave Propagation Over Rough Surfaces," *RCA Review*, Vol. XX, No. 2, p. 308, June (1959).
71. H. Head, "The Influence of Trees on Television Field Strengths at Ultra-High Frequencies," *Proc. I.R.E.*, Vol. 48, p. 1016, June (1960).
72. A. H. LaGrone and C. W. Chapman, "Some Propagation Characteristics of High UHF Signals in the Immediate Vicinity of Trees," *Trans. I.R.E.*, Vol. AP-9, p. 487, Sept. (1961).

Depolarization

73. P. Beckmann, "The Depolarization of Electromagnetic Waves Scattered from Rough Surfaces," Czech Academy of Sciences, Institute of Radio Eng. and Elect., Report No. 12 (1961).
74. P. Beckmann, "The Depolarization of Electromagnetic Waves by Inclined Planes," Czech Academy of Sciences, Institute of Radio Eng. and Elect., Report No. 19 (1961).
75. B. Chytil, "The Depolarization of Electromagnetic Waves Back-Scattered from Certain Bodies," Czech Academy of Sciences, Institute of Radio Eng. and Elect., Report No. 17 (1961).
76. B. Chytil, "Depolarization by Randomly Spaced Scatterers," Czech Academy of Sciences, Institute of Radio Eng. and Elect., Report No. 20 (1961).

Surface Conductivity

77. B. Abeld, "Contribution on VHF Propagation Over the Sea," *Tech. Hausmitt Nordwidsch Rundfunk*, Vol. 8, p. 103, Dec. (1956).

78. Y. Aons and K. Muramatsu, "Measurement of Field Intensity of Ground Wave Over Mixed Paths," *Jour. Radio Res. Lab.*, Vol. 2, p. 51, Jan. (1955).
79. J. Bazer and S. N. Karp, "Propagation of Plane Electromagnetic Waves Past a Shoreline," *N.Y.U. Res. Rep. No. EM-46* (1952).
80. H. Bremmer, "The Extension of Sommerfeld's Formula for the Propagation of Radio Waves over a Flat Earth to Different Conductivities of the Soil," *Physica*, Vol. 20, p. 441 (1954).
81. P. C. Clemmow, "Radio Propagation over a Flat Earth Across a Boundary Separating Two Different Media," *Phil. Trans*, Vol. A246, p. 1 (1953).
82. P. S. Epstein, "On the Possibility of E-M Surface Waves," *Proc. Nat. Acad. Sci.* (Washington) Vol. 40, p. 1158, Dec. (1954).
83. E. L. Feinberg, "Propagation of Radio Waves over an Actual Surface," *Izdatel'stbo Akademi SSSR* (Moscow), p. 109 (1944).
84. E. L. Feinberg, "On the Propagation of Radio Waves Along an Imperfect Surface," *Jour. Phys.* (USSR), Vol. 10, p. 410 (1946).
85. E. L. Feinberg, "Propagation of Radio Waves along an Inhomogeneous Surface," *Nuova Cimento*, Vol. 11, p. 60 (1959).
86. K. Furutsu, "Propagation of E-M Waves over a Flat Earth Across Two Boundaries Separating Three Different Media," *Jour. Radio Res. Labs.* (Japan), in three parts: Vol. 2, p. 1, Jan. (1955); Vol. 2, p. 239, July (1955); and Vol. 2, p. 345, Oct. (1955).
87. K. Furutsu and S. Koimai, "The Calculation of Field Strength over Mixed Paths on a Spherical Earth," *Jour. Radio Res. Lab.*, Japan, Vol. 3, p. 331, Oct. (1956).
88. J. Grosskopf and K. Vogt, "Effective Conductivity of the Earth," *Hochfrequenztech, Electroak*, Vol. 62, p. 14 (1943).
89. K. Horiuchi, "E-M Fields due to Current Flowing Parallel to Interface of Two Different Media," *Jour. Phys. Soc.* (Japan), Vol. 12, p. 170, Feb. (1957).
90. H. L. Kirke, "Calculation of Ground Wave Field Strength over a Composite Land Path," *Proc. I.R.E.*, Vol. 37, p. 489 (1949).
91. G. Millington, "Ground Wave Propagation Across a 'Land-Sea' Boundary," *Nature*, Vol. 163, p. 128 (1949), and *Nature*, Vol. 164, p. 114 (1949).
92. G. Millington, "Ground Wave Propagation over an Inhomogeneous Smooth Earth," *Proc. I.E.E.*, Vol. 96, Part III, p. 53 (1949); and Vol. 97, Part III, p. 209 (1950).
93. G. Millington and J. C. Thackray, "Ground-Wave Propagation Curves for Frequencies from 150 kc/s to 10 Mc/s," *Marconi Review*, Vol. 16, p. 109, 3rd Quarter (1953).

94. G. D. Monteith, "Application of the Compensation Theorem to Certain Radiation and Propagation Problems," Monograph No. 3, *Proc. I.E.E.*, Vol. 98, p. 1 (1959).
95. Y. Nomura, "On the Theory of Electric Waves over a Plane Surface of the Inhomogeneous Earth," *Sci. Rep. Res. Inst. Tohoku Univ.*, Ser. B, Vol. 6, p. 19 (1954).
96. K. A. Norton, "Calculation of the Ground-Wave Field Intensity," *Proc. I.R.E.*, Vol. 29, p. 623 (1941).
97. B. G. Pressy, G. E. Ashwell, and C. S. Fowler, "Change of Phase With Distance of a Low-Frequency Ground Wave Propagated Across a Coastline," *Proc. I.E.E.*, Part B, Vol. 103, p. 527, July (1956).
98. B. G. Pressy and G. E. Ashwell, "The Deviation of Low Frequency Ground Waves at a Coast Line," *Proc. I.E.E.*, Part B, Vol. 103, p. 535, July (1956).
99. L. Robin, "On a Problem of Diffraction of E-M Waves at the Separation of Two Media," *Compt. Rend. Acad. Sci. (Paris)*, Vol. 218, p. 135 (1944); and Vol. 218, p. 989 (1944). See also *Rev. Sc.*, Vol. 84, p. 7 (1946).
100. R. A. Rowden and J. W. Stark, "Long-Distance Propagation at 94.5 Mc/s over the North Sea," *Proc. I.E.E.*, Part B, Vol. 194, p. 210, May (1957).
101. T. B. A. Senior, "Radio Propagation over a Discontinuity in the Earth's Electrical Properties," Part I and Part II, *Proc. I.E.E.*, Part C, Vol. 104, p. 43 and p. 139, March (1957).
102. K. Suda, "Field Strength Calculation," *Wireless Eng.*, Vol. 31, p. 249, Sept. (1954).
103. K. Ventkitaraman, "Ground-Wave Propagation over a Non-Homogeneous Earth," *Inst. Telecommun. Engrs.*, India, Vol. 1, p. 155, Sept. (1955).
104. R. W. Vice, "A Survey of Ground-Wave Propagation Conditions in South Africa," *Trans. S. Afr. Inst. Elect. Eng.*, Vol. 45, p. 139, April (1954).
105. J. R. Wait, "On the Theory of Propagation Along A Curved Surface," *N.B.S. Report* 3583, May (1956).
106. J. R. Wait, "Mixed Path Ground Wave Propagation — I Short Distances," *Jour. Res. N.B.S.*, Vol. 57, No. 1, p. 1, July (1956); and "II Larger Distances," Vol. 59, No. 1, p. 19, July (1957).
107. J. R. Wait, "Propagation of a Pulse Across a Coastline," *Proc. I.R.E.*, Vol. 45, p. 1550, Nov. (1957).
108. J. R. Wait, "On the Theory of Mixed-Path Ground-Wave Propagation on a Spherical Earth," *N.B.S. Jour. Res.*, Vol. 65D, No. 4, p. 401 (1961).

Field Measurements

109. A. P. Barsis and R. S. Kirby, "VHF and UHF Signal Characteristics Observed on a Long Knife Edge Diffraction Path," *N.B.S. Jour. Res.*, Vol. 65D, p. 437, Sept.-Oct. (1961).
110. S. YaBraude, "Propagation of Ultrashort Waves in a Mountainous Locality," *Ukrainian Phys. Jour.*, Vol. 3, p. 246, May (1959).
111. J. H. Crysdale, "Large Reduction of VHF Transmission Loss and Fading by the Presence of a Mountain Obstacle in Beyond-line-of-sight Paths," *Proc. I.R.E.*, Vol. 43, p. 627, May (1955).
112. J. H. Crysdale, J. W. B. Day, W. S. Cook, M. E. Psutka, and P. E. Robillard, "An Experimental Investigation of the Diffraction of Electromagnetic Waves by a Dominating Ridge," *Trans. I.R.E.*, Vol. AP-5, p. 203, April (1957).
113. J. F. Day and L. G. Trolese, "Propagation of Short Radio Waves over Desert Terrain," *Proc. I.R.E.*, Vol. 38, p. 165, Feb. (1950).
114. F. H. Dickson, J. J. Egli, J. W. Herbstreit, and G. S. Wickizer, "Large Reduction of VHF Transmission Loss and Fading by the Presence of a Mountain Obstacle in Beyond-line-of-sight Path," *Proc. I.R.E.*, Vol. 41, p. 967, Aug. (1953).
115. J. Dufour, "Study of Ultra-Short-Wave Propagation over the Barrier Presented by the Alps," *Tech. Mitt. Schweiz Telegr.-Teleph. Verw.*, Vol. 31, p. 124, May 1 (1953).
116. M. Hirai, Y. Fujii, and H. Saito, "An Experimental Investigation of the Diffraction of VHF and UHF by Mountain Ridges," *Jour. Radio Res. Labs. (Japan)*, Vol. 5, p. 189, July (1958).
117. R. E. Lacy, "Mountain Obstacle Measurements," *I.R.E. Convention Record*, Part I, p. 32 (1957).
118. R. E. Lacy, "Measurement of Gain Across Mountain Obstacles in California (U.S.A.)," *Ann. Telecommun.*, Vol. 12, p. 200, May (1957).
119. J. K. S. Jowett, "VHF Field Strength Measurements over Paths in the Irish Sea Involving Mountain Obstacles," *Proc. I.E.E.*, Pt. B, Vol. 107, p. 141, March (1960).
120. R. S. Kirby, H. T. Dougherty, and P. L. McQuate, "Obstacle Gain Measurements Over Pikes Peak at 60 to 1,046 Mc," *Proc. I.R.E.*, Vol. 43, p. 1467, Oct. (1955).
121. R. S. Kirby, H. T. Dougherty, and P. L. McQuate, "VHF Propagation Measurements in the Rocky Mountain Region," *Trans. I.R.E.*, Vol. VC-6, p. 13, July (1956).
122. T. Kono, Y. Uesugi, M. Hirai, S. Niwa, and H. Irie, "Measurements of Field Intensity of VHF Radio Waves Behind Mount

- Fuji," *Jour. Radio Research Labs.* (Japan), Vol. 1, p. 1, June (1954).
123. T. Kono, K. Nishikori, M. Fukushima, M. Ikeda, and N. Yoshida, "Experimental Studies on Diffracted Waves from a Mountain at 3000 Mc/s," *Jour. Radio Res. Labs.* (Japan), Vol. 2, p. 163, April (1955).
124. T. Kono, M. Hirai, Y. Uesugi, "Uses of Diffraction Effect of Mountains for VHF Radio Communication," *Jour. Radio Res. Labs* (Japan), Vol. 2, p. 293, July (1955).
125. E. C. S. Megaw, "Experimental Studies of the Propagation of Very Short Radio Waves," *Jour. I.E.E.* (London), Part I, Vol. 93, p. 462 (1946); and Part IIIA, Vol. 93, p. 79 (1946).
126. J. S. McPetrie and L. H. Ford, "Some Experiments on the Propagation of 9.2 cm. Wavelength, Especially on the Effects of Obstacles," *Jour. I.E.E.*, Part IIIA, Vol. 93, p. 108 (1946).
127. J. S. McPetrie and L. H. Ford, "Experiments on Propagation of 9.2 cm. Wavelength, Especially on the Effects of Obstacles," *Jour. Inst. Elec. Eng.* (London), Vol. 93, Pt. IIIA, p. 531, March-May (1946).
128. K. Nishikori, Y. Kurihara, M. Fukushima, and M. Ikeda, "Broad and Narrow-Beam Investigations of SHF Diffraction by Mountain Ridges," *Jour. Radio Res. Labs.* (Japan), Vol. 4, p. 407, Oct. (1957).
129. G. C. Rider, "Some VHF Experiments Upon the Diffraction Effect of Hills," *Marconi Review*, Vol. 16, p. 96, 2nd Quarter (1953).
130. J. A. Saxton, K. S. Kreielsheimer, G. W. Luscombe, "Measurement of Height-Gain at Meter Wavelengths," *Electronic Radio Engr.*, Vol. 34, p. 89, March (1957).
131. G. W. Swensen, Jr., "VHF Diffraction by Mountains of the Alaska Range," *Proc. I.R.E.*, Vol. 44, p. 1049, Aug. (1956).
132. R. Vikramsingh, M. N. Rao, and S. Uda, "Microwave Field Strength and Fading in the Presence of Intervening Ridges," *Jour. Inst. Telecommun. Eng.* (India), Vol. 4, p. 18, Dec. (1957).

RCA TECHNICAL PAPERS†

Fourth Quarter, 1962

Any request for copies of papers listed herein should be
addressed to the publication to which credited.

“Cerenkov Radiation as Leaky Surface Waves,” L. W. Zelby (Correspondence), <i>Proc. I.R.E.</i> (October)	1962
“Comments on ‘Broad-Band Parametric Amplifiers by Simple Experimental Techniques,’” B. B. Bossard and R. M. Kurzrok (Correspondence), <i>Proc. I.R.E.</i> (October)	1962
“Comments on ‘Symmetrical RC Distributed Networks,’” J. Pearl (Correspondence), <i>Proc. I.R.E.</i> (October)	1962
“Demonstration of a Speech Processing System Consisting of a Speech Analyzer, Translator, Typer, and Synthesizer,” H. F. Olson, H. Belar, and R. De Sobrino, <i>Jour. Acous. Soc. Amer.</i> (October)	1962
“An Electrostatically Focused Vidicon,” J. E. Kuehne and R. G. Neuhauser, <i>Jour. S.M.P.T.E.</i> (October)	1962
“The Measurement of the Velocity of Light,” A. C. Schroeder (Correspondence), <i>Proc. I.R.E.</i> (October)	1962
“Minute Resistivity Variations in Germanium Crystals and Their Effect on Devices,” G. Meltzer, <i>Jour. Electrochem. Soc.</i> (October)	1962
“Multiple-Target Data Handling with a Monopulse Radar,” M. Korff, C. M. Brindley, and M. H. Lowe, <i>Trans. I.R.E. PGME</i> (October)	1962
“Non-directional Stereo Effects,” C. J. Hirsch, <i>Electronics World</i> (October)	1962
“Project Relay — Another Step in Satellite Communications,” R. W. Wilmotte, <i>Signal</i> (October)	1962
“The Theory of Cerenkov Effect Based on Lorentz Transformations,” L. W. Zelby, <i>Jour. Appl. Phys.</i> (October)	1962
“Tree-Like Structure of Block Codes,” D. M. Jones and Coauthor (Correspondence), <i>Trans. I.R.E. PGIT</i> (October)	1962
“Tunneling-Assisted Photon Emission in Gallium Arsenide p-n Junctions,” J. I. Pankove, <i>Phys. Rev. Letters</i> (October 1)	1962
“Properties of Cadmium Sulfide Crystals with High Impurity Concentrations,” R. H. Bube, E. L. Lind, and A. B. Dreeben, <i>Phys. Rev.</i> (October 15)	1962
“Some Aspects of the Kapitza Resistance,” J. I. Gittleman and S. Bozowski, <i>Phys. Rev.</i> (October 15)	1962
“The Design and Operational Philosophy of the Ballistic Camera Systems at the Atlantic Missile Range,” A. E. Gleis, <i>Jour. S.M.P.T.E.</i> (November)	1962
“The Design and Performance of a High-Resolution Vidicon,” R. G. Neuhauser, B. H. Vine, J. E. Kuehne, and G. A. Robinson, <i>Jour. S.M.P.T.E.</i> (November)	1962

† Report all corrections to *RCA Review*, RCA Laboratories, Princeton, N. J.

"Effects of Random Errors on the Performance of a Linear Butler Array," M. J. Kiss, <i>Trans. I.R.E. PGAP</i> (November)	1962
"Fast High-Sensitivity Silicon Photodiodes," R. L. Williams, <i>Jour. Opt. Soc. Amer.</i> (November)	1962
"Feed Assembly for Furnaces which Utilize the Verneuil Single-Crystal Growth Technique," M. Kestigian (Notes), <i>Rev. Sci. Instr.</i> (November)	1962
"Frequency Multipliers and Harmonic Generators Using Varactor Diodes," H. C. Lee, <i>Semiconductor Products</i> (November)	1962
"A High Performance AM/FM Receiver Using an Autodyne Converter," H. Thanos and L. Plus, <i>Trans. I.R.E. PGBTR</i> (November)	1962
"The Increasing Competition for Engineers," E. I. Anderson, <i>Trans. I.R.E. PGBTR</i> (November)	1962
"New Modulation and FM Multiplex Monitor," H. J. Shay, <i>Broadcast News</i> (November)	1962
"Practical FM Stereo," A. H. Bott, <i>Broadcast News</i> (November)	1962
"Radiation-Induced Changes in Silicon Photovoltaic Cells," J. A. Baicker and B. W. Faughnan, <i>Jour. Appl. Phys.</i> (November)	1962
"A Transistorized Multiplex Demodulator for FM Stereophonic Reception," J. W. Englund and L. Plus, <i>Trans. I.R.E. PGBTR</i> (November)	1962
"Transistorized Video Distribution Amplifiers," <i>Broadcast News</i> (November)	1962
"TR-22 All-Transistor TV Tape Recorder," A. C. Luther and R. N. Hurst, <i>Broadcast News</i> (November)	1962
"Photoemissive Studies of the Band Structure of Silicon," W. E. Spicer and R. E. Simon, <i>Phys. Rev. Letters</i> (November 1)	1962
"Electron Paramagnetic Resonance of Manganese in Gallium Arsenide," N. Almeleh and B. Goldstein, <i>Phys. Rev.</i> (November 15)	1962
"Magnetoplasma Resonance in Germanium," R. E. Michel and B. Rosenblum, <i>Phys. Rev.</i> (November 15)	1962
"Photoconductivity in Cubic Cadmium Sulfide," E. L. Lind and R. H. Bube, <i>Jour. Chem. Phys.</i> (Notes) (November 15)	1962
"An All-Transistor Television Tape Recorder," A. H. Lind, <i>Jour. S.M.P.T.E.</i> (December)	1962
"An Analysis of the Effects of Reactances on the Performance of the Tunnel-Diode Balanced-Pair Logic Circuit," J. J. Gibson, <i>RCA Review</i> (December)	1962
"Breakdown Voltage of GaAs Diodes Having Nearly Abrupt Junctions," H. Kressel, A. Blicher, and L. H. Gibbons, Jr. (Correspondence), <i>Proc. I.R.E.</i> (December)	1962
"The Business Radio Service," G. W. Pettengill, <i>Electronics World</i> (December)	1962
"Design Considerations for Double-Diffused Silicon Switching Transistors," H. Kressel, H. S. Veloric, and A. Blicher, <i>RCA Review</i> (December)	1962
"An Evaluation of Tunnel-Diode Balanced-Pair Logic Systems," H. S. Müller and R. A. Powlus, <i>RCA Review</i> (December)	1962
"Microaperture High-Speed Ferrite Memory," R. Shahbender, T. Nelson, R. Lochinger, and J. Valentine, <i>RCA Review</i> (December)	1962
"Non-Directional Stereo," C. J. Hirsch (Letters from our Readers), <i>Electronics World</i> (December)	1962
"Prediction of Rise Time in Junction Transistors," P. E. Kolk (Correspondence), <i>Proc. I.R.E.</i> (December)	1962
"Rapid Measurement of Transistor Junction-to-Case Thermal Resistance," P. A. Peckover, <i>Semiconductor Products</i> (December)	1962
"Reciprocal Ferrite Phase-Shifter Measurements," M. J. Schindler (Correspondence), <i>Proc. I.R.E.</i> (December)	1962
"Tunnel Diode Decade Counter," B. Rabinovici, <i>Rev. Sci. Instr.</i> (December)	1962

"Vapor Pressure Data for the Solid and Liquid Elements," R. E. Honig, <i>RCA Review</i> (December)	1962
"Temperature Dependence of Photo-Hall Effects in High-Resistivity Gallium Arsenide. I. One-Carrier Effects," R. H. Bube and H. E. MacDonald, <i>Phys. Rev.</i> (December 1)	1962
"Temperature Dependence of Photo-Hall Effects in High-Resistivity Gallium Arsenide. II. Two-Carrier Effects," R. H. Bube and H. E. MacDonald, <i>Phys. Rev.</i> (December 1)	1962
"Electrodynamic Properties of a Quantum Plasma in a Uniform Magnetic Field," J. J. Quinn and S. Rodriguez, <i>Phys. Rev.</i> (December 15)	1962
"Quantum Effects in Ultrasonic Attenuation in Metals in a Magnetic Field," J. J. Quinn and S. Rodriguez, <i>Phys. Rev.</i> (December 15)	1962
"Radiation Defect Introduction Rates in n- and p-Type Silicon in the Vicinity of the Radiation Damage Threshold," H. Flicker, J. J. Loferski, and J. Scott-Monck, <i>Phys. Rev.</i> (December 15)	1962
"Image Processing with Optical Panels," H. O. Hook and H. Weinstein, <i>Electronics</i> (December 21)	1962

AUTHORS



MORREL P. BACHYNSKI received the B.E. degree in Engineering Physics in 1952 and the M.Sc. degree in 1953, both from the University of Saskatchewan, and the Ph.D. degree from McGill University in 1955. Until October 1955, as a member of the Eaton Electronics Research Laboratory, McGill University, he was engaged in investigations on microwave optics. Since that time, he has been with the RCA Victor Research Laboratories, Montreal, Canada, concerned primarily with electromagnetic wave propagation, microwaves and plasma physics. He is presently Director of the Microwave and

Plasma Physics Laboratories. Dr. Bachynski is a senior member of the Institute of Electrical and Electronics Engineers, a member of the American Physical Society and of the Canadian Association of Physicists. He served on the Defence Research Board of Canada Advisory Committee on Gas Dynamics (1960-1963), is Chairman of Commission VI of the Canadian National Committee of the International Scientific Union (URSI) and is associated with the Graduate School of McGill University.

ALVIN S. CLORFEINE studied electrical engineering at the College of the City of New York where he was granted a B.S. in 1959. He received his M.S. in Electrical Engineering the following year, from the Carnegie Institute of Technology. Since joining RCA Laboratories in 1961, he has been engaged in research in tunnel diodes and superconductive devices. Mr. Clorfeine is a member of Eta Kappa Nu, Tau Beta Pi, and Sigma Xi.





AUGUSTE B. EL-KAREH received the equivalent of a B.S. degree from the Polytechnic, University of London in 1955 and the Dip. Elec. Ing. degree and the D.Sc. degree from the Technische Hogeschool of Delft, Netherlands, in 1956 and 1962, respectively. From 1956 till 1958 he worked as a research engineer in the Technische Hogeschool of Delft. From 1959 till 1960 he taught in the electrical engineering department of the University of New Mexico and the University of Pennsylvania. He joined RCA Laboratories in 1960, where he has been working in the area of electron-optical devices and, more

recently, on microwaves. Dr. El-Kareh is a member of the Institute of Electrical and Electronics Engineers.

HENRY S. MILLER received the B.S. and M.S. degrees in Electrical Engineering from the University of Illinois and the University of Pennsylvania. In 1958, he joined RCA Laboratories, where he has been involved in work on ultra-high-speed computer circuits utilizing microwave phase-locked oscillators and tunnel diodes. His current interests relate to tunnel-diode-transistor hybrid digital circuits and systems. Mr. Miller is a member of the Institute of Electrical and Electronics Engineers and Eta Kappa Nu.



DONALD W. PETERSON received the B.S. degree in E.E. from the University of Wisconsin in 1936. In that year he joined the Service Department of RCA Manufacturing Co. in Camden, N. J. From 1942 to 1961, he was a member of the technical staff of RCA Laboratories in Princeton, N. J. In 1961 he was transferred to the Antenna Skill Center of the Missile and Surface Radar Division of RCA in Moorestown, N. J. He is currently engaged in work on antennas and propagation. Mr. Peterson is a member of the Institute of Electrical and Electronics Engineers.



